

Investigation of Gut-Derived Circulating Succinate in Metabolism and Liver Signaling

by

Wenxin Tong

Department of Pharmacology and Cancer Biology
Duke University

Date: _____

Approved:

Mark. A. Herman, Supervisor

Christopher Newgard, Chair

Deborah Muoio

Donald Fox

John Rawls

Dissertation submitted in partial fulfillment of
the requirements for the degree of Doctor
of Philosophy in the Department of
Pharmacology and Cancer Biology
in the Graduate School of Duke University

2022

ABSTRACT

Investigation of Gut-Derived Circulating Succinate in Metabolism and Liver Signaling

by

Wenxin Tong

Department of Pharmacology and Cancer Biology
Duke University

Date: _____

Approved:

Mark. A. Herman, MD, Supervisor

Christopher Newgard, PhD, Chair

Deborah Muoio, PhD

Donald Fox, PhD

John Rawls, PhD

Dissertation submitted in partial fulfillment of
the requirements for the degree of Doctor
of Philosophy in the Department of
Pharmacology and Cancer Biology
in the Graduate School of Duke University

2022

Copyright by
Wenxin Tong
2022

Abstract

The tricarboxylic acid (TCA) cycle is the epicenter of cellular aerobic metabolism and accounts for the majority of cellular ATP production. In addition to its use in anabolic and catabolic processes, TCA cycle intermediates may serve as signaling molecules. The TCA cycle intermediates succinate and α -ketoglutarate are specific natural ligands for previously orphan receptors GPR91 (Sucnr1) and GPR99 (Oxgr1), respectively. The function of Sucnr1 is more extensively studied and its activation by succinate regulates pleiotropic biological processes. The physiological range of circulating succinate coincides with the pharmacological range (EC50) of Sucnr1 activation, suggesting that changes in circulating succinate levels have the potential to affect the activity of Sucnr1 and its downstream targets. This supports the potential for a signaling role of succinate in health and disease.

Despite the potential importance of circulating TCA cycle metabolites as signaling molecules, the source of circulating TCA cycle intermediates remains uncertain. Although prior studies showed that exogenous succinate via activating Sucnr1 regulates biological function in various tissues, succinate concentrations used in such studies typically far exceed circulating levels. Thus, it is uncertain whether circulating succinate signals through Sucnr1 and whether there are specific cell-types or tissue-types where this is more or less likely to occur. As a result, the physiological roles for circulating succinate as a signaling molecule remains speculative.

In my thesis work, we set out to address three major questions. First, we explored the major source of circulating TCA cycle metabolites and found the gut plays a major role in this. Second, we investigated the role of intestinal-derived circulating succinate in signaling with a focus on the role of *Sucnr1* signaling in the liver. Third, using our new knowledge that the intestine is a major production site of circulating TCA cycle metabolites including succinate, we used this knowledge to develop a method to further probe intestinal and systemic metabolism.

Our work elucidating the site of circulating TCA cycle metabolites began when we first observed that TCA cycle intermediates levels are much higher in the portal vein compared with tail vein plasma. This observation led directly to our hypothesis that the gut might be a major contributor to circulating TCA cycle metabolites. With a focus on succinate as a representative TCA cycle intermediate with known signaling activities and using a combination of germ-free mice and isotopomer tracing, we demonstrated that intestinal microbiota are not major contributors to circulating TCA cycle metabolites. Moreover, we demonstrated that endogenous succinate production is markedly higher than intestinal succinate absorption in normal physiological conditions. Altogether, these results showed that endogenous succinate production within the intestinal tissue is a major physiological source of circulating succinate.

We next sought to determine whether gut-derived succinate may function as a metabolic signal and regulate biological function. This could occur through activation of

the previously described succinate receptor, *Sucnr1*, or through other, unknown mechanism. *Sucnr1* is highly expressed in multiple metabolic tissues including the liver. This combined with our evidence that the intestine is a major source of circulating succinate led to the hypothesis that cells within the liver expressing *Sucnr1* might be a major target of intestine-derived, circulating succinate. By analyzing single-cell RNA-sequencing data, we found that *Sucnr1* is expressed in both hepatocytes and liver non-parenchymal cells including hepatic stellate cell, endothelial cells and the Kupffer cells. Using distinct methods to generate liver-selective versus hepatocyte-selective *Sucnr1* knockout mice, we demonstrated that *Sucnr1* is predominantly expressed in hepatocytes and to a much lesser degree in non-parenchymal cells.

As *Sucnr1* is a Gi coupled GPCR, we further hypothesized that succinate mediated activation of *Sucnr1* might antagonize the glucagon receptor (GCGR), the most abundant Gs-coupled GPCR expressed in hepatocytes. Initially, succinate infusion experiments and assessment of its effects on glucagon signaling in mouse liver appeared to support the possibility that succinate might antagonize hepatocyte glucagon signaling. However, subsequent experiments in liver specific *Sucnr1* knockout mice did not strongly support this hypothesis.

Therefore, to investigate the potential role of gut-derived succinate and its effects on liver *Sucnr1* from a more unbiased perspective, we conducted RNA-sequencing of liver samples from liver-specific *Sucnr1* knockout mice and their littermate controls which

suggested that hepatic *Sucnr1* may play modest regulatory role in regulating amino acid metabolism and in some infections. Altogether, our work indicates that hepatocytes are a major site of *Sucnr1* expression. However, whether it has a major role in responding to circulating succinate and what that role might be remains less certain. Our results suggest that hepatic *Sucnr1* does not play a major role in antagonizing hepatic glucagon signaling. Hepatic RNA-seq analysis suggests that hepatic *Sucnr1* may have a role in infection and this may be consistent with a putative role for *Sucnr1* in responding to intestinal parasitic infections and in immunity more generally.

In the course of this work, we demonstrated that the intestine tissue is a major contributor to circulating TCA cycle intermediates. Additionally, recent studies from our lab and others showed that fructose is largely metabolized in the intestine tissue and readily incorporated into the TCA cycle intermediates. Therefore, we hypothesized that we could use intestinal fructose metabolism and its incorporation into circulating TCA cycle metabolites as a methodology to investigate intestinal metabolism in live, conscious animals. Metformin is the most widely prescribed anti-diabetic drug and concentrates at high levels within enterocytes. Its mechanism of action to enhance systemic metabolism and reduce or delay the progression to type 2 diabetes remains highly controversial. Therefore, we hypothesized that isotope-tracing metabolomics performed after gavaging U-C-13 fructose could be used to investigate the role of metformin in intestinal and systemic metabolism. Consistent with this, we have now demonstrated that metformin

significantly diminished intestinal fructose metabolism, flux of metabolites into the TCA cycle within the intestine, and intestinal glucose production. Metformin also reduced the delivery of ingested fructose to the liver. Altogether, these results indicate that isotopomer tracing of intestinal fructose metabolism and TCA cycle intermediate production may serve as a non-invasive method to investigate intestinal metabolism and the mechanism of action of metformin.

Overall, our work provides insight into the major source of circulating TCA cycle intermediates, potential function of the succinate sensing receptor, *Sucnr1*, in hepatocytes, and the role of metformin in regulating intestinal metabolism and TCA cycle production. These data provide a foundation for further investigation into the role of the intestine in regulating circulating TCA cycle metabolites and related signaling effects in health and disease. Furthermore, these data clarify that *Sucnr1* is predominantly expressed in the liver hepatocyte, in contrast with prior findings that suggested that *Sucnr1* within the liver was predominantly expressed in non-parenchymal cells. The contributions and novel insight provided here will be important to fully understand the regulatory role of succinate-*Sucnr1* axis in liver functions and provide a novel approach for using intestinal fructose metabolism and TCA cycle intermediates production to probe intestinal and systemic metabolism.

Dedication

I dedicate this dissertation and my success in academic endeavors to my grandfather Laibin Tong. I would not be interested in science in the first place had he not inspired me with science stories and hands-on “science projects” like tearing down flashlights, fans, and TV controllers when I was a child. As one of the very few college graduates in China back in the 1960s, he is always curious and passionate about science and takes every minute to absorb knowledge of all kinds. His passion and hardwork encourage me to pursue my interests with determination and stimulate me to carry on when I feel “things are too hard”. I hope he finds satisfaction and enjoyment in knowing that my Doctorate of Philosophy is largely inspired by him.

Contents

Abstract	iv
List of Tables.....	xiv
List of Figures	xv
List of Equations.....	xvii
List of Abbreviations	xviii
Acknowledgements	xxi
1.1 Tricarboxylic acid cycle	1
1.2 TCA cycle and other metabolic pathways	2
1.3 Circulating succinate as metabolic signal	3
1.4 Circulating succinate and metabolic disease	5
1.5 Goals of dissertation work	6
2. Methods and Materials.....	8
2.1 Animal Experiments	8
2.1.1 Mouse models.....	8
2.1.2 Mouse procedures	10
2.2 Molecular biology techniques and procedures	14
2.2.1 Primary tissue/cell isolation procedures and <i>in vitro</i> culturing techniques.....	14
2.2.2 Molecular biology techniques.....	18
2.2.3 Metabolomic techniques.....	26
2.2.4 Transcriptome techniques	33

2.3 Statistics and data analysis.....	34
3. Intestinal tissue is a major contributor to circulating TCA cycle intermediates	36
3.1 Introduction.....	36
3.2 Results	38
3.2.1 The gut contributes to circulating TCA cycle metabolites.....	38
3.2.2 Microbiota are not essential to maintain the portal levels of TCA cycle intermediates.....	42
3.2.3 Labeled precursors produce distinct succinate labeling patterns when exposed to intestinal organoids versus microbiota.....	44
3.2.4 Portal succinate is produced from the intestinal tissue and not the microbiota	47
3.2.5 Need of generating a model to estimate the intestinal capacity for absorption of orally administered succinate	49
3.2.6 Generating a Relative quantification model for assessing endogenous production versus external absorption	49
3.2.7 Compared to endogenous production, intestinal succinate absorption capacity is limited.	56
3.3 Discussion.....	59
3.4 Conclusion.....	64
4. Sucnr1 is predominantly expressed in hepatocytes where its physiological role remains unclear	65
4.1 Introduction.....	65
4.2 Results	67
4.2.1 Sucnr1 is expressed in multiple liver cell types.	67
4.2.2 Sucnr1 is predominantly expressed in parenchymal cells in the liver.	72

4.2.3 Acute exposure of the liver to succinate attenuates phosphorylation of some targets of hepatic glucagon signaling	77
4.2.4 Hepatic Sucnr1 knock-out has minimal effects on metabolic parameters	82
4.2.4 Explore hepatic Sucnr1's role on hepatic gene expression	86
4.2.5 Exploration of Sucnr1 function in human exome sequencing data	92
4.3 Discussion.....	93
4.4 Conclusion.....	97
5. Investigation into the use of the gut-derived TCA cycle intermediates as biomarkers of intestinal metabolism in metabolic disease	98
5.1 Introduction.....	98
5.2 Results	99
5.2.1 Establish a short-term metformin intervention animal model	99
5.2.2 Short-term metformin treatment improves glucose tolerance.....	100
5.2.3 Short-term metformin treatment decreased fructose metabolism in the intestine tissue.....	102
5.2.4 Metformin treatment decreases the flux from pyruvate into TCA cycle of PDH in the intestine tissue.....	104
5.2.5 Metformin altered citrate concentrations in the intestine tissue and portal plasma	106
5.2.6 Decreased intestinal fructose metabolism induced by metformin is associated with increased AMPK signaling.....	107
5.2.7 Short-term metformin treatment inhibits intestinal glucose production	110
5.2.8 Short-term metformin treatment decreases the delivery of fructose and fructose-derived metabolites to the liver	112
5.3 Discussion.....	114
5.4 Conclusion.....	118

6. Conclusions and future directions.....	119
Appendix A.....	122
References	124
Biography	143
Wenxin Tong.....	143
Education.....	143
Publication.....	143
Honors and Awards.....	144

List of Tables

Table 1: Primers for genotyping.....	19
Table 2: Primers for qPCR.....	25
Table 3: metabolites detected by GC/MS.....	32
Table 4: All murine GPCRs detected in hepatocytes	71
Table 5: Top 20 up-regulated KEGG Pathways in LiSucnr1KO than controls.....	90
Table 6: Top 20 down-regulated KEGG Pathways in LiSucnr1KO than controls	91
Table 7: Top 50 differentially expressed genes between the LiSucnr1KO liver versus controls using the p values smaller than 0.05 as criteria	122

List of Figures

Figure 1: Targeting strategy used to generate the Alb-Cre Sucnr1KO.....	10
Figure 2: A consistent portal to tail gradient of TCA cycle intermediates.....	39
Figure 3: Providing isotope precursors to the gut increases isotope enrichment of TCA cycle intermediates without changing their quantities	41
Figure 4: Microbiota are not essential to maintain the portal levels of TCA cycle intermediates	43
Figure 5: Succinate production from isotope tracers	45
Figure 6: Intestinal organoids in contrast to cecal/fecal content generate distinct succinate labeling patterns from labeled precursors.....	46
Figure 7: The succinate labeling pattern in portal plasma is similar to that in the intestinal tissue while distinct from that in the cecal contents following oral-gavage with U-C13-fructose.....	48
Figure 8: The outline of the relative quantification model.....	50
Figure 9: Equations of the relative quantification model	53
Figure 10: Validation of the relative quantification model using fructose	55
Figure 11: The intestinal absorption of succinate is limited.....	58
Figure 12: Sucnr1 is expressed in multiple cell types in the liver	68
Figure 13: Sucnr1 does express in hepatocytes.....	70
Figure 14: Sucnr1 is exclusively knocked out in the liver-specific Sucnr1 knock-out (LiSucnr1KO) mice.....	72
Figure 15: Liver parenchymal and non-parenchymal fragment isolation after 2-step <i>in situ</i> liver digestion.....	73
Figure 16: Sucnr1 expressed higher in the hepatocytes versus non-parenchymal cells ...	74
Figure 17: Sucnr1 is predominantly expressed in the hepatocytes.....	76

Figure 18: Succinate attenuates the phosphorylation of selected hepatic substrates that are phosphorylated following glucagon treatment.	79
Figure 19: Protein discovery of phospho-PKA-substrates bands that responsive to acute portal succinate perfusion.....	81
Figure 20: Hepatic Sucnr1 knockout does not change metabolic phenotypes in high fat high sucrose induced metabolic disorder model	83
Figure 21: Liver Sucnr1 has modest regulatory effects of amino acid homeostasis	85
Figure 22: Liver Sucnr1 knockout induce modest gene expression changes	87
Figure 23: Differentially expressed pathways induced by liver Sucnr1 knockout	89
Figure 24: Timeline of the metformin study.....	100
Figure 25: Short-term of metformin treatment improves glucose tolerance	101
Figure 26: Intestinal fructose metabolism.....	102
Figure 27: Metformin decrease fructose metabolism in the intestine tissue.....	103
Figure 28: Metformin decreased the flux of labeled substrate into the TCA cycle in association with reduced pyruvate dehydrogenase	105
Figure 29: Metformin decreased citrate levels in the intestine tissue and portal plasma	106
Figure 30: The effects of decreased intestinal fructose metabolism induced by metformin associates with increased activity of AMPK signaling	109
Figure 31: Metformin decrease intestinal glucose production	111
Figure 32: Metformin decrease fructose delivery to the liver	113

List of Equations

Equation 1: First-order transport	51
Equation 2: Transported labeled metabolites correspond to the ratio of labeled to unlabeled metabolites in the gavage solution.....	52
Equation 3: Transported unlabeled metabolites are the sum from both external absorption and endogenous production	52
Equation 4: Estimate the intestinal absorption to endogenous production by the labeling of metabolites in the portal blood.....	53

List of Abbreviations

36B4 – ribosomal protein, large, P0

AAV – Adeno-associated viruses

Acta2 – actin alpha 2, smooth muscle

ACN – acetonitrile

Alb – albumin

AldoB – aldolase B

AMP – adenosine monophosphate

AMPK – adenosine monophosphate-activated protein kinase

ATP – adenosine triphosphate

BCAA – branched-chain amino acids

BMI – body mass index

CD68 – cluster of differentiation 68

CD31 – cluster of differentiation 31 or platelet endothelial cell adhesion molecule

DCLK3 – doublecortin like kinase 3

DTT – dithiothreitol

ETC – electron transport chain

F1P – fructose-1-phosphate

FADH₂ – flavin adenine dinucleotide

G6pc – glucose-6-phosphatase, catalytic subunit

GA3P – glyceraldehyde 3-phosphate

GABA – γ -aminobutyrate

GAPDH – glyceraldehyde-3-phosphate dehydrogenase

GCGR – glucagon receptor

GC/MS – gas chromatography / mass spectrometry

GPCRs – G-protein coupled receptors

HFHS – high-fat/high-sucrose

HIF-1 α – hypoxia-induced-factor 1 α

HOMA-IR – Homeostatic Model Assessment for Insulin Resistance

IFN- γ – interferon- γ

Khk – ketohexokinase

LPS – lipopolysaccharide

NAD⁺ – nicotinamide adenine dinucleotide

NADH – nicotinamide adenine dinucleotide

NAFLD – non-alcohol fatty liver disease

NASH – non-alcohol steatohepatitis

P85 – phosphatidylinositol 3-kinase 85 kDa regulatory subunit alpha

PCK1 – phosphoenolpyruvate carboxykinase 1

PCR – polymerase chain reaction

PDH – pyruvate dehydrogenase

PDHA – pyruvate dehydrogenase E1 component subunit alpha

PKA – protein kinase A

Sucnr1 – succinate receptor

T2D – type 2 diabetes

TBDMS – tertbutyldimethylchloros

TMS – trimethylsilyl

Tbg – thyroxine-binding globulin

TCA – tricarboxylic acid

TG – triglyceride

Tpmt – thiopurine methyltransferase

Acknowledgements

I would like to thank my advisor Mark Herman, M.D., and the Herman lab for their constant support of my research endeavors. I thank the members of my dissertation committee, Chris Newgard, Ph.D., John Rawls, Ph.D., Deb Muoio, Ph.D., and Don Fox, Ph.D., for their instruction throughout my graduate tenure. I thank members of the Duke Molecular Physiology Institute for their welcoming and diverse community. Special thanks to Guofang Zhang, Ph.D., from the DMPI metabolomics core, for his generous help and offer with the metabolomics training.

I would like to give special thanks to my significant other Canqi Cui, MD, Ph.D., who is always there for me with uppermost enthusiasm. I would hardly have made it through the completion of my thesis without her constant encouragement. I thank my parents for their respect for my insistence on pursuing a distinct career path and their cultivation of my independence to survive in a foreign country. And I appreciate the graduate training opportunity offered by Duke Pharmacology and Cancer Biology department. This five years' study at Duke provides me not only the professional skills as a qualified researcher, but also the appreciation and embrace of diversity from various disciplines including culture, religion, lifestyles, and politics. I believe this experience would be one of my most valuable adventures.

1. Introduction: General overview of dissertation work

1.1 *Tricarboxylic acid cycle*

The tricarboxylic acid (TCA) cycle, or Krebs' cycle, was first described by Sir Hans Krebs in 1937 [1]. The TCA cycle includes a series of chemical reactions that oxidize acetyl-CoA derived from common nutrients including carbohydrates, proteins, and fats. The complete oxidation of acetyl-CoA into 2 molecules of carbon dioxide yields an estimated 12.5 molecules of adenosine triphosphate (ATP) in aerobic conditions which accounts for the majority of energy production in cells [2].

In eukaryotic cells, the TCA cycle occurs in the mitochondrial matrix and is closely coupled to the electron transport chain (ETC) [3]. Indeed, the Nicotinamide adenine dinucleotide (NADH) and flavin adenine dinucleotide (FADH₂) generated from the TCA cycle donates its electron to the ETC which generates the electrochemical gradient across the inner mitochondrial membrane that drives ATP synthesis. Additionally, the conversion of succinate from succinate-CoA in the TCA cycle flux directly contributes to ATP production by substrate-level phosphorylation. Altogether, the extensive ATP generation via processes mentioned above make the TCA cycle the epicenter of cellular and organismal energy homeostasis.

1.2 TCA cycle and other metabolic pathways

Apart from contributing to the energy production, TCA cycle intermediates are localized at the crossroads of multiple metabolic pathways. As mentioned earlier, glucose and fatty acids are catabolized through glycolysis and fatty acid oxidation, respectively, to generate acetyl-CoA which is then fully oxidized in the TCA cycle. In contrast, TCA cycle intermediates can also be used for anabolic purposes. For instance, oxaloacetate can be exported from the mitochondria and decarboxylated into phosphoenolpyruvate and enter the gluconeogenesis pathway [4]. Additionally, the TCA cycle intermediate citrate can be transported to the cytosol and used for fatty acid synthesis [5]. Moreover, TCA cycle intermediates also serve as a major source of carbon for production of common amino acids. Specifically, oxaloacetate and α -ketoglutarate are readily converted to the amino acids aspartate and glutamate and participate in nitrogen homeostasis [6].

In addition to serving as the anabolic precursors of amino acids and fatty acids, TCA cycle intermediates are also the end products of various substrates outside of canonical biochemical pathways. Specifically, TCA cycle intermediate succinate serves as the end products of valine and isoleucine catabolism, regulating the balance of branched-chain amino acids (BCAA) metabolism [7]. Further, succinate is the end product of γ -aminobutyrate (GABA) catabolism, which is an important regulator of intercellular GABA levels and is crucial to protect from multiple neurological diseases including Alzheimer's disease, seizures and Parkinson's disease [8].

Although the majority of TCA cycle metabolites are produced within the mitochondria and participate in nutrient metabolism, TCA cycle intermediates could also regulate responses outside the mitochondria. To be specific, in hypoxia conditions, absence of electron acceptors impairs mitochondrial function and leads to the accumulation of succinate in the mitochondrial [9]. The excessive mitochondrial succinate escapes to the cytosol. This increased cytosolic succinate during hypoxia stabilizes the activated hypoxia-induced-factor 1 α (HIF-1 α) and regulates the hypoxia induced proliferation, migration and inflammation in various cell types [10]. This succinate regulated hypoxia responses has crucial clinical significance in the disease conditions such as myocardial infarction [11], liver ischemia [12], and ischemic renal disease [13]. On the other hand, succinate in the nuclei can regulate DNA and histone methylation and modulate the expression of the transcriptome [14].

Altogether, TCA cycle intermediates serve pleiotropic functions in maintaining cellular energy homeostasis, nutrient interconversion, and hypoxia effects.

1.3 Circulating succinate as metabolic signal

Recently, TCA cycle intermediates succinate, and α -ketoglutarate to a lesser potency, have been shown to act as specific ligands for a previously discovered orphan cell surface G-protein receptor (GPR-91, or Sucnr1), opening the possibility of TCA cycle intermediates serving as metabolic signals outside of cells. This succinate-Sucnr1 axis has

been demonstrated to be a crucial regulator of multifarious physiological and pathophysiological functions [15, 16].

Studies to date have shown that the succinate-Sucnr1 signaling axis is important for cell-to-cell communication in regulating the adaptive and innate immune responses that maintain immune homeostasis. For instance, in chronic autoimmune diseases including systemic lupus erythematosus, large amounts of succinate are released by activated T cells [17]. Additionally, the expression of cell-surface Sucnr1 is necessary for the activation of B cell from naïve B cell [18]. Moreover, succinate can be produced and secreted by the pro-inflammatory M1 macrophages following metabolic reprogramming when stimulated by inflammatory signals like lipopolysaccharide (LPS) and interferon- γ (IFN- γ) [19]. This M1 macrophage-derived succinate causes hyperpolarization of M2 macrophages to induce anti-inflammatory responses [20]. Thus, the succinate-Sucnr1 axis is an important mediator of M1 to M2 macrophage communication to maintain pro-inflammatory and anti-inflammatory balance [21-23].

In addition to its role in inflammation, circulating succinate is also thought to serve as a metabolic signal that participates in maintenance of systemic energy homeostasis and muscle remodeling. For instance, global Sucnr1 knockout mice have increased energy expenditure and decreased fat pad volume when fed on a chow diet. [24]. Also, physical exercise could induce a transient surge of circulating succinate and chronic exercise induces skeletal muscle fiber remodeling and increased explosive strength via Sucnr1

signaling [25]. This regulatory effect of succinate-Sucnr1 axis on muscle remodeling is supported by studies showing that the lack of Sucnr1 abolished succinate induced up-regulation of explosive strength during exercise [26].

Altogether, circulating succinate functions as crucial signals to regulate immune and inflammatory responses and energy expenditure homeostasis.

1.4 Circulating succinate and metabolic disease

Recent studies suggest that circulating level of TCA cycle intermediate may also serve as biomarkers of metabolic disease. Serena and colleagues noted increased circulating succinate levels in obese and type 2 diabetes (T2D) patients [27]. Moreover, circulating succinate levels correlate with multiple metabolic traits, including circulating glycemia, insulin, and triglyceride (TG), as well as body mass index (BMI) and Homeostatic Model Assessment for Insulin Resistance (HOMA-IR) [27]. Indeed, circulating succinate levels are significantly elevated in multiple metabolic disease associated animal models including genetically obese ob/ob and db/db mice and spontaneously hypertensive rats [28]. Moreover, chronic western-style diet (30 weeks) can also significantly increase the circulating succinate levels in mice in accordance with the development of metabolic disorders [29]. Moreover, Osuna-Prieto and colleagues demonstrated that elevated plasma succinate levels are positively correlated with higher cardiovascular disease risk factors [30]. Additionally, increased basal preoperative

succinate levels correlate with diabetes remission after bariatric surgery in a randomized controlled clinical trial [31]. Altogether, these studies strongly suggest the circulating succinate could serve as a biomarker for metabolic disease in both human and animal models. It follows that investigation of factors or regulatory processes contributing to regulation of circulating succinate levels may provide insight into the pathogenesis of metabolic disease that could lead to new diagnostic and therapeutic strategies.

1.5 Goals of dissertation work

Altogether, TCA cycle intermediates facilitate energy homeostasis, modulate intercell and/or interorgan communication as metabolic signals, and serve as biomarkers of multiple metabolic diseases. However, the major sources of circulating TCA cycle intermediates and the key target tissues that sense circulating TCA cycle intermediates and that might contribute to the pathogenesis of metabolic disease remain largely unknown. Therefore, for my dissertation work, we sought 1) to identify the major source of circulating TCA cycle intermediates, and 2) to identify potential targets and effects of circulating succinate. In support of the first goal, we have demonstrated that the intestine is a major contributor to circulating TCA cycle intermediates. In follow-up of the methods and conclusions developed in pursuit of the first goal, we proposed a third goal, to investigate whether intestinal TCA cycle intermediate production could be used to interrogate intestinal metabolism in association with metabolic disease. To this end, we

have used this knowledge in combination with our knowledge of intestinal fructose metabolism to approach the regulatory role of metformin on intestinal metabolism and systemic glucose homeostasis. These multiple approaches enabled us to achieve a deeper understanding of the intestine tissue as a major contributor of succinate and a potential regulator of liver functions via the succinate-Sucnr1 axis in hepatocytes. The work also frames a promising strategy to evaluate intestinal metabolism using non-interventional techniques.

2. Methods and Materials

2.1 Animal Experiments

Animal studies were conducted under protocols approved by Duke University's Animal Care and Use program Committee (protocol number A147-19-07 and A204-18-08). All animals were maintained at constant temperature (~ 22°C) on a 12-hour light-dark cycle (8 AM to 8 PM). The housing, husbandry, and care of animals were monitored by the Duke Department of Laboratory Animal Resources, which is accredited by the Association for Assessment and Accreditation of Laboratory Animal Care (AAALAC).

2.1.1 Mouse models

2.1.1.1 Conventional reared wild-type mice

Conventional wild-type male mice on either C57/BL6J, C57/BL6N, and C3H/HeJ background were purchased from The Jackson Laboratory (Stock# 000664, 005304, and 000659, respectively) and maintained in the animal facility under standard conditions. Conventionally reared animals were maintained in Duke University's specific pathogen free environment with corn cob bedding for at least one week before any experimental procedure or intervention. Except where otherwise noted with respect to specific

experiments, specified treatments or euthanasia were performed at 2 PM after 5 hours food removal (9 AM to 2 PM).

2.1.1.2 Germ-free wild-type mice

Germ-free mice were obtained from the Duke Gnotobiotic Core. These mice were originally obtained from Taconic (C57BL/6NTac). All germ-free animals were fed autoclaved Envigo 2020SX diet. Germ-free animals were maintained in a flexible film isolator (Class Biologically Clean, Madison, WI) with Alpha Dri bedding.

2.1.1.3 Generation of the liver-selective *Sucnr1* knock-out and hepatocyte-specific *Sucnr1* knock-out mice models

Mouse ES cells were generated containing the *Sucnr1* gene with LoxP sites flanking exon 2 on C57/BL6J background (*Sucnr1*^{flox/flox}) by standard recombineering techniques. To generate the liver-specific *Sucnr1* knock-out model, *Sucnr1*^{flox/flox} mice were crossed with C57/BL6J mice that expressed Albumin-Cre (Alb-Cre, The Jackson Laboratory Stock #000664) as indicated by Figure 1. Mice were backcrossed with *Sucnr1*^{flox/flox} animals to generate the homozygous *Sucnr1*^{flox/flox}, Alb^{Cre/-} mice and maintained at homozygosity for the floxed *Sucnr1* allele and hemizyosity for the Alb-Cre transgene. For hepatocyte-specific *Sucnr1* knockout, rAAV8-TBG-Cre and rAAV8-TBG-eGFP were purchased from University of Michigan Virus Core (VVC061119.2, and VVC061119.1, respectively). Animals were anesthetized under isoflurane for retro-orbital

injection of AAVs (dose: 6.9×10^{11} viral genomes of either Cre or eGFP). Animals were genotyped by PCR using genomic DNA from the tail nicks that were harvested at 3-weeks of age at weaning. A detailed genotyping strategy will be discussed in 2.2.3.1.

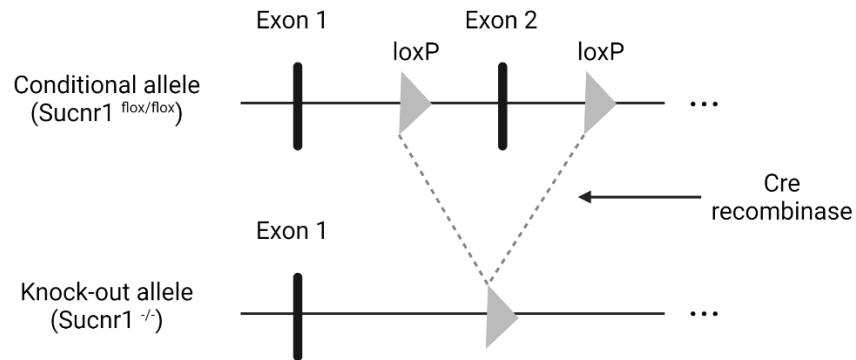


Figure 1: Targeting strategy used to generate the Alb-Cre Sucnr1KO

Targeting strategy of generating the liver selective Sucnr1KO mice. A map of the Sucnr1 genomic locus shows the conditional allele (upper panels) and the KO allele (lower panels). Arrowheads indicate LoxP sites. Vertical bars depict respective exons.

2.1.2 Mouse procedures

2.1.2.1 Body weight and body composition characterization

For chronic dietary intervention studies, animals' body weights were measured at 10 AM weekly. Otherwise, body weights were assessed prior to terminal procedures. Whole body composition was measured by Bruker Minispec LF 90II system. For this, body weight was recorded before mice were carefully placed into a plastic tube which was then inserted into the minspec magnetic body. The minspec system uses Nuclear

Magnetic Resonance (NMR) to precisely quantify the weight of lean tissue, fat, and fluids in living mice. The percentages of lean mass and fat mass were calculated by dividing the weight of lean tissue and fat tissue by total body weight.

2.1.2.2 Glucose tolerance test

Animals were fasted for 5 hours starting at 8 AM. At 1PM, body weight of animals was measured, and sterile glucose solution was injected intraperitoneally at a dose of 1.5 g/Kg body weight. Glycemia was measured using a drop of blood drawn from a nicked tail vein via glucometer (Bayer Contour) at the 0, 15, 30, 60, 90, and 120 minutes time points post injection.

2.1.2.3 Mix-meal tolerance test

Animals were fasted for 5 hours starting at 8 AM. At 1PM, body weights were measured and Ensure® milkshake was orally gavaged at a dose of 10 µl/g body weight. Glycemia levels of animals were recorded using a drop of blood drawn from a nicked tail vein by glucometer (Bayer Contour) at 0, 15, 30, 45, and 60 minutes time points post gavage.

2.1.2.4 Portal plasma sample preparation

As this project investigated potential communication between the intestine tissue and the liver tissue, this required sampling blood from the portal vein. To obtain portal vein blood samples, mice were anesthetized under continuous isoflurane administration following the guidelines recommended by the Duke Institutional Animal Care and Use Committee. Specifically, animals were anesthetized using a precision vaporizer and induced with 5% isoflurane (0.5 - 1 L/min) and then switched to a nose cone at 2-3% isoflurane with a constant oxygen flow (1.5 L/min). Once deep anesthesia is confirmed by a toe pinch, laparotomy was performed, and the portal vein was exposed. Clean scissors were used to make a small incision in the the portal vein, and blood (200 ul) was be extracted using a 1 ml syringe from the peritoneal cavity and transferred to EDTA-coated blood collection tube (Sarstedt, 16.440.100). This was stored on ice for no longer than 60 minutes prior to centrifugation at 7,500 g for 10 minutes in a microcentrifuge at 4 °C to obtain plasma. The upper layer plasma was then transferred to a fresh tube and snap frozen in liquid nitrogen for storage at - 80 °C prior to further analysis.

2.1.2.5 Liver perfusion via the portal vein

Animals were continuously anesthetized with isoflurane using precision vaporizer: induction with 5% isoflurane (0.5 - 1 L/min) and then switched to a nose cone at 2-3% isoflurane with a constant oxygen flow (1.5 L/min). Respiration was monitored

by visualizing the movement of the chest wall and adequate anesthetic depth was assessed via a toe pinch. Once deep anesthesia was confirmed, laparotomy was performed, and the portal vein was exposed. A perfusion needle was then introduced into the portal vein and secured using a tissue-specific glue (3M tissue adhesive). Perfusion solutions containing either 66.7 nM glucagon, 13.2 mM sodium succinate, or both were perfused directly to the liver at the rate of 30 μ l/min via a syringe perfusion pump (Scientific Instrument, NE-1002X) for 5 minutes. Based on an estimated portal blood flow rate of 2 ml/min [32], the final concentrations of glucagon and sodium succinate in the portal vein are expected to be 1 nM and 200 μ M respectively after dilution by the portal blood flow. These doses of glucagon and sodium succinate are approximately 2- to 4-fold higher than their physiological concentrations in the portal blood, thus providing reasonable stimulation to investigate signaling. After perfusion, liver tissue was quickly excised and rinsed in ice-cold PBS before transferring to a fresh Eppendorf tube and snap frozen in liquid nitrogen for future analysis.

2.1.2.6 Liver *in situ* digestion

Liver *in situ* digestion is a two-step liver perfusion procedure where preparation and portal cannulation is performed as described in 2.1.2.5. First, following portal cannulation, animals were perfused with 20 mL liver perfusion buffer (Invitrogen, 17701-038) that was pre-heated to 42 °C at a rate of 1.6 mL/min. Immediately after starting the

perfusion, a sharp cut is made on the inferior vena cava to allow perfused fluid to flow out of the mice to avoid vascular overload. Next, 20 mL pre-heated liver digestion buffer (Invitrogen, 17701-034) was perfused via the portal vein at 1.6 mL/min. Once the 20 mL liver digestion buffer was completely finished (approximately 13 minutes), liver was carefully excised and used for the separation of parenchymal and non-parenchymal cells for further analysis. The procedure of enriching parenchymal versus non-parenchymal cells will be detailed in 2.2.1.3.

2.2 Molecular biology techniques and procedures

2.2.1 Primary tissue/cell isolation procedures and *in vitro* culturing techniques

2.2.1.1 Cell-line culturing

The HEK-293T cell line that continuously expresses Noggin (HEK293-mNoggin-Fc) was a kind gift from our collaborator Dr. Jatin Roper, MD at Duke University [33]. The constitutively R-spondin-1 expressing 293T cell line (HA-R-spondin1-Fc) was purchased from ATCC (Trevigen, 3710-001-01). Both cell lines were used to generate conditional media for intestinal organoid culturing. Cells were first grown in growth medium which consists of DMEM and 10% FBS (Sigma, D0819 and F0926 respectively). Cells were grown to confluency and then were then split at a ratio of 1:5 and then cultured in selection media which is growth medium supplemented with antibiotics: 500 µg/mL Geneticine (Thermo

Fisher, 10131035) for HEK293-mNoggin-Fc cells, and 300 µg/mL Zeocin (Thermo Fisher, R25001) for HA-R-spondin1-Fc cells. Once these cells passed selection and became confluent, cells were further split at a ratio of 1:5 and cultured with growth media. At 80% confluency, growth media was replaced with expression medium which consists of advanced DMEM/F12 and 1% GlutaMAX (Thermo Fisher, 12634010 and 35050061 respectively) without FBS. Cells were incubated in the expression medium for 7-14 days without medium replacement. After 7-14 days, the conditioned media containing Noggin and R-spondin-1 was harvested and centrifuged at 1,500 g at 4 °C. Media supernatants were harvested and filtered through a 0.22 µm strainer before freezing at –80 °C for future usage.

2.2.1.2 3D Intestinal organoids culturing

Intestinal crypts were isolated from 8-week old mice and used to grow enterocyte-enriched intestinal organoids as previously reported using ENR-growth media [33]. The ENR-growth media is based on advanced DMEM/F12 (Thermo Fisher, 12634010) and supplemented with 50 ng/mL murine EGF (Peprotech, 315-09), 1 µM N-acetylcysteine (MP Bio, 194603), 100 nM GSK269962 (Tocris, 4009), 2% B27 (ThermoFisher, 12587010), 2% Noggin conditioned media, and 2% R-spondin-1 conditioned media [34]. The Noggin and R-spondin-1 conditioned media was harvested from confluent 293T cells as described in 2.2.1.1.

Briefly, small intestines were removed, incised longitudinally, and cut into 0.5- to 1-cm fragments before being washed 3 times with ice-cold PBS (ThermoFisher, 10010049). Washed intestinal fragments were then incubated in ice-cold PBS containing 10 mM EDTA (ThermoFisher, AM9260G) for 30 minutes on a rocker at 4 °C. Tissues were removed from solutions contacting EDTA and placed in ice-cold PBS, then mechanically shaken by hand for 30 seconds in PBS. Crypts were enriched by filtering through a 70- μ m cell strainer (VWR, 431751) to remove the villi. Enriched crypts were resuspended in ENR-growth media after centrifugation at 300 g for 5 minutes. After manually counting, crypts were further diluted and embedded in Matrigel (3:1, Corning, 356231) and seeded on 12-well plates at a density of approximately 900 crypts per well and incubated with ENR-growth media. After 5 days of proliferation and differentiation, intestinal organoids were treated with either 10 mM glucose or 10 mM U-C13-fructose overnight (5 PM to 9AM) at 37 °C. Immediately after incubation with glucose or fructose, media was harvested for measurement of succinate labeling using GC/MS as detailed in 2.2.2.3.

2.2.1.3 Culturing of fresh fecal and cecal contents

Fecal and cecal contents were freshly harvested from the anus and cecum respectively of 8-week old male mice. To obtain feces, mice are carefully scuffed by the neck and their abdomens are massaged until a fresh piece of feces was defecated. The freshly defecated feces were placed into a 2 mL Eppendorf centrifuge tube at room

temperature for future experiment. After harvesting fresh feces, animals were euthanized by decapitation. The cecum was exposed by laparotomy and the distal end of the cecum was incised. Tweezers were used to push cecal contents out of cecum into fresh tubes. The freshly isolated cecal/fecal contents were next incubated with or without 10 mM U-C13 fructose in 0.05% cysteine supplemented PBS for 30 minutes at 37 °C in a temperature-controlled incubator with regular air. Immediately after incubation, culture media was sampled and prepared for analysis by GC/MS as detailed in 2.2.2.3.

2.2.1.4 Primary hepatic parenchymal and non-parenchymal cell isolation

After digestion of livers *in situ* as detailed in 2.1.2.6, the liver tissue was carefully excised from the mice and immediately submerged in Leibovitz's L-15 medium (ThermoFisher, 11415064) supplemented with 20% FBS and GlutaMAX on ice. The liver was gently shaken to dissociate and release as many cells as possible. The Leibovitz's L-15 medium containing cells was filtered through a 70- μ m cell strainer to remove undigested cell clusters and debris. Multiple rounds of centrifugation and filtration were further conducted to enrich for hepatic parenchymal and non-parenchymal cells respectively. Briefly, cell suspensions were centrifuged at low speed (50 g for 3 minutes at 4 °C) three times. Parenchymal cells were found within the pellet whereas the supernatant from each round of centrifugation were pooled and filtered through a 40- μ m cell strainer for non-parenchymal cell enrichment. For parenchymal cell enrichment, the cellular pellet

was resuspended in 6 mL ice-cold DMEM plus 2mL Percoll® beads (Sigma, P1644) before centrifuge at 60 g for 3 minutes at 4 °C. The pellet was further washed for 3 times with Hepatocyte Wash Buffer (Invitrogen, 17704024) before resuspension in 5 mL of DMEM medium supplemented with 10% FBS and GlutaMAX. On the other hand, non-parenchymal cells contained in the pooled filtered supernatant was pelleted by centrifuge at 160 g for 10 minutes at 4 °C and then resuspended with 35 mL DMEM medium supplemented with 10% FBS and GlutaMAX, this cellular suspension was centrifuge again at 25 g for 3 minutes at 4 °C. After aspiration of the supernatant, the cells were again centrifuged at 160 g for 10 minutes. The resulting cell pellet enriched for non-parenchymal cells was resuspended in 5 mL of DMEM medium supplemented with 10% FBS and GlutaMAX. Both the parenchymal cell fragments and non-parenchymal cell fragments were observed under the microscope after staining with Trypan Blue (ThermoFisher, 15250061). After confirming enrichment for cells under microscope, cell fragments were pelleted at 160 g for 5 minutes and kept in 1 mL TRI reagent for RNA isolation which will be described in detail in 2.2.2.3.

2.2.2 Molecular biology techniques

2.2.2.1 Genomic DNA extraction and genotyping

Genomic DNA was isolated from the tail of animals using tail digestion buffer that contains 670 mM Tris-HCl (PH=8.8), 166 mM ammonium sulfate, 65 mM magnesium chloride, 1% beta-mercaptoethanol, and 0.5% Triton X-100. After preheated for 5 minutes at 95 °C, proteinase K was added to the tail digestion buffer at the final concentration of 2 mg/mL. The tail and digestion buffer were incubated overnight at 55 °C. After incubation at 95 °C for 10 minutes to deactivate proteinase K, the tail and digestion buffer were centrifuged at 12,000 g for 2 minutes. 1 µL of supernatant was used for the genotyping PCR. PCR for genotyping was conducting using MyTaq Red Mix (Meridian bioscience, BIO-25043) with primers targeting both the floxed allele, and Cre transgene (Table 1).

Table 1: Primers for genotyping

Gene Name	Forward primer sequence (5' – 3')	Reverse primer sequence (5' – 3')
Sucnr1_flox	GTCAGGAAAAGTCGCCCATGA	CTCTCTGTCCATGCACTGGG
Cre	GCCTGCATTACCGGTTCGATGCAACGA	GTGGCAGATGGCGCGGCAACACCA

2.2.2.2 Protein extraction, quantification, and immunoblots

For immunoblotting, 20 to 30 mg tissue samples (intestine and/or liver) were homogenized in 0.5 mL cell signaling lysis buffer that contains 20 mM Tris-HCl, 150 mM NaCl, 1 mM Na₂EDTA, 1 mM EGTA, 1% Triton and further supplemented with protease inhibitors (Sigma-Aldrich, P8340) and phosphatase inhibitor cocktail (Pierce, A32957).

After centrifugation at 12,000 g for 15 minutes, the supernatant was transferred to a fresh tube to measure protein concentration using the BCA method (ThermoFisher, 23225). Approximately 35 ug of protein was loaded per lane for SDS-PAGE electrophoresis. After electrophoresis, immunoproteins were transferred to PVDF membranes. The membranes were then incubated with primary antibodies overnight at 4 °C with gentle rocking after blocking with 5% solution of BSA (Cytivia, SH30574.02) at room temperature for 1 hour. Primary antibodies used in this work are listed as following: anti-phospho-PKA substrate (Cell Signaling 9624), anti-PDHA1 (phospho S293) antibody (Abcam, ab92696), Pyruvate Dehydrogenase (Cell Signaling, 3205), anti-AMPK (Cell Signaling, 5831S), anti-AMPK (phospho T172) antibody (Cell Signaling, 2635S), anti-KHK (Abcam, 15405), anti-AldoB (Thermo Fisher, 18065-1-AP), anti-P85 (Upstate, 06-496). Blots were incubated with appropriate secondary antibody after washing with TBST for 3 times. Chemiluminescence was conducted using the Clarity Western ECL substrate kit (Bio-Rad, 1705061) and membranes were imaged on ChemiDoc XP (Bio-Rad). Quantification of blots was conducted using ChemiDoc XP associated Image Lab software v6.0. For loading normalization, whole lane proteins were quantified using Bio-Rad Stain free technology.

2.2.2.3 Immunoprecipitation

Protein samples were extracted from liver tissues and protein concentrations were measured as described in 2.2.2.2. 25 µL Dynabeads Protein A (Thermo Fisher,

10001D) were transferred to a clean tube. After removing the supernatant by applying magnetic field to concentrate and hold the beads, the Dynabeads were then mixed with 2 μg anti-phospho-PKA substrate antibody (Cell Signaling 9624) in 500 μL PBS with Tween[®]-20. The mixture was gently rotated and incubated at room temperature for 10 minutes. The magnetic field was applied, and the supernatant was removed. Bead-antibody complexes were washed twice with 200 μL PBS with Tween[®]-20 to remove excessive antibody. Then the bead-antibody complexes were further washed twice with 200 μL BS3 Conjugation Buffer (20 mM Sodium Phosphate, 0.15M NaCl (pH=8)). The beads were then incubated in 250 μL BS3 solution at room temperature for 30 minutes with rotation. The cross-linking reaction was quenched by adding 12.5 μL 1M Tris-HCl (pH 7.5) buffer and incubation with rotation for 15 minutes at room temperature. Crosslinked bead-antibody complexes were then washed three times with 200 μL PBS with Tween[®]-20. 400 μg total protein in 500 μL lysis buffer was added to the crosslinked bead-antibody complexes and incubated with rotation at 4 $^{\circ}\text{C}$ for 2 hours. The magnetic field was then applied to the system and the supernatant was removed. The bead-antibody-antigen complexes were washed three times with 500 μL PBS with Tween[®]-20 for 3 times with gentle vortexing. To elute the bead-antibody-antigen complexes, 20 μL 50 mM Glycine Buffer (PH=2.8) plus 10 μL premixed NuPAGE[®] LDS Sample Buffer (Thermo Fisher, NP0008) and NuPAGE[®] Sample Reducing Agent (Thermo Fisher, NP0009) was added to the system and heated at 70 $^{\circ}\text{C}$ for 10 minutes.

After incubation, magnetic fields were applied to the samples to remove the beads. 25 μ L supernatant was then loaded on 4–12% Criterion™ XT Bis-Tris Protein Gel (BioRad, 3450123) for electrophoresis.

2.2.2.4 In-gel digestion and sample preparation for protein discovery

After electrophoresis, the gel was stained with Colloidal Blue (Thermo Fisher, LC6025) for 3 hours at room temperature with constant agitation, and extensively washed with ddH₂O for 7 hours. Bands between 25 to 37 KD and the band between 75 to 90 KD were carefully excised with a new razor blade for each band per sample. The excised gel fragments were chopped into approximately 2 mm cubes and placed into new 1.5 ml Eppendorf tubes. Gel pieces were incubated with 75 μ L 100mM ammonium bicarbonate: acetonitrile (1:1) for 15 minutes at room temperature. After removing the supernatant, 75 μ L 100% acetonitrile was used to dehydrate gel pieces for 30 seconds. Gel pieces were then incubated with 75 μ L 10 mM dithiothreitol (DTT) in 50 mM ammonium bicarbonate at 56 °C for 1 hour to rehydrate. After briefly centrifuge, DTT solution is removed and the gel was incubated with 75 μ L 55 mM iodoacetamide in 50 mM NH₄HCO₃ in dark room for 30 minutes. After removing the iodoacetamide solution post a brief centrifuge, gels were washed with 75 μ L 100mM ammonium bicarbonate: acetonitrile (1:1) twice and dehydrated with 100% acetonitrile. The gel fragments were then incubated with digestion buffer (50 mM NH₄HCO₃, 5 mM CaCl₂,

5 ng/ μ L trypsin) for 15 minutes on ice. After brief centrifuge, the digestion buffer was replaced with 70 μ L solutions with 50 mM NH_4HCO_3 , 5 mM CaCl_2 and incubated at 37 $^\circ\text{C}$ overnight in a warm-air incubator. The supernatant that containing digested peptides was harvested and transferred to a new tube and dried by speed vacuum. The peptides were then desalted using the C18 Millipore Ziptips (Sigma, Z720070). Specifically, the dried peptide samples were reconstituted with 13 μ L reconstitution buffer (5% Acetonitrile, 0.1% Trifluoroacetic acid in H_2O , $\text{PH}<3$). 10 μ L reconstituted samples were loaded to the equilibrated ziptips and triturated for 10 times. After washing the ziptips with wash solution (0.1% Trifluoroacetic acid in H_2O , $\text{PH}<3$) for 5 times, samples were eluted with 1.7 μ L elution buffer (50% Acetonitrile, 0.1% Trifluoroacetic acid in H_2O , $\text{PH}<3$). The eluted samples were dried by speed vacuum to remove the Acetonitrile and ready to load on the LC-MS machine for protein/peptide discovery.

2.2.2.5 RNA isolation, cDNA generation, and real-time qPCR

Tissue samples (intestine and/or liver) were carefully weighed (15 to 20 mg) and homogenized in 1 mL TRI reagent (Sigma, T9424) for RNA isolation. 100 μ L 1-bromo-3-chloropropane (BCP) was added to every 1 mL suspension at room temperature. After centrifugation at 12,000 g for 15 minutes post incubating at room temperature for 10 minutes, 400 μ L of upper aqueous phase was transferred to a fresh tube containing 400 μ L ice-cold isopropanol. After vigorous vortex, the RNA containing suspension was

centrifuged at 12,000 g, 4 °C for 20 minutes. The barely visible pellets were air-dried after carefully washed with 1 mL ice-cold 75% ethanol twice. 20 to 50 µL nucleotide-free water was added to the dried pellets to resolve RNA with constant vigorous vortex. The purity and quantity of RNA were measured by spectrophotometric measurement. The RNA integrity was assessed by agarose electrophoresis. RNA samples with the OD_{260/280} higher than 1.8 and rRNA 28S/18S approximately to 2 were acceptable for further cDNA generation or RNA sequencing.

To synthesize cDNA, 100 ng RNA was reverse transcribed using a SuperScript VILO kit (Invitrogen) according to the manuscript. Synthesized cDNA was used for Gene expression analysis with the ABI Prism sequence detection system (SYBR Green; Applied Biosystems). Gene-specific primers were synthesized by Thermo-Fisher (Table 2). Each sample was run in duplicate and normalized to 36B4 (liver tissues) or TBP (intestine tissues).

Table 2: Primers for qPCR

Gene Name	Forward primer sequence (5' – 3')	Reverse primer sequence (5' – 3')
Sucnr1	CAGCTCCTGGCAGAGTTTTTC	CCTCTGTTGCCAACCAATTCTC
Alb	CCACTAGCCTCTGGCAAAAT	GCCTTGAAATGTTGTTCTCC
Tbg	ATGGGTAGAAGCAGCCATGT	CCAAGGTCATATGTGGCAGA
Acta2	CGCCATGTATGTGGCTATTC	CCTCATAGATAGGCACGTTGTG
CD36	CCTGCAAATGTCAGAGGAAA	GCGACATGATTAATGGCACA
CD68	GCTTATAGCCCAAGGAACAGAG	CTGTAGGTGTCATCGTGAAGGA
Cre	GCGGTCTGGCAGTAAAAACTATC	GTGAAACAGCATTGCTGTCACTT
36B4	AGATTCGGGATATGCTGTTGGC	TCGGGTCCTAGACCAGTGTTTC
Glut2	GGAACCTTGGCTTTCACCTGT	TGTAAGTGGGGTGTCTGTGC
Glut5	GAGCCCCTCGTAGGTTTTTC	TCCAGACTTCTGGTTGGAATC
Chrebp- α	GAGCCCCTCGTAGGTTTTTC	TCCAGACTTCTGGTTGGAATC
Chrebp- β	TCTGCAGATCGCGTGGAG	CTTGTCCCGGCATAGCAAC
Khk	GGACAGTGCAGGAGTTGGAT	GGACATCATCAATGTGGTGG
AldoB	GCTGGCAATTTTCAGAGAGC	GAGGACTCTTCCCCTTIGCT
G6pc	GTGTCCAGGACCCACCAATA	ACTGTGGGCATCAATCTCCT
PCK1	TCTGGATGGTTTTAATGGCA	TGCCTGGATGAAGTTGATG
Tbp	CCCTATCACTCCTGCCACAC	ACGAAGTGCAATGGTCTTTAGG

2.2.3 Metabolomic techniques

2.2.3.1 Plasma sample preparation for mass spectrometry

Plasma was prepared from collected blood by centrifugation at 2,000 g, 4°C for 15 minutes. 0.1 mmol norvaline or 0.2 mM 2-Deoxy-D-glucose (2DG) was added to 10 µL plasma samples as an internal standard for the relative quantification of TCA cycle intermediates or fructose and glucose respectively. 0.5 nmol D4-succinate was added to 10 µL plasma samples as an internal standard for the absolute quantification of succinate. To 10 µL plasma samples, 400 µL MeOH, 400 µL ddH₂O, and 400 µL chloroform were added sequentially and briefly vortexed after each addition. After centrifugation at 12,000 g for 15 minutes, supernatants were collected and dried under nitrogen gas.

2.2.3.2 Culture media sample preparation for mass spectrometry

Culture media samples from intestinal organoids and cecal/fecal contents following fructose treatment were obtained and centrifuged at 12,000 g to remove cell debris. 0.5 mmol norvaline was added to 100 µL media samples as an internal standard for the analysis of TCA cycle intermediates. 400 µL MeOH, 400 µL ddH₂O, and 400 µL chloroform were added sequentially to the samples and briefly vortexed after each addition. After centrifugation at 12,000 g for 15 minutes, supernatants were collected and dried under nitrogen gas.

2.2.3.3 Tissue and food sample preparation for mass spectrometry

Tissue samples and food samples were powdered under liquid N₂. 400 µL ice-cold 1:1 MeOH and ddH₂O were added to 10 mg powdered samples. 0.1 mmol norvaline and 0.5 mmol 2FDG6P were added in methanol as an internal standard for enrichment analysis of TCA cycle intermediates and G6P respectively. 10 nmol D₄-succinate was added in methanol as an internal standard for succinate quantification in food. These samples were homogenized (TissueLyser) for 2 minutes at 30 H and centrifuged at 12,000 g, 4°C for 20 minutes. 50 µL supernatants were combined with another 350 µL ice-cold 1:1 MeOH and ddH₂O prior to adding 400 µL chloroform per sample and vortexed for 30 seconds. Samples were centrifuged at 12,000 g for 15 minutes and supernatants were collected and dried completely under nitrogen gas.

2.2.3.4 Relative quantification and enrichment measurements of TCA cycle intermediates by gas chromatography-mass spectrometry (GC/MS)

Dried residues were derivatized with methoxylamine hydrochloride and tertbutyldimethylchloros (TBDMS) sequentially as previously described [3]. Specifically, 25 µL of methoxylamine hydrochloride (2% (w/v) in pyridine) was added to the dried residues and incubated for 90 minutes at 40°C before the addition of 35 µL of TBDMS and incubation for 30 minutes at 60°C. The samples were then centrifuged for 2 minutes at 12,000 g and the supernatants of derivatized samples were transferred to GC vials for further analysis. GC/MS analysis was conducted as previously described using an Agilent

7890B GC system and Agilent 5977A Mass Spectrometer [3]. Specifically, 1 μL of the derivatized sample was injected into the GC column. GC temperature gradient started at 80°C for 2 minutes, increased to 280°C at the speed of 7°C per minute, and held at 280°C for until the completion of a run time of 40 minutes. Ionization was conducted by electron impact (EI) at 70 eV with Helium flow at 1 mL/min. Temperatures of the source, the MS quadropole, the interface, and the inlet were maintained at 230°C, 150°C, 280°C, and 250°C respectively. Mass spectra were recorded in mass scan mode from m/z 50 to 700.

2.2.3.5 Absolute quantification of succinate and quantification of G6P by GC/MS

Dried sample residues were derivatized with methoxylamine hydrochloride and trimethylsilyl (TMS) sequentially. Specifically, 25 μL of methoxylamine hydrochloride (2% (w/v) in pyridine) was added to the dried residues and incubated for 90 minutes at 40°C before the addition of 35 μL of TMS and incubation for 30 minutes at 60°C. The samples were then centrifuged for 2 minutes at 12,000 g and the supernatants of derivatized samples were transferred to GC vials for further analysis. GC/MS analysis was conducted using Agilent 7890B GC system and Agilent 5977A Mass Spectrometer. To be specific, 1 μL of the derivatized sample was injected into the GC column. GC temperature gradient start at 80°C for 2 minutes, increased to 280°C at the speed of 7°C per minute, and held at 280°C for until the completion of a run time of 40 minutes. Ionization was conducted EI at 70 eV with Helium flow at 1 mL/min. Temperatures of the source, the MS

quadrupole, the interface, and the inlet were maintained at 230°C, 150°C, 280°C, and 250°C respectively. Mass spectra were recorded in mass scan mode from m/z 50 to 700.

2.2.3.6 Relative quantification and enrichment measurements of fructose and glucose by GC/MS

The dried residues were derivatized with methoxylamine hydrochloride and propionic anhydride sequentially adapted from a previously described method [35]. 25 μ L of methoxylamine hydrochloride (2% (w/v) in pyridine) was added to the dried residues and incubated for 60 minutes at 70°C. After centrifugation for 2 minutes at 12,000 g, 50 μ L propionic anhydride was added and incubated for 30 minutes at 60°C prior to another round of drying under nitrogen. The dried residues were resuspended with 55 μ L pure ethyl acetate and transferred to GC vials for analysis. GC/MS analysis was conducted using the Agilent 7890B GC system and Agilent 5977A Mass Spectrometer. Specifically, 1 μ L of the derivatized sample was injected into the GC column. GC temperature gradient started at 90°C, increased to 260°C at the speed of 9°C per minute and further increased to 290 °C at the speed of 30°C per minute. Then temperature was held at 290°C for 5 minutes with a run time of 24.9 minutes. Ionization was conducted by EI at 70 eV with Helium flow at 1 mL/min. Temperatures of the source, the MS quad, the interface, and the inlet were maintained at 230°C, 150°C, 280°C, and 250°C, respectively. Mass spectra were recorded from m/z 50 to 700 in mass scan mode.

2.2.3.7 Absolute quantification of butyrate by liquid chromatography with tandem mass spectrometry (LC-MS/MS)

Plasma samples were prepared the same way as described above. A modified LC-MS/MS method was developed to analyze the absolute quantity of butyrate as previously reported [36]. Specifically, 30 μ l plasma samples were mixed with 30 μ l 20 μ M 2,2,3,3,4,4,4-²H₇-butyrate (D₇-butyrate, internal standard) before adding to 1 ml acetonitrile to remove protein by precipitation. After centrifuge for 20 minutes at 1,200 g, supernatant was collected and transferred to a new Eppendorf tube, then dried completely by nitrogen gas. The dried residue was resuspended in a mixture solution consists of 50 μ l HPLC water, 20 μ l 3-Nitrophenylhydrazine hydrochloride (EDC, 120 mM), and 20 μ l (N-(3-Dimethylaminopropyl)-N'-ethylcarbodiimide (3-NPH, 200 mM) for derivatization at 40 °C for 30 minutes. After centrifuge for 10 minutes at 1,200 g in room temperature, supernatant was transferred to an LC-MS/MS vial for butyrate analysis. LC-MS/MS was conducted using a Sciex QTRAP 6500+ MS connected with a Sciex AD UHPLC. Specifically, an Agilent C18 column (Pursuit XRs C18 150 \times 2.0 mm, 5 μ m) was employed to generate a flow rate at 0.4 ml/min for separation. Gradient methods were conducted within two mobile phases. Mobile phase A was composed of 98% H₂O and 2% acetonitrile with 0.1% formic acid. On the other hand, mobile phase B was consisting of 98% acetonitrile and 2% H₂O containing 0.1% formic acid. At first, gradient started with 98% phase A and 2% phase B for 30 seconds. After 7.5 minutes, phase B was increased to 90% while phase A was decreased to 10% at 8 minutes. After maintaining at 90% phase B and

10% phase A for another 4.5 minutes, phase B was returned to initial 2% within 0.5 minutes. Finally, the column was re-equilibrated for 9 minutes with 98% phase A and 2% phase B before the next injection. The injection volume was 3 μ l. MRM in negative mode was used for butyrate assay. The MS/MS parameters were set as following: curtain gas: 35 psi, source temperature: 600 °C, Gas 1: 55 psi, Gas 2: 55 psi, CAD: 10, Ion spray voltage: -4500 V, EP: -10 V, and CXP: -14.

2.2.3.8 Stable Isotope Analysis

Isotopologues that containing 0, 1, to n heavy atom(s) in a molecule were referred as M+0, M+1, to M+n respectively. The retention times (RT) of individual metabolites and their isotopomers are described in Table 3. Isotope enrichment and labeling analysis in this study were corrected for natural isotope distribution as previously described [37, 38]. Specifically, the stable isotope enrichment of each metabolite in plasma, tissue, organoids, and fecal/cecal content was corrected based on the natural isotope distribution measured in the same type of samples treated without labeled substrates. For example, the natural isotope distribution matrix of individually measured metabolites in the blood samples were experimentally determined by assaying and averaging the blood samples from animals who had not received any treatments involving isotopically labeled substrates.

Table 3: metabolites detected by GC/MS

Metabolites and their isotopomers	m/z	RT (min)
M+0 Succinate (Relative quantification and enrichment -TBDMS method)	289.1	18.0
M+1 Succinate (Relative quantification and enrichment -TBDMS method)	290.1	18.0
M+2 Succinate (Relative quantification and enrichment -TBDMS method)	291.1	18.0
M+3 Succinate (Relative quantification and enrichment -TBDMS method)	292.1	18.0
M+4 Succinate (Relative quantification and enrichment -TBDMS method)	293.1	18.0
M+0 Succinate (Absolute quantification-TMS method)	247.0	10.8
M+4 Succinate (Absolute quantification-TMS method)	251.0	10.7
M+0 Fumarate	287.1	18.4
M+1 Fumarate	288.1	18.4
M+2 Fumarate	289.1	18.4
M+3 Fumarate	290.1	18.4
M+4 Fumarate	291.1	18.4
M+0 Malate	419.3	23.0
M+1 Malate	420.3	23.0
M+2 Malate	421.3	23.0
M+3 Malate	422.3	23.0
M+4 Malate	423.3	23.0
M+0 Citrate	459.3	29.0
M+1 Citrate	460.3	29.0
M+2 Citrate	461.3	29.0
M+3 Citrate	462.3	29.0
M+4 Citrate	463.3	29.0
M+5 Citrate	464.3	29.0
M+6 Citrate	465.3	29.0
Norvaline	288.2	16.6
M+0 Fructose	328.0	19.8
M+1 Fructose	329.0	19.8
M+2 Fructose	330.0	19.8
M+3 Fructose	331.0	19.8
M+4 Fructose	332.0	19.8
M+5 Fructose	333.0	19.8
M+6 Fructose	334.0	19.8
2DG	182.1	17.1
2FDG6P	357.0	25.0
M+0 Glucose	416.0	18.7
M+1 Glucose	417.0	18.7
M+2 Glucose	418.0	18.7
M+3 Glucose	419.0	18.7
M+4/6 Glucose	420.0	18.7
M+0 G6P	471.0	26.1
M+3 G6P	474.0	26.1

2.2.4 Transcriptome techniques

2.2.4.1 RNA-sequencing and data processing

RNA samples used for RNA-sequencing were prepared as detailed in 2.2.2.3. After confirming the purity and integrity of the RNA samples, RNA library was prepared with all the RNA samples using the Illumina Stranded Total RNA Prep Kit (Illumina, 20040525) according to the manual. After that, samples are ready to sequence by Illumina NovaSeq 6000 using the S1-50 bp mode.

The original output base-calling files from Illumina sequencers were converted to FASTQ files for further analysis. After checking the quality of RNA-sequencing by the percentage of unmapped reads and percentage of adapter content using FASTQC program [39], the qualified raw FASTQ files were aligned to the mouse reference genome (Mus_musculus_GRCm39) using the STAR aligner [40]. FeatureCounts program from the Subread package was used to count reads based on the mouse transcriptome[41] . Pairwise comparisons of expression changes between the LiSucnr1KO and controls were conducted after normalization by the generalized log-linear model through the glm.fit function using the edgeR package [42]. Pathway analysis of the differentially expressed genes was conducted using the enrichR package [43]. R (4.1.2) and R studio (1.4.1717) were used for data analysis and visualization.

2.2.4.1 Public single-cell RNA-sequencing dataset access and data processing

Raw data from studies where single-cell RNA-sequencing was performed in mouse livers was downloaded from the public Gene Expression Omnibus (GEO) database GSE129516, and GSE84498 respectively [44, 45]. Similar to the analysis of RNA-seq data, the raw data were aligned to the mouse reference genome by STAR. After trimming low quality bases reads, Salmon was used to count and annotate the read counts and generate an expression matrix [46]. The library size normalization between samples was conducted using the CRAN program. t-Distributed Stochastic Neighbor embedding (t-SNE), a statistical dimensionality reduction technique, was used to visualize the single-cell RNA-sequencing data based on the similarity of gene expression in single cells [47]. The algorithm to determine liver cell types were adapted from the previous publication that established marker genes for each cell types [48]. R (4.1.2) and R studio (1.4.1717) were used for data analysis and visualization.

2.3 Statistics and data analysis

Guidance for statistical analyses was provided by Dr. Theodore Slotkin during the course PHARM 733: experimental design & statistics. Statistical analyses were conducted using R and GraphPad Prism 9. Data in this study were presented as mean \pm standard deviation. A p-value of ≤ 0.05 was considered significant. Outlier detection was conducted by a two-sided Grubb's test on datasets with $n > 6$. No more than one outlier

per group was removed. For studies comparing a single parameter between two groups, student's t-test was performed. For studies comparing more than one parameter between two groups, one-way ANOVA and Fisher's post hoc analysis was performed. Repeated measured ANOVA was conducted to compare parameter(s) that were measured over multiple time points. For studies with 4 conditions (genotype * location, genotype * diet, and genotype * cell type), a two-way ANOVA and Bonferroni correction was conducted, and a corrected p-value of ≤ 0.05 was considered significant. For RNA-seq data analysis, differentially expressed genes refers to genes that have a p-value of ≤ 0.05 from student's t-test between LiSucnr1-floxed and LiSucnr1KO. Additionally, significantly expressed genes from the RNA-seq analysis were adjusted by Benjamini-Hochberg procedure with a false discovery rate (FDR) of 2. For protein discovery using proteomics study, differentially expressed proteins/peptides refers to proteins/peptides that have a p-value of ≤ 0.05 from student's t-test between saline group and glucagon group. Additionally, significantly expressed differentially expressed proteins/peptides from the protein discovery analysis were adjusted by Benjamini-Hochberg procedure with a false discovery rate (FDR) of 2.

3. Intestinal tissue is a major contributor to circulating TCA cycle intermediates

3.1 Introduction

Animals rely on aerobic metabolism to produce chemical energy for energy intensive physiological functions like locomotion and mentation. Aerobic metabolism occurs in mitochondria where acetyl-CoA, the common two carbon metabolite derived from the catabolism of carbohydrates, proteins, or lipids, is oxidized to carbon dioxide and water producing ATP via the tricarboxylic acid cycle (TCA cycle or Krebs cycle). The TCA cycle is the epicenter of cellular aerobic metabolism and TCA cycle intermediates play essential roles in this process to facilitate cellular and organismal energy homeostasis.

While the role of TCA cycle intermediates in facilitating energy production is well defined, TCA cycle metabolites can serve other roles outside of the mitochondria. For example, TCA cycle metabolites including citrate and oxaloacetate can be exported from the mitochondria and used in synthesis of glucose and lipids [49]. Additionally, the TCA cycle metabolites succinate and alpha-ketoglutarate function as natural ligands for cell surface G-protein coupled receptors (GPCRs) indicating that TCA cycle derived metabolites may serve as metabolic signals [50]. Succinate signals through the succinate receptor 1 (Sucnr1), a GPCR that regulates pleiotropic biological activities including urine filtration [51], immune responses [52, 53], thermogenesis [54], and liver damage and fibrosis [12, 55]. This succinate-Sucnr1 signaling system suggests that circulating TCA

cycle intermediates have the potential to regulate interorgan communication in coordination of fuel and immune homeostasis.

Although TCA cycle intermediates are produced within the mitochondria of all cells, the major sources of circulating TCA cycle intermediates in physiological conditions are less clear. Some, but not all studies have suggested that the gut microbiota is a source of circulating TCA cycle intermediates [27, 56]. A small study in humans with obesity and type 2 diabetes observed that circulating succinate levels are positively associated with enrichment for specific succinate-generating microbial strains, suggesting that gut microbiota contribute to circulating succinate [27]. In contrast, colonization of mice with succinate producing bacterial species increased succinate levels in cecal matter, but did not increase portal succinate levels [56].

These results raise questions regarding the ability of the intestine to absorb intestinal and/or dietary succinate. This is of importance as chronic supplementation of succinate in the diet or drinking water impacts metabolic homeostasis in animal models, but no evidence has been provided that such supplementation studies impact circulating succinate [54, 56]. Thus, it remains unclear whether diet or microbiota are crucial contributors to circulating succinate levels.

In this section, with a focus on succinate as a representative circulating and signaling TCA cycle intermediate, we demonstrate that endogenous production within the gut is a major source of circulating TCA cycle intermediates and far exceeds the dietary

contribution in normal physiological circumstances. Furthermore, using both *in vivo* and *in vitro* models, we show that intestinal tissue, and not microbiota, are the predominant sources of gut-derived succinate. These results advance our knowledge of the source of circulating TCA cycle metabolites, interorgan metabolite communication, and will also provide guidance in investigating the physiological and/or pathophysiological functions of circulating TCA metabolites in health and disease.

3.2 Results

3.2.1 The gut contributes to circulating TCA cycle metabolites

The TCA cycle and its intermediates are essential for ATP production in mitochondria under aerobic conditions. As meal-derived nutrients are typically absorbed from the intestine and delivered to the liver prior to mixing with systemic circulation, we sampled blood from the portal vein and tail vein of mice to establish the baseline levels of the TCA cycle intermediates. We observed that relative levels of succinate, fumarate, and malate are 4- to 9-folds higher in the portal blood when compared to tail blood, specifically 3.8-fold for succinate, 8.5-fold for fumarate, 4.3-fold for malate (Figure 2A). Citrate levels were also higher in portal compared to tail blood, but only ~ 2-fold higher (Figure 2A). Conducting absolute quantification of succinate in the portal versus tail plasma using a labeled succinate internal standard confirmed the increase in portal blood demonstrating

a succinate level of $150.4 \pm 20.9 \mu\text{M}$ in portal blood compared to $51.9 \pm 17.2 \mu\text{M}$ in tail blood, a difference that is similar to what we observed in the relative quantification model ($P < 0.001$, Figure 2B). This marked portal-peripheral gradient indicates that circulating TCA cycle intermediates are gut-derived, and either absorbed from the intestinal lumen or generated from the intestinal tissue.

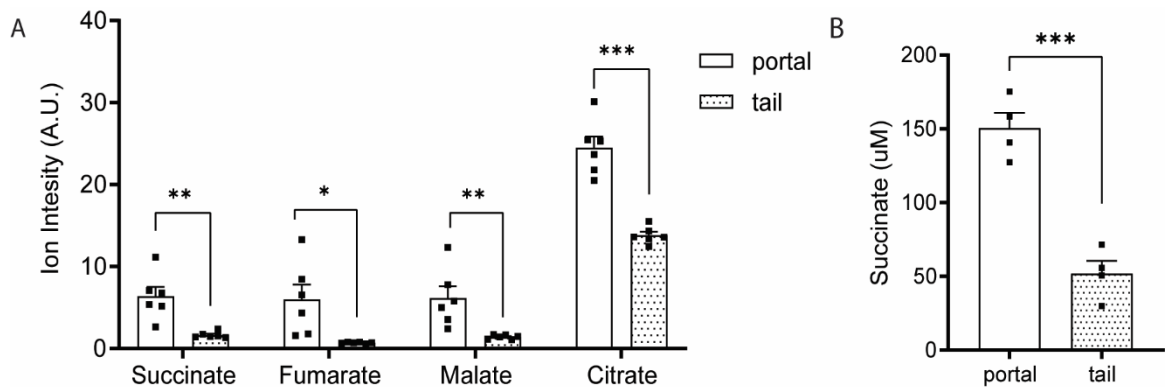


Figure 2: A consistent portal to tail gradient of TCA cycle intermediates

Relative quantification of TCA cycle metabolites (A) and absolute quantification of succinate (B) in the portal versus tail plasma samples from 8-weeks old wild-type C3H/HeJ males that have been fasted for 5 hours. * $p < 0.05$; ** $p < 0.01$; *** $p < 0.001$. Norvaline and D4-sodium succinate were used as internal standards for relative and absolute quantification by GC/MS. $n=6$ in experiments

To examine the contribution of gut carbohydrate metabolism to portal TCA cycle intermediates we orally gavaged mice with U-C13-fructose (0.48 g/kg) as fructose can be metabolized at high rates by both microbiota and enterocytes in the gut [57, 58]. The relative quantification and enrichment of TCA cycle intermediates in the portal blood were assessed by GC/MS at intervals for 2 hours following gavage. The rapid appearance of labeled carbons in portal TCA cycle intermediates supports the hypothesis that orally administered fructose can be readily metabolized into TCA cycle intermediates in gut (Figure 3A, C, E). While fructose-derived carbons were readily incorporated into portal TCA cycle intermediates, the quantity of the TCA cycle intermediates (succinate, malate, and citrate) in the portal vein remained relatively constant over this two-hour period (Figure 3B, D, F). The increase in isotope enrichment without changing in quantity suggests that TCA cycle intermediates are constitutively produced in the gut although the source of TCA cycle intermediates derived carbons varies based on available substrate.

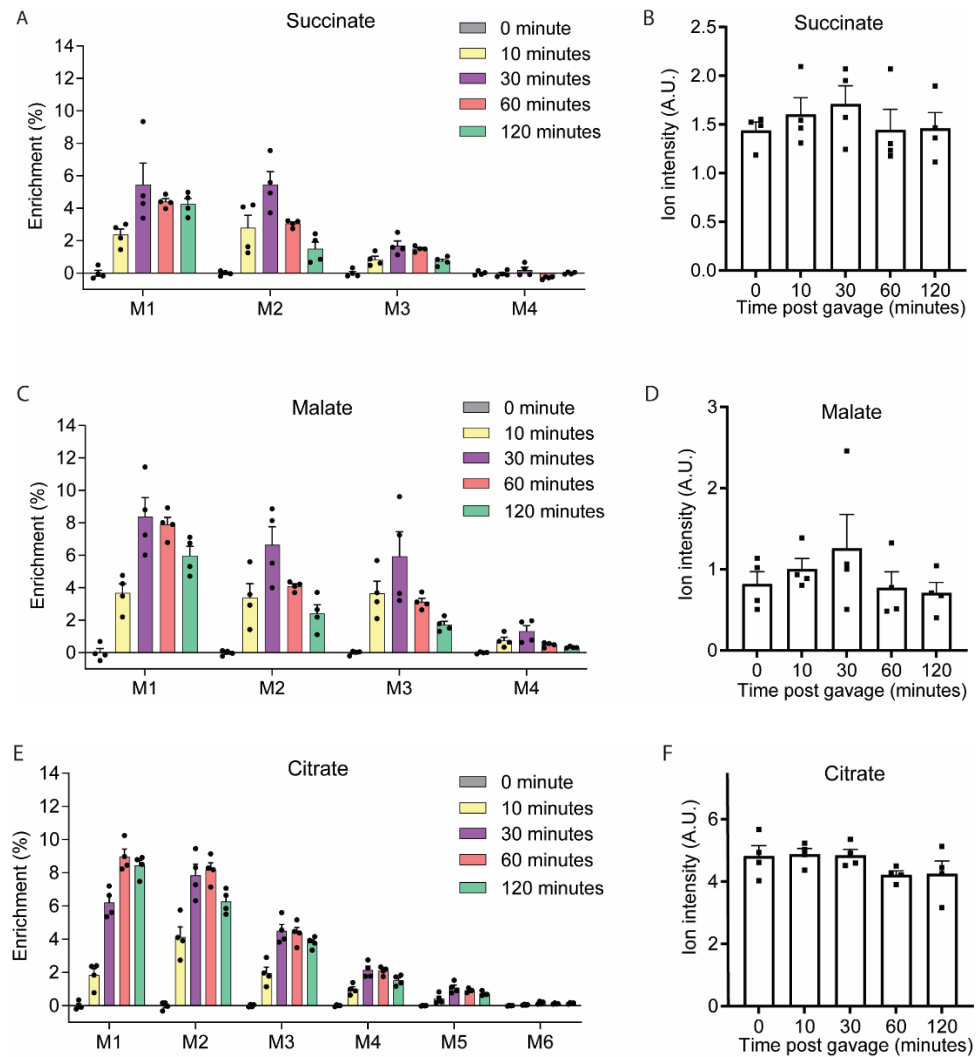


Figure 3: Providing isotope precursors to the gut increases isotope enrichment of TCA cycle intermediates without changing their quantities

Relative quantification of TCA cycle metabolites (A) and absolute quantification of succinate (B) in portal versus tail plasma samples from 8-weeks old, male mice after 5 hours food removal. Norvaline and D4-sodium succinate were used as internal standards for relative and absolute quantification measurement by GC/MS, respectively (n=6 per group). Enrichment (C, D, E) and relative quantification (F, G, H) of portal TCA cycle intermediates after oral-gavage in 8-weeks old male mice with U-C13-fructose (0.48 g/Kg body weight, n=4 per group). Data represent means \pm SEM. * p<0.05; ** p<0.01; *** p<0.001. Analysis in A and B performed via paired student t-test. Analysis in panel F - H performed via one-way ANOVA and Fisher's LSD for post-hoc analysis comparing to baseline (0 minutes).

3.2.2 Microbiota are not essential to maintain the portal levels of TCA cycle intermediates

TCA cycle intermediates found in portal blood appear to be constitutively produced in the gut. The cellular origin of these TCA cycle intermediates is uncertain as both the intestinal tissue and microbiota residing in the gut have the capacity to produce them. We measured TCA cycle intermediates levels in blood samples of conventionally reared mice to age- and strain-matched mice that were reared in a germ-free environment. Butyrate is a well-established circulating metabolite produced largely by microbiota [59]. As expected, portal butyrate levels are 143-fold higher in the portal blood of the conventional reared mice compared to the germ-free mice (Figure 4A). In contrast, TCA cycle intermediates levels in the portal blood of germ-free mice were similar to that of conventional reared animals (Figure 4B). Indeed, the portal malate levels are higher in the germ-free mice. Thus, intestinal microbiota are not a major source of circulating TCA cycle intermediates.

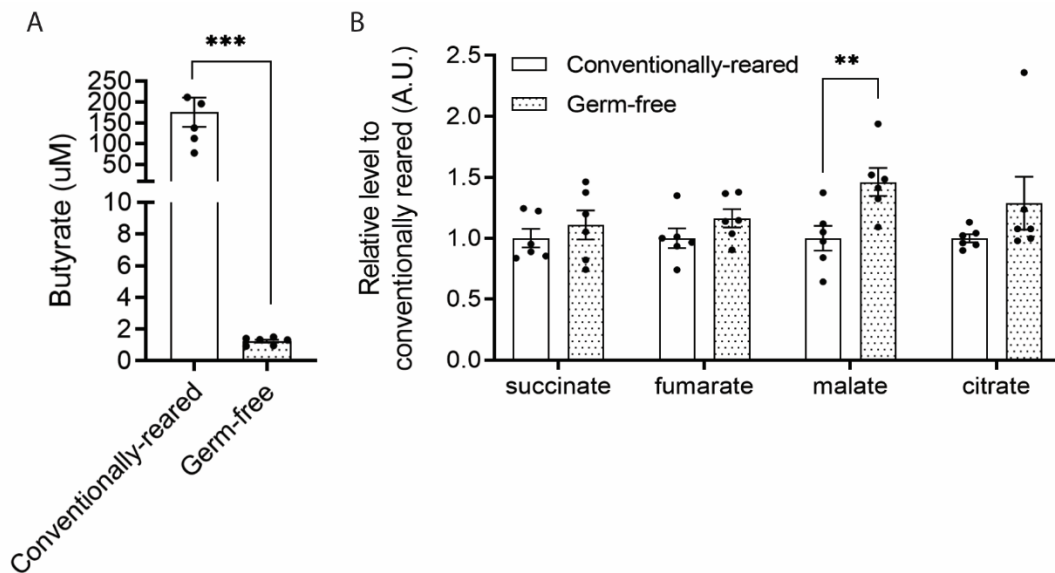


Figure 4: Microbiota are not essential to maintain the portal levels of TCA cycle intermediates

Absolute quantification of butyrate (A) and TCA cycle intermediates (B) in plasma samples from portal vein and inferior vena cava of 12-weeks old germ-free wild-type C57/BL6J males versus their conventionally bred littermates. Butyrate levels were measured by LC-MS/MS using D7-butyrate as internal standard. TCA cycle intermediates levels were measured by GC/MS using norvaline as internal standard. n=6 in each group. * indicate statistical significance ($p < 0.05$) of metabolite levels between conventional and germ-free mice

3.2.3 Labeled precursors produce distinct succinate labeling patterns when exposed to intestinal organoids versus microbiota

Although intestinal microbiota are not essential for intestinal succinate production, this does not exclude the possibility that microbiota can contribute to circulating TCA cycle intermediates in conventionally bred animals, and that other undefined mechanisms maintain portal TCA cycle intermediates levels. Given interest in succinate as a metabolic signal [60], we focused on succinate as a representative TCA cycle intermediate in the remainder of this study. Whereas eukaryotes generate succinate from carbohydrate precursors exclusively via the TCA cycle, microbiota could generate succinate from carbohydrate precursors via the glyoxylate shunt other from TCA cycle (Figure 5). Thus, the labeling pattern of succinate produced from C-13-labeled carbohydrate-derived three-carbon substrates are likely to be different when produced in mammalian cells versus microbiota [61]. Specifically, mammalian cells using predominantly the TCA cycle will generate M+2 succinate in the first turn of the cycle and M+1 succinate in the second turn of the cycle, leading to predominant enrichment in M+1 and M+2 succinate (Figure 5). In contrast, microbiota use a highly active PEP carboxykinase which converts PEP into oxaloacetate and then condenses acetyl-CoA and oxaloacetate via isocitrate lyase into isocitrate which is used to generate glyoxylate and succinate. The succinate generated in this pathway from C-13-labeled carbohydrate-derived three-carbon substrates will be enriched for M+3 and M+4 succinate (Figure 5).

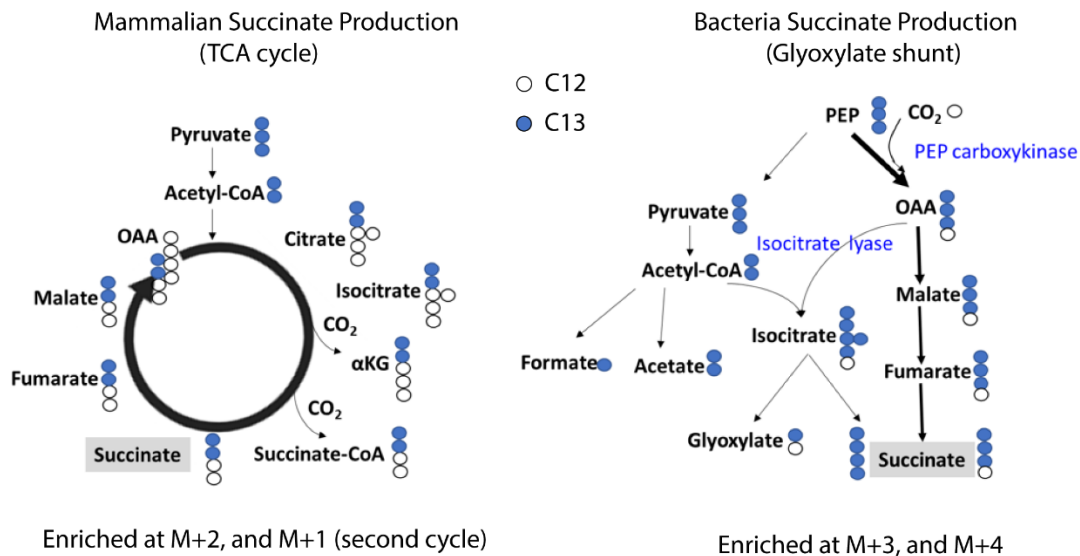


Figure 5: Succinate production from isotope tracers

Theoretical isotope-labeling patterns of succinate produced from C13-labeled three carbon substrates in mammalian cells versus bacteria.

We examined succinate enrichment within fecal/cecal contents *in vitro* and in cultured intestinal organoids after incubation with U-C13-fructose. As expected, isotope-labeled succinate was identified in both the intestinal organoids and fecal/cecal contents when cultured with U-C13-fructose. In the intestinal organoid experiment, the M+1 and M+2 succinate accounts for 83.7% of the labeled succinate (Figure 6 A), consistent with the hypothesis that mammalian cells predominantly use the TCA cycle to generate succinate from carbohydrate precursors. In contrast, fecal/cecal contents generated a much higher proportion of M+3 and M+4 labeled succinate, accounting for nearly 44.8% to 46.6% of the labeled succinate (Figure 6 B, C). These substantial differences demonstrate that the

contribution of microbiota versus mammalian tissue to succinate production can be distinguished based on labeling patterns following administration of labeled carbohydrate precursors.

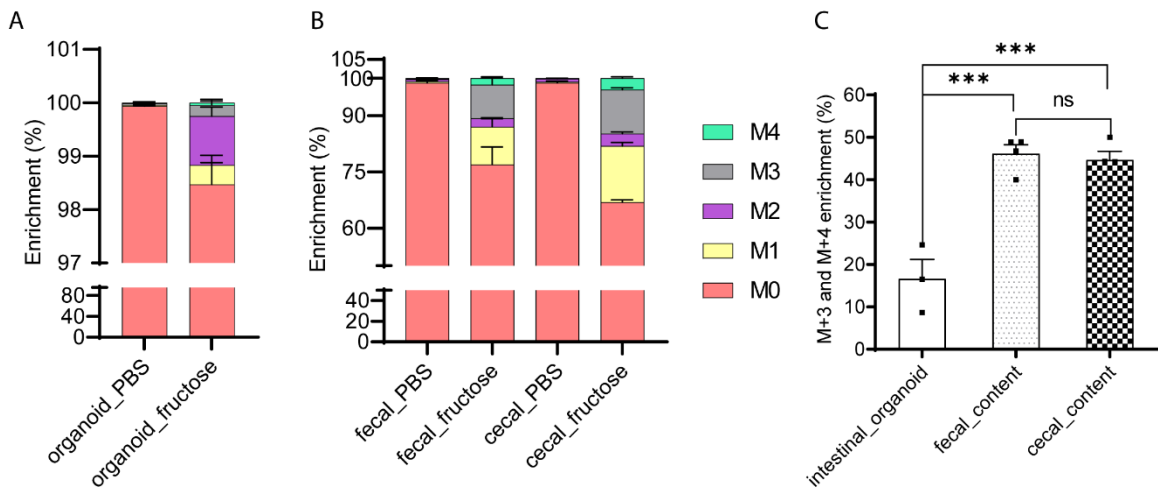


Figure 6: Intestinal organoids in contrast to cecal/fecal content generate distinct succinate labeling patterns from labeled precursors

Measured labeling pattern in (A) mammalian cells and (B) microbial enriched samples. Intestinal crypts and fresh cecal and fecal contents were harvested from 8-weeks-old male mice. Intestinal organoids were differentiated into enterocytes prior to treatment with 100 mM U-C13-fructose for 24 hours (n=3 per group). Freshly harvested cecal and fecal contents were cultured with 100 mM U-C13-fructose for 30 minutes (n=4 per group). (C) Quantification of the ratio of M+3 and M+4 succinate to total labeled succinate in cultured intestinal organoids and cecal/fecal contents described in (A) and (B). Data represent means \pm SEM. * p<0.05; ** p<0.01; *** p<0.001. Data were analyzed by one-way ANOVA and Fisher's LSD for post-hoc analysis between intestinal organoids, fecal contents, and cecal contents.

3.2.4 Portal succinate is produced from the intestinal tissue and not the microbiota

We next compared the succinate labeling pattern in portal blood, intestinal tissue, and cecal contents in mice after providing large amounts of labeled precursors in the form of U-C13-fructose. The fructose dose, 4 g/kg, is higher than the amount that mice can fully absorb in the small intestine, thus providing adequate labeling in both intestinal tissue and the bulk of intestinal bacteria present in the cecum and colon [57, 62]. Portal blood, intestinal tissue, and cecal contents were harvested from animals that are not gavaged or at either 10 minutes or 2 hours post gavage. The two time points were chosen based on the liquid transition speed in typical mice. Specifically, 10 minutes is sufficient for liquid transition to small intestine, but not cecum, whereas 2 hours is aimed at ensuring cecal fructose metabolism [57, 62]. The portal succinate labeling pattern and specifically the proportion of M+1 and M+2 labeled succinate consistent with production in the eukaryotic TCA cycle were similar in portal blood and intestinal tissue, and distinct from the pattern in the cecal contents at both time points (Figure 7 A-B). These data demonstrate that portal succinate is predominantly produced by intestinal tissue and not microbiota.

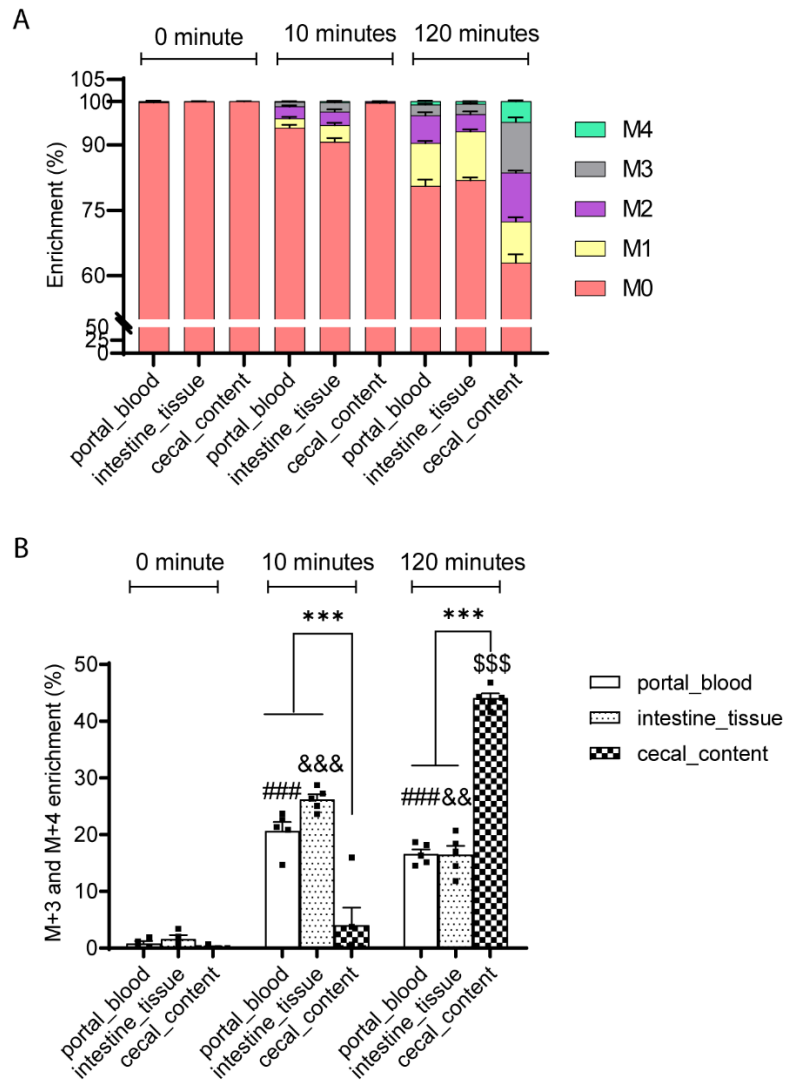


Figure 7: The succinate labeling pattern in portal plasma is similar to that in the intestinal tissue while distinct from that in the cecal contents following oral-gavage with U-C13-fructose

(A) The enrichment and (B) the ratio of M+3 plus M+4 to total labeled succinate in the portal plasma, intestinal tissue, and cecal contents after gavage of 8-weeks-old male mice with U-C13-fructose (4g/Kg body weight) (n=4 per group at each time point). Data represent means \pm SEM. * $p < 0.05$; ** $p < 0.01$; *** $p < 0.001$. Data were analyzed by two-way ANOVA and Tukey's test was applied for post hoc comparisons. # portal plasma comparisons across time points, & intestinal tissue comparisons across time points, \$ cecal content comparisons across time points, * comparisons between tissues within time points.

3.2.5 Need of generating a model to estimate the intestinal capacity for absorption of orally administered succinate

Prior studies have suggested that dietary succinate supplementation can regulate multiple systemic biological activities through the effects of absorbed succinate on the Sucnr1 receptor in diverse tissues [54, 63, 64]. However, there is limited data demonstrating that oral or dietary succinate supplementation increases circulating succinate levels. Our data indicates that succinate produced by microbiota in the large intestine is not readily absorbed, but this does not exclude the possibility that dietary succinate could be absorbed in the small intestine. Thus, we sought to examine the intestinal capacity for absorption of orally administered succinate and compare this to the rate of endogenous intestinal succinate production.

3.2.6 Generating a Relative quantification model for assessing endogenous production versus external absorption

The simplified relative quantification model used here is based on standard isotope dilution methodologies. Specifically, wildtype animals were given a bolus of 1:1 isotope-labeled and unlabeled metabolites by oral gavage. Animals were then sacrificed during a 2-hour time period with the following time points: 0 (no gavage), 10, 30, 60, and 120 minutes for the harvest of portal blood. The relative quantity and labeling pattern of metabolites in the portal blood samples were measured by GC/MS. A brief summary of conducting this model is described in diagram as shown in Figure 8.

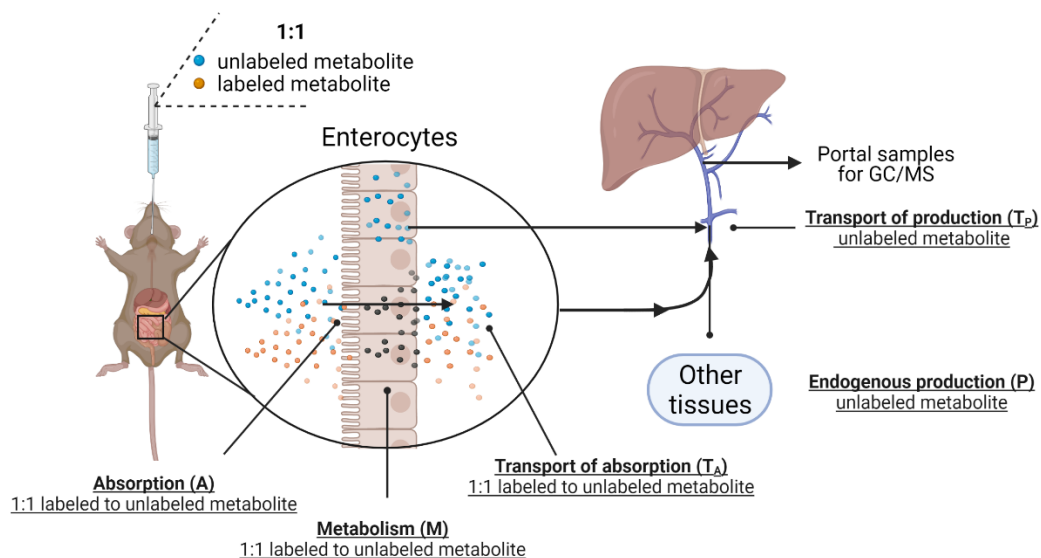


Figure 8: The outline of the relative quantification model

Diagram of a relative quantification model that crudely estimates intestinal absorption versus endogenous production of circulating metabolites.

Metabolites in the portal blood are a mixture of metabolites transported into portal circulation following absorption as well as recirculation of metabolites from systemic circulation include metabolites derived from endogenous production which may occur in the intestine or other tissues. Thus, the labeling of absorbed isotope-labeled metabolites are diluted by the endogenously produced metabolites and recirculating metabolites which can be assessed in portal blood samples. The endogenously produced metabolites are assumed to be exclusively unlabeled because the natural isotopomer labeling of their

substrates is negligible [65]. One assumption made by this model is that the redistribution of intestinal absorbed metabolites is limited during our acute oral gavage experiment. Ignoring the redistribution may overestimate the absorption rate since all labeled metabolites were assumed to be from absorption. Another major assumption made by this model is that the metabolism of absorbed nutrients in intestinal tissues follows first-order kinetics, which is approximately true for most drugs and nutrients [66]. Assuming first-order kinetics - that metabolites are metabolized in proportion to their concentration - the fraction of transported labeled metabolites following absorption will be the same as transported unlabeled metabolite from endogenous production within the intestine:

Equation 1: First-order transport

The fraction of transported labeled metabolites (T_A) following absorption (A) is the same as transported unlabeled metabolites (T_P) produced endogenously (P).

$$\frac{E_A}{A} = \frac{E_P}{P}$$

As we gavaged a bolus of metabolites at a 1:1 labeled to unlabeled ratio, the transported labeled metabolites are proportional to half of the total absorbed metabolite:

Equation 2: Transported labeled metabolites correspond to the ratio of labeled to unlabeled metabolites in the gavage solution

The transported labeled metabolites ($T_{labeled}$) are proportionally to half of the total absorbed metabolites (T_A)

$$T_{labeled} \propto \frac{1}{2} T_A$$

As transported unlabeled metabolites originate from both external absorption and endogenous production, transported unlabeled metabolites are proportional to the sum of half transported absorption and transported intestinal production:

Equation 3: Transported unlabeled metabolites are the sum from both external absorption and endogenous production

The transported unlabeled metabolites ($T_{labeled}$) are proportionally to half of the total absorbed metabolites (T_A) plus the endogenous production

$$T_{labeled} \propto \left(\frac{1}{2} T_A + T_P \right)$$

Combining these equations, we crudely estimate the ratio of external absorption to endogenous production using the transported labeled and unlabeled metabolites amount measured by GC/MS in portal blood samples:

Equation 4: Estimate the intestinal absorption to endogenous production by the labeling of metabolites in the portal blood

The transported unlabeled metabolites (T_{labeled}) are proportionally to half of the total absorbed metabolites (T_A) plus the endogenous production

$$\frac{A}{P} = \frac{T_A}{T_P} \propto \frac{2 \times T_{\text{labeled}}}{T_{\text{unlabeled}} - T_{\text{labeled}}}$$

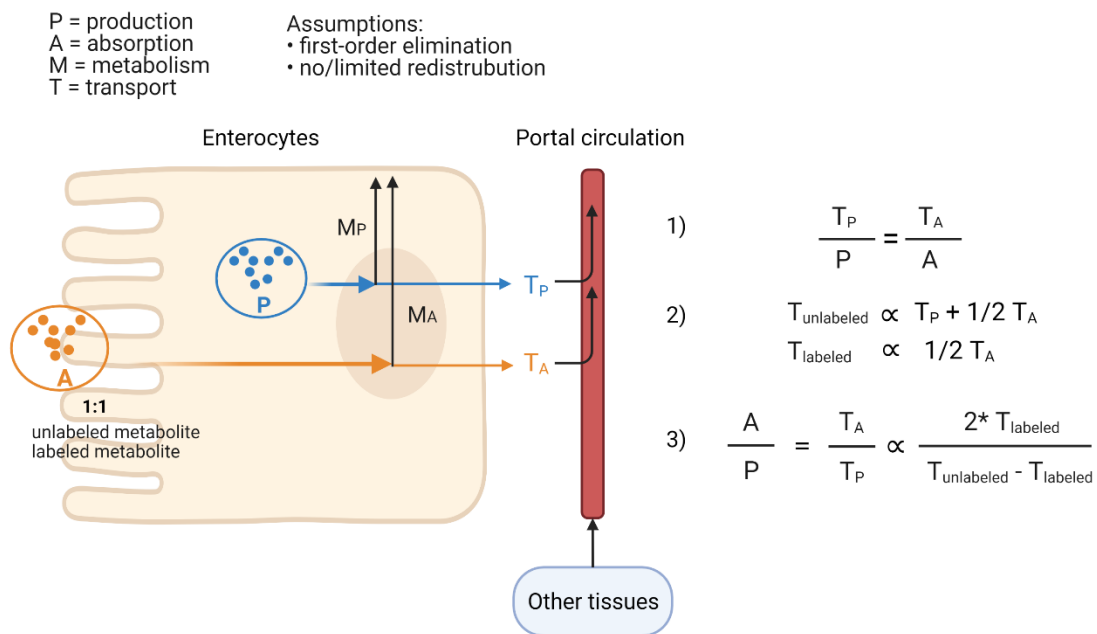


Figure 9: Equations of the relative quantification model

Description and equations of a relative quantification model that crudely estimates intestinal absorption versus endogenous production of circulating metabolites.

We tested this model using fructose, taking advantage of the fact that fructose is quickly absorbed and readily metabolized in the intestine and that endogenous fructose production is likely small relative to fructose absorption in mammals [67]. As expected, within 10 minutes of fructose gavage, both portal and tail fructose levels rapidly and robustly increased approximately 50-fold and 20-fold above their baseline levels, respectively (Figure 10A). The relative abundance of M+6 fructose was similar to that of M+0 fructose at the 10-minute time point and comparable to the 1:1 ratio of labeled and unlabeled fructose that was provided by gavage. The lack of dilution of M+6 fructose with M+0 fructose indicates that endogenously produced fructose was not a major contributor to portal fructose at this time point. The gradual decline in M+6 compared to M+0 fructose from 30 minutes on is indicative of the dilution of the gavaged mixture of labeled and unlabeled fructose with endogenously produced fructose (Figure 10B). Based on the relative quantification model (Figure 10), we estimate that the rate of intestinal fructose absorption is approximately 25-fold greater than the rate of endogenously produced fructose production at the 10-minute time point (Figure 10C). These findings are consistent with known aspects of fructose metabolism in mice [68] and illustrate that this simplified relative quantification model may be useful in estimating the relative amounts of absorbed versus endogenously produced substrates *in vivo*.

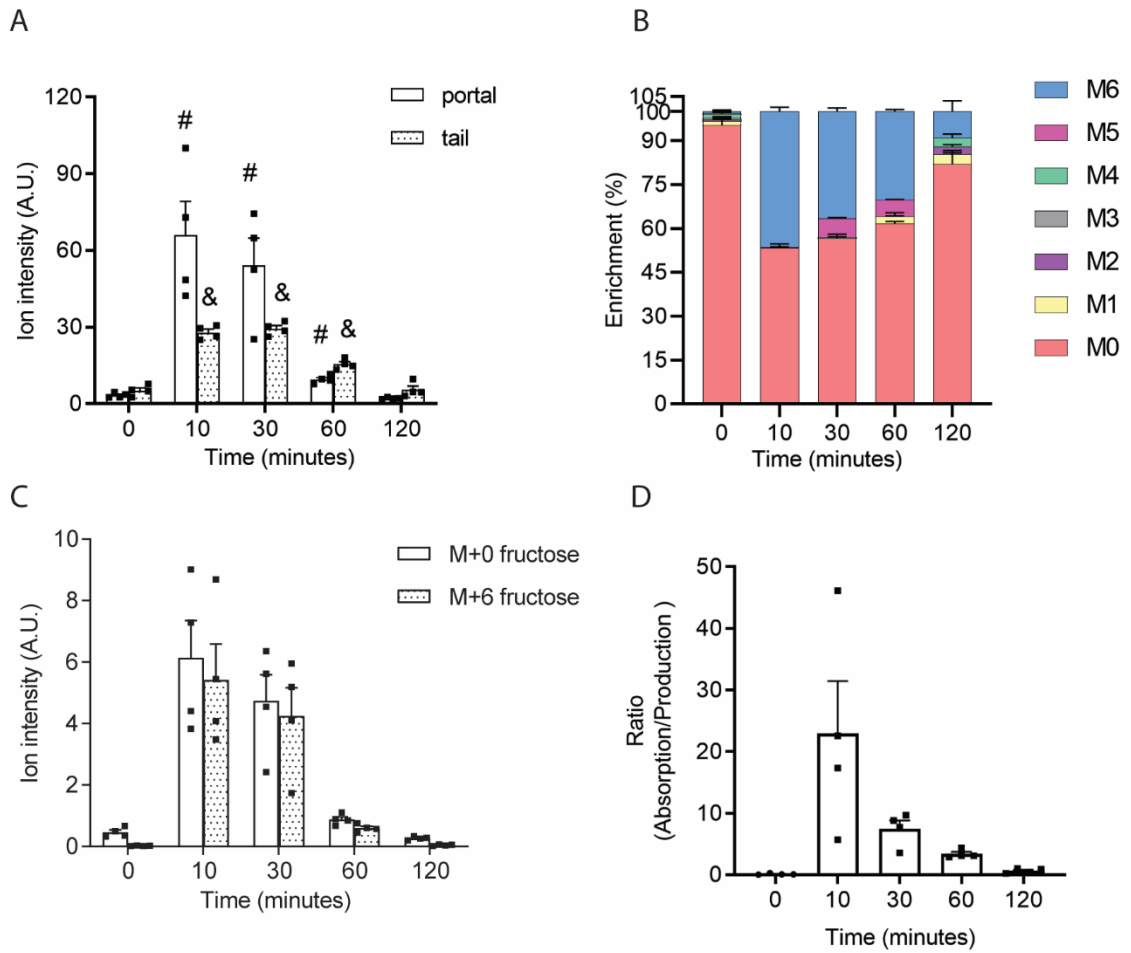


Figure 10: Validation of the relative quantification model using fructose

The relative quantification (A) and enrichment (B) of portal fructose after oral-gavaged with 1:1 U-C13-fructose and unlabeled fructose (0.48 g/Kg body weight). C. The ratio of intestinal absorption to endogenous production of fructose based on the relative quantification model we described in figure 10. n=4 in each group.

3.2.7 Compared to endogenous production, intestinal succinate absorption capacity is limited.

The content of succinate in typical human or mouse diets is not well defined. Succinate may be added to foods as a flavor enhancer at levels not to exceed 0.08% (g/g) in condiments and less than 0.006% (g/g) in meat products per FDA guidelines (21CFR184, Sec. 184.1091). By GC/MS measurement, the succinate content of a standard mouse chow diet (LabDiet 5053), is 146.5 $\mu\text{g/g}$, comprising less than 0.015% of food by weight (Figure 11A).

To define the upper limits of intestinal succinate absorption and to compare this to the rate of endogenous gut succinate production, we gavaged mice with 1:1 disodium succinate-2,2,3,3-D4 and unlabeled disodium succinate at a dose of 1.46 g/kg which is close to the solubility of succinate in water. This amount of succinate (~ 36.5 mg for a 25g mouse) is more than 60-fold higher than the amount of succinate consumed by a mouse on a standard chow diet in a day (~ 0.6 mg succinate for a mouse that eats 4g food per day). After gavage of this supraphysiological succinate bolus, both portal and tail succinate levels increased within 10 minutes and declined to baseline levels after ~ 1 hour (Figure 11B). This suggests that succinate can be absorbed from the intestinal lumen. Interestingly, at the time point of 10 minutes, the increase magnitude for M+0 succinate (from 3.35 ± 1.32 to 8.70 ± 5.10 A.U.) is higher than M+4 succinate (from 0.41 ± 0.08 to 3.44 ± 2.99 A.U.), suggesting the osmolarity stress of the supraphysiological succinate bolus may promote the secretion of endogenous gut-derived succinate (Figure 11C). During the

2 hours' time period, the maximum proportion of M+4 succinate accounts for total succinate only range from 20 to 25% (Figure 11D). This indicates that the absorbed exogenous 1:1 labeled to unlabeled succinate was substantially diluted by endogenous unlabeled succinate (Figure 11E). Using our model detailed above, we estimated that at peak absorption of this supraphysiological succinate bolus, the contribution of endogenous succinate and absorbed succinate are approximately equal (Figure 11E). These results indicate that in normal physiological circumstances, where succinate is present in ingested foods in limited amounts, the vast majority of circulating succinate is produced endogenously, and that succinate absorption likely contributes negligibly to portal succinate levels.

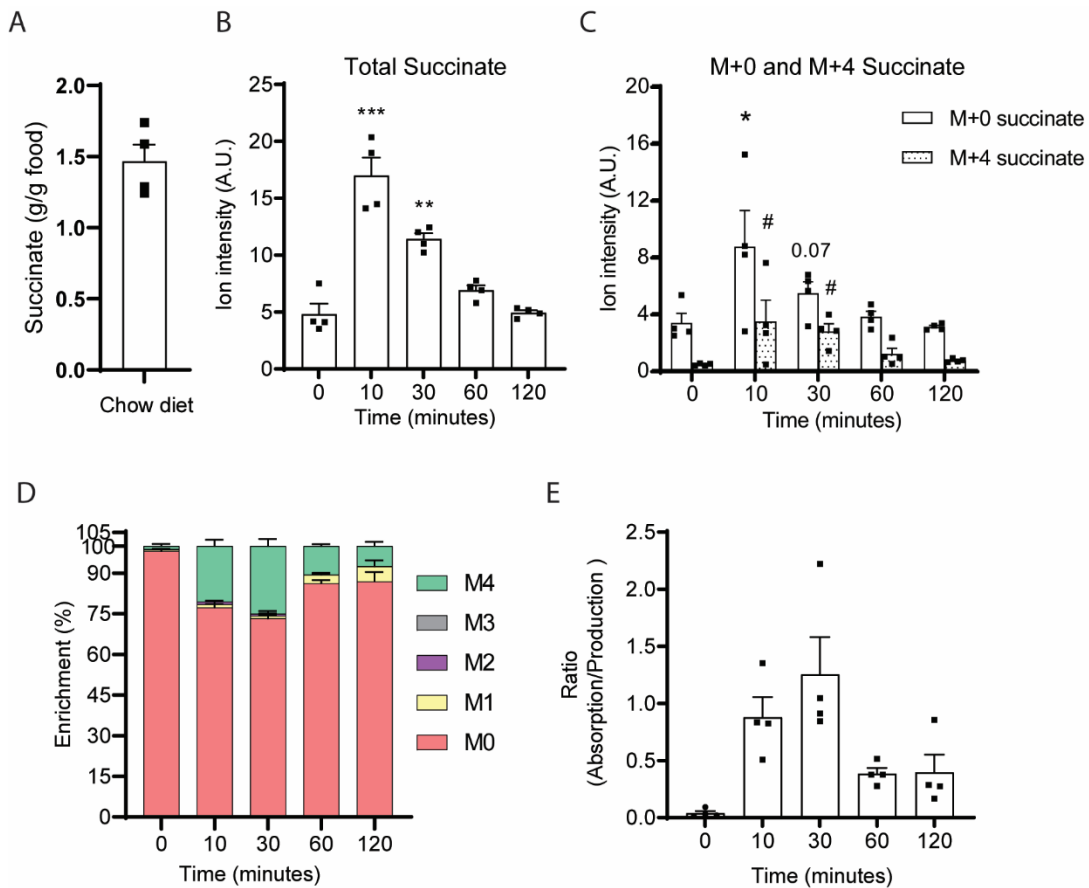


Figure 11: The intestinal absorption of succinate is limited

A. Succinate content in normal chow diet (LabDiet 5053) based on 4 different measurements. The total (B), M+0, and M+4 (C) succinate levels, and succinate enrichment (D) in the portal circulation after given a bolus of 1:1 D-4 succinate and unlabeled succinate in sodium salts (1.46 g/Kg body weight) by oral gavage. Norvaline was used as internal standard. E. The ratio of intestinal absorption to endogenous production of succinate based on the relative quantification model we described above. n=4 in each group

3.3 Discussion

Recent studies illustrate important roles for TCA cycle intermediates outside of their role in energy production including important roles for circulating TCA cycle intermediates as metabolic signals [50, 60]. This field has advanced with the discovery of cell-surface receptors sensitive to specific TCA cycle metabolites including succinate and alpha-ketoglutarate [69]. While the role of metabolites like succinate in regulating cellular function and organismal homeostasis is rapidly advancing, few studies have assessed the source of circulating TCA cycle intermediates.

We observed that the levels of TCA cycle intermediates are markedly higher in the portal blood than the peripheral circulation indicating the gut is a major source of circulating TCA cycle intermediates (Figure 2A, B). Recently Jang and colleagues used steady-state stable isotopic tracer infusions to assess sites of production and consumption of a wide range of metabolites including TCA cycle metabolites in pigs [70]. Based on sampling of the pancreaticoduodenal vein, they concluded that the pancreas was a major source of circulating TCA cycle metabolites. However, as this vein carries venous blood from both the pancreas and duodenum, these investigators could not discriminate whether the duodenum versus pancreas is the actual source. Moreover, in this study analysis of blood obtained from the splenic vein which drains the pancreas tail was not consistent with the pancreas as a source of TCA cycle intermediates.

Fructose is a dietary sugar that is preferentially metabolized in selected cell types including enterocytes in the intestine, hepatocytes in the liver, and proximal tubule cells in the kidney [67, 68]. Fructose is not readily metabolized in the pancreas [68]. Gavaging mice with labeled fructose rapidly and robustly labels TCA cycle intermediates in the portal vein and to comparable degrees within duodenal tissue (Figure 4 and Figure 8). Although multiple intestinal epithelial cell types (enterocytes, goblet cells, and paneth cells) may express the Glut5 luminal fructose transporter and fructolytic enzymes [71], these are expressed at high levels in absorptive enterocytes which are thought to mediate the bulk of intestinal fructose metabolism [68, 72]. Altogether, these results indicate that enterocytes in the proximal intestine are major contributors to gut-derived circulating TCA cycle metabolites.

According to studies conducted by us and others, the physiological circulating succinate levels range from 0 to 50 μM in humans [27], and 0 to 100 μM in rodents [63]. This range of succinate coincides with the pharmacological range (EC_{50}) of succinate receptor (Sucnr1) activation - 20 to 50 μM in human and 10 to 100 μM in rodents [50]. Thus, changes in the circulating succinate level within the physiological range have potential to affect the activity of Sucnr1 and its downstream signaling. This supports succinate's potential role as an important circulating metabolic signal.

While our results indicate that enterocytes are major sources of circulating succinate in physiological circumstances, other tissues may also play important roles.

For example, acute cellular hypoxia such as myocardial infarction, ischemia of the kidney, or liver ischemia are known to result in succinate production, and this may increase circulating succinate levels [9, 73, 74]. Exercise-induced hypoxia in skeletal muscles can produce substantial amounts of succinate which can transiently increase circulating succinate levels [75]. Chronic, mild increases in circulating succinate are associated with cardiometabolic diseases including obesity, hypertension, and type-2 diabetes and the source of this succinate is unclear [27, 28]. Additional studies will be required to determine whether intestinal TCA cycle metabolite production is a contributor to changes in circulating succinate associated with pathological conditions.

Intestinal microbiota are increasingly recognized as a major source of bioactive metabolites in systemic circulation which may have pleiotropic physiological effects [76]. As examples, microbiota-derived short-chain fatty acids and acetate both play important roles in hepatic gluconeogenesis and de novo lipogenesis participating in diet-induced metabolic disease [58, 77]. Serena et al. observed an enrichment of succinate-generating microbiota in association with circulating succinate levels in patients with metabolic diseases and hypothesized that the microbiota contributes to this increase (9). De Vadder et al. subsequently transplanted one of these succinate-generating microbial strains, *P. copri*, into conventional mice and observed significantly increased succinate in cecal contents in association with improved glucose tolerance [56]. However, this was not associated with increased circulating succinate indicating that increased levels of

succinate in the intestinal lumen are not sufficient to increase circulating succinate levels [56]. De Vadder et al. interpreted this data to suggest that microbially-derived succinate is absorbed and consumed within the intestine as gluconeogenic substrate. However, intestinal gluconeogenesis is largely restricted to the small intestine whereas succinate production from microbiota occurs predominantly in the colon [78]. As we cannot rule out the possibility of nutrient exchange between the small and large intestine, we assessed portal succinate levels in conventional and germ-free mice (Figure 3B), directly demonstrating that gut microbiota are not essential for maintaining circulating succinate levels. Moreover, by comparing portal succinate labeling patterns after oral administration of labeled substrate, we demonstrate that intestinal tissue rather than microbiota are the predominant contributor to portal succinate in conventional mice (Figure 3A, B). Altogether, we and others have demonstrated that although microbiota can generate substantial amounts of succinate in the intestinal lumen, this microbiota-produced succinate is distinct from that produced endogenously in the small intestine. Thus, microbiota are not a major contributor to circulating succinate. These results raise questions as to the causal nature of the improvements in glucose homeostasis after transplantation of succinate-generating microbiota. At a minimum, the improvements in metabolism associated with this transplant cannot be attributed to changes in circulating succinate as a metabolic signal.

These studies also raise questions about the capacity of the intestine to absorb succinate from the lumen. This question is important as several studies have suggested that dietary supplementation of succinate can increase circulating succinate and regulate biological functions through activation of *Sucnr1* in multiple organs including the liver and adipose tissue [54, 63, 79]. However, none of these studies assessed the impact of dietary succinate supplementation on circulating succinate levels. Here, we examined intestinal succinate absorption capacity and determine the relative importance of succinate absorption compared to endogenous production.

To approach this problem, we first sought literature regarding the succinate content of typical diets and were surprised to find no clear reference for this in typical human or animal diets. Hence, we measured succinate levels a standard mouse chow diet and found that succinate contributes no more than 0.015% g/g diet. We elected to gavage mice with a quantity of labeled succinate that far exceeds the typical dietary content. At this extreme, supraphysiological dose, succinate absorption transiently approached the levels of endogenous succinate production (Figure 11 B-E). These results suggest that the modest amounts of succinate present in typical diets contributes negligibly to gut-derived circulating succinate levels.

While the results from this study support the conclusion that enterocytes are a major source of circulating TCA cycle metabolites, there are several limitations. The model used to compare the relative rates of succinate absorption versus endogenous

production relies on several assumptions which include: 1) metabolism of absorbed and endogenously produced succinate follows first-order kinetics, and 2) the recirculation of labeled succinate is negligible. First, although most of metabolites follow first-order elimination kinetics [66], it is possible that succinate elimination actually follows zero-order elimination rule. However, the rapid peak and return to baseline after within 1 hour of gavage is inconsistent with a zero-order elimination model. Second, although we disregard the recirculation of intestinal absorbed labeled metabolites in our model, this assumption could lead to an overestimation of the absorption of succinate. Thus, if recirculation is substantial, the actual intestinal absorption rate would be even smaller than what we estimated here and would further support our conclusion that intestinal absorption of succinate makes a minor contribution.

3.4 Conclusion

Intestinal tissue is a major source of circulating TCA cycle metabolites. The role of intestinally derived circulating TCA cycle intermediates as metabolic signals remains to be investigated in future studies.

4. Sucnr1 is predominantly expressed in hepatocytes where its physiological role remains unclear

4.1 Introduction

The TCA cycle produces large amounts of ATP that is crucial for maintaining cellular and systemic energy homeostasis. While the role of TCA cycle intermediates in facilitating energy production is well defined, they can also serve other roles outside of the mitochondria [49]. Specifically, recent studies suggest that circulating succinate is a metabolic signal that participates in multiple physiological and pathological processes in various tissues [50]. In our prior work (Section 3), we showed that the intestine constitutively produces and export large amounts of succinate to the systemic circulation. Whether gut-derived circulating succinate plays a significant biologic/regulatory role remains unclear.

Succinate receptor (Sucnr1) is a cell-surface G-protein receptor that is highly expressed in metabolic tissues including kidney, liver, skeletal muscle and adipose tissues [80]. Sucnr1 is activated by succinate with an EC_{50} between 20 to 50 μM in human and 10 to 100 μM in rodents [50]. This overlaps with the range of circulating succinate levels, which have been reported to range from 0 to 50 μM in humans [27], and 0 to 100 μM in rodents [63]. In our study, the systemic succinate levels range from 20 μM to 65 μM in C57/BL6J background mice (Figure 4) and 25 μM to 75 μM in the mice with C3H/HeJ background (Figure 2). Succinate levels trend to be higher in the portal vein, with 40 μM

to 80 μM in C57/BL6J background mice (Figure 4) and 120 μM to 180 μM in the mice with C3H/HeJ background. Thus, normal physiological levels of circulating succinate have the potential to regulate biological functions downstream of *Sucnr1* signaling.

Sucnr1 is highly expressed in liver tissue [80]. As we have shown that the intestine is a major contributor to portal and peripheral succinate (Section 3) and levels in the portal circulation exceed those in systemic circulation, likely in part due to the first pass metabolism in the liver [70]. I propose that liver *Sucnr1* may be a crucial target of intestine-derived succinate, since the liver is exposed to higher levels of circulating succinate than other tissues.

The precise cell types that express *Sucnr1* within the liver has been a controversial topic. Previous studies suggested that liver *Sucnr1* is predominantly expressed in hepatic stellate cells, with only low levels in hepatocytes, based on qPCR and immunochemistry measurements performed on cultured hepatocytes, hepatic stellate cells, and other liver cell types *in vitro* [12, 81]. However, this approach may be misleading as it is well-established that primary hepatocytes quickly dedifferentiate in culture [82], and that this dedifferentiation significantly diminishes the expression of almost all GPCRs [83]. Additionally, the published immunochemistry studies lack antibody validation experiments in *Sucnr1* knockout tissues versus controls. Unfortunately, there is no accessible antibody for *Sucnr1* currently, partially due to the fact that GPCRs are typically expressed at low levels and hard to approach using immunoblot techniques. Thus, it

remains challenging to evaluate the expression of *Sucnr1* in precise cell types within the liver.

In this section, I have analyzed publicly available single-cell RNA-sequencing data to demonstrate that *Sucnr1* mRNA is expressed at high levels in hepatocytes in addition to non-parenchymal cells. In addition, using hepatocyte specific *Sucnr1* KO mice, I confirmed that the vast majority of liver *Sucnr1* is expressed in hepatocytes and not in non-parenchymal cells. Moreover, I conducted unbiased transcriptomic analyses in liver selective *Sucnr1* KO mice to begin to define the role of *Sucnr1* in liver function.

4.2 Results

4.2.1 *Sucnr1* is expressed in multiple liver cell types.

As discussed above, *Sucnr1* is highly expressed in the liver but it remains uncertain which cell types contribute to this expression. To explore the cellular expression level of *Sucnr1* from an unbiased perspective, I analyzed two publicly available single-cell RNA-sequencing datasets [44, 45]. Raw data from these datasets are accessible through the NCBI GEO database platform with the specific series number GSE129516 and GSE84498, respectively [84]. These single-cell RNA-sequencing datasets were used to conduct enrichment procedures to obtain gene expression levels selectively from non-parenchymal cells (GSE129516, [84]) or liver parenchymal cells (GSE84498, [84]).

The non-parenchymal cell enriched dataset (GSE129516) indicates that *Sucnr1* is expressed in multiple cell-types including cholangiocytes, hepatic stellate cells, dendritic cells, and endothelial cells (Figure 12A). Even though this dataset was depleted for hepatocytes, *Sucnr1* was detected in the small numbers of hepatocytes that were detected. Moreover, the expression level of *Sucnr1* in hepatocytes was as high or higher than that in hepatic stellate cells, dendritic cells, or endothelial cells (Figure 12B). This finding appeared to contradict the prevailing view that *Sucnr1* is predominantly expressed in liver non-parenchymal cells and not in hepatocytes [12, 81].

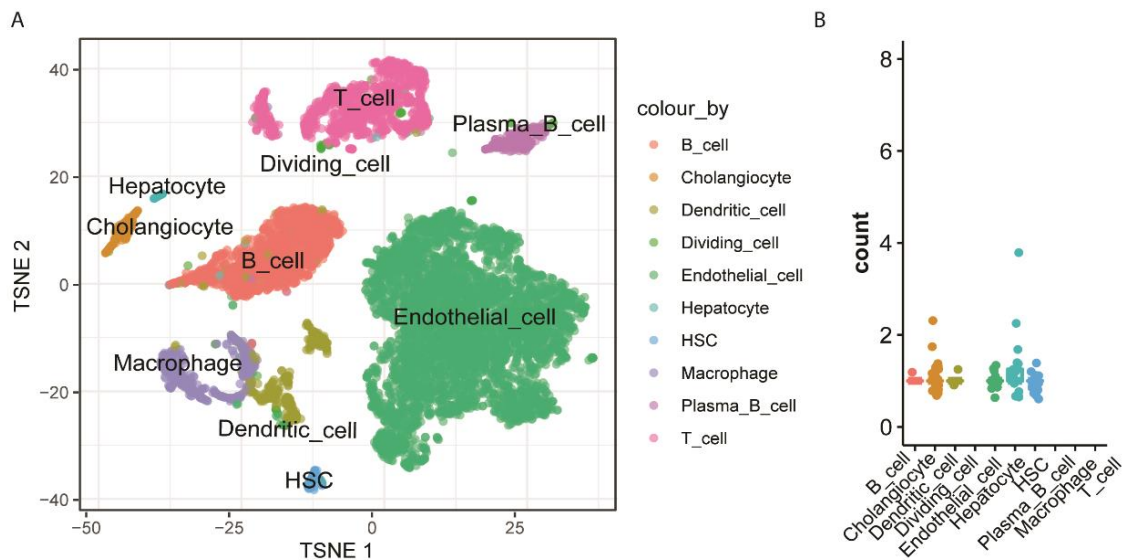


Figure 12: *Sucnr1* is expressed in multiple cell types in the liver

A. Cluster map showing cell-type specific clusters. B. Expression levels of *Sucnr1* in cell-type specific clusters. Data were derived from GSE129516. HSC: Hepatic stellate cell.

To further investigate this finding, I analyzed the liver parenchymal cell enriched dataset GSE84498. As expected, nearly 90% of cells included in this dataset are labeled as hepatocytes (Figure 13A). *Sucnr1* is readily detectable in a large number of hepatocytes, but not other cell types in this analysis (Figure 13B), which again indicates that *Sucnr1* is expressed in hepatocytes. Additionally, we further compared the hepatic expression level of *Sucnr1* to that of all 384 reported murine GPCRs in this dataset [80]. A total of 81 GPCRs was identified in the hepatocytes in this specific dataset (Table 4). Consistent with the known critical regulating effects of glucagon signaling on liver functions, *Gcgr* is the most abundantly expressed GPCR in the hepatocytes (Figure 13C). Previous studies suggested that *Sucnr1* couples to the G_i subunit and activates G_i -mediated inhibition of cAMP formation and contributes to ERK pathway activation in a dose-dependent manner [50]. Interestingly, we find that *Sucnr1* is among the top 10 most abundant GPCRs, and the most highly expressed G_i -coupled GPCR (Figure 13C). Altogether, these data suggest that *Sucnr1* mRNA is expressed in hepatocytes.

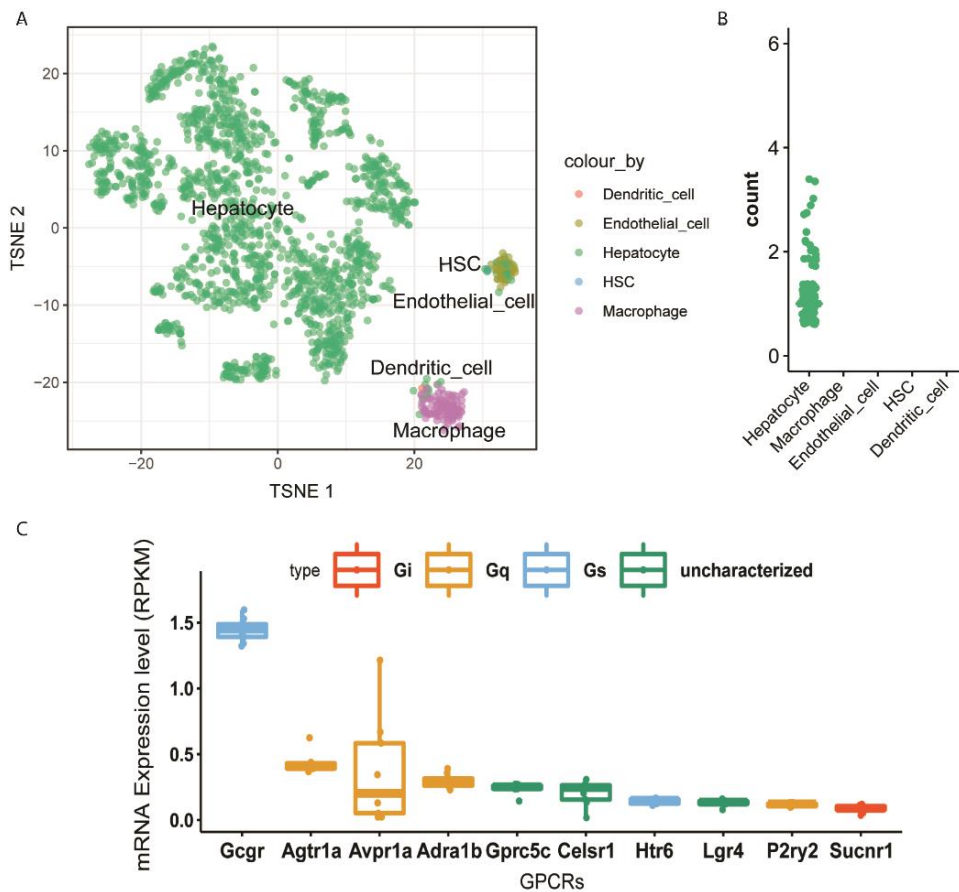


Figure 13: Sucnr1 does express in hepatocytes

A. Cluster map showing the cell-type specific clusters. B. Expression levels of Sucnr1 in cell-type specific clusters. C. Expression levels of the 10 most highly expressed GPCRs in hepatocytes. Data were derived from GSE84498.

Table 4: All murine GPCRs detected in hepatocytes

Rank	Gene Symbol	Expression Level	Rank	Gene Symbol	Expression Level
1	Gcgr	1.45E-04	42	Ednrb	4.82E-07
2	Agtr1a	4.29E-05	43	Ltb4r2	4.60E-07
3	Avpr1a	3.60E-05	44	Adra2a	4.54E-07
4	Adra1b	3.02E-05	45	Gpr160	4.45E-07
5	Gprc5c	2.41E-05	46	Cmklr1	4.42E-07
6	Celsr1	2.06E-05	47	Vmn2r29	4.16E-07
7	Htr6	1.45E-05	48	Npr3	4.01E-07
8	Lgr4	1.30E-05	49	S1pr3	3.69E-07
9	P2ry2	1.17E-05	50	P2ry1	3.42E-07
10	Sucnr1	8.53E-06	51	Chrm3	3.21E-07
11	Inpp5k	8.40E-06	52	Gpr135	3.15E-07
12	Fzd1	8.31E-06	53	Kiss1r	2.92E-07
13	S1pr2	6.57E-06	54	Calcr1	2.92E-07
14	Fzd8	5.65E-06	55	Sphk2	2.89E-07
15	F2r	3.90E-06	56	Htr5b	2.69E-07
16	Adra1a	3.89E-06	57	Pth1r	2.68E-07
17	Gabbr2	3.59E-06	58	Lpar1	2.48E-07
18	Fzd6	3.29E-06	59	S1pr4	2.37E-07
19	Fzd7	3.19E-06	60	Gpr12	2.25E-07
20	Lpar6	3.12E-06	61	Adrb1	2.19E-07
21	Gpr19	2.89E-06	62	Gpr171	1.97E-07
22	Fzd5	2.78E-06	63	Celsr2	1.97E-07
23	Gpr182	2.40E-06	64	Gpr4	1.80E-07
24	S1pr5	2.38E-06	65	Cxcr4	1.48E-07
25	Fzd4	2.27E-06	66	Opn3	1.40E-07
26	Adra2b	2.16E-06	67	Cxcr5	1.31E-07
27	Ltb4r1	1.24E-06	68	Ccr5	1.20E-07
28	Adrb3	1.16E-06	69	Fzd3	1.06E-07
29	P2ry13	1.00E-06	70	Ptger2	1.06E-07
30	Gpr157	9.00E-07	71	Fpr1	1.03E-07
31	Vipr1	8.43E-07	72	Gpr183	9.76E-08
32	Ccr2	7.20E-07	73	Tas1r1	8.54E-08
33	Mrgpre	6.91E-07	74	Cxcr2	8.41E-08
34	Mtnr1a	6.37E-07	75	Gpr35	6.65E-08
35	Ramp1	6.21E-07	76	Fzd9	5.84E-08
36	Agtrap	5.88E-07	77	Ednra	5.74E-08
37	Adora1	5.88E-07	78	Gpr18	5.03E-08
38	Ccr7	5.84E-07	79	Gpr153	2.55E-08
39	Ccr12	5.34E-07	80	Lpar3	2.34E-08
40	Gpr25	5.28E-07	81	Vmn1r4	1.68E-08
41	Adrb2	4.92E-07			

4.2.2 Sucnr1 is predominantly expressed in parenchymal cells in the liver.

We generated liver-selective Sucnr1 knock-out (LiSucnr1KO) mice using the Cre-LoxP recombination system by crossing Sucnr1-floxed mice with Alb-Cre mice as detailed in 2.1.1.2. As expected, Sucnr1 mRNA was exclusively depleted in the liver of LiSucnr1KO mice and not in controls (Figure 14). In contrast, the levels of Sucnr1 remains constant across genotypes in the kidney where Sucnr1 is also highly expressed, demonstrating the specificity of liver knockout (Figure 14). The Alb-Cre directed knockout resulted in a ~90% decrease of Sucnr1 mRNA expression in whole liver tissue, suggesting robust Sucnr1 knockout in this LiSucnr1KO mouse model (Figure 14).

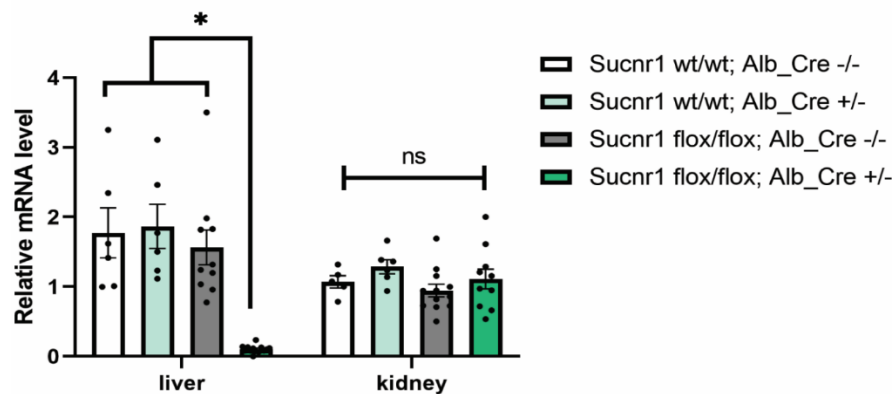


Figure 14: Sucnr1 is exclusively knocked out in the liver-specific Sucnr1 knock-out (LiSucnr1KO) mice

The mRNA levels of Sucnr1 were measured by qPCR in the whole liver and kidney tissue samples of mice as noted above. n= 6-9 in each group. * indicate the p value is statistical significance (<0.05) of Sucnr1 expression between LiSucnr1KO with others by one-way ANOVA.

To further compare the intensity of *Sucnr1* expression in hepatocytes versus other hepatic non-parenchymal cells, we isolated liver parenchymal-enriched and non-parenchymal-enriched cellular fractions after liver *in situ* digestion. The liver *in situ* digestion and parenchymal/non-parenchymal cell enrichment procedures are detailed in 2.1.1.4 and 2.1.2.6 respectively and illustrated in Figure 15.

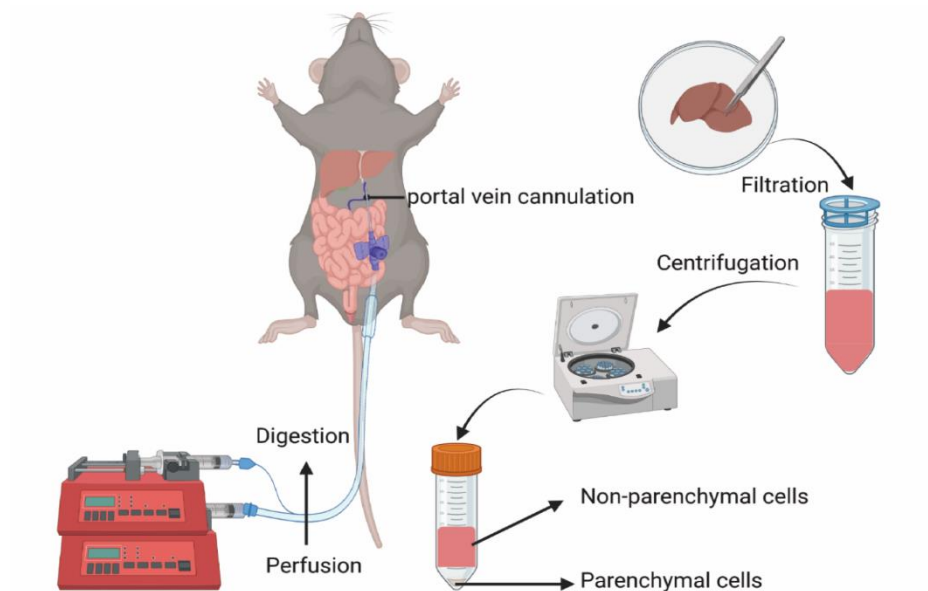


Figure 15: Liver parenchymal and non-parenchymal fragment isolation after 2-step *in situ* liver digestion

Diagram cartoon of *in situ* liver digestion by portal vein cannulation and portal infusion of perfusion-digestion buffers and liver parenchymal versus non-parenchymal cell isolation by gradient centrifuge.

By conducting qPCR, we have confirmed that hepatocyte and non-parenchymal cell fraction were well separated, as the hepatocyte-enriched fraction has significantly higher expression of hepatocyte marker Alb and Tbg while the non-parenchymal cell fragment has higher expression of non-parenchymal cell markers like Acat2 (hepatic stellate cell) and CD68 (macrophage) (Figure 16) [85]. Interestingly, the *Sucnr1* expression level is 6-fold higher in the hepatocyte enriched fraction than the non-parenchymal cell enriched fraction, indicating that *Sucnr1* is predominantly expressed in the hepatic parenchymal cells (Figure 16).

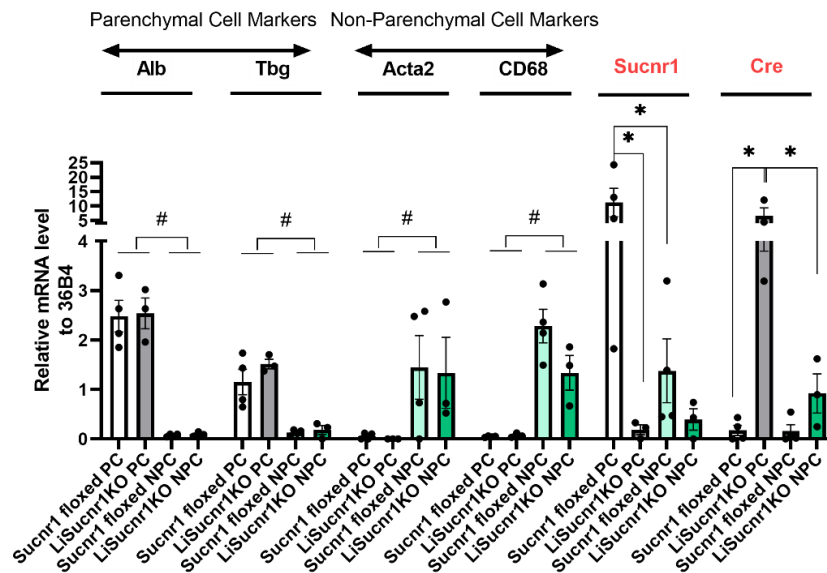


Figure 16: *Sucnr1* expressed higher in the hepatocytes versus non-parenchymal cells

The mRNA levels of genes were assessed in the liver parenchymal fraction (PC) versus non-parenchymal (NPC) fraction in ad-lib sacrificed *Sucnr1*-floxed and *LiSucnr1KO* males by qPCR. n= 4 in each group. * indicate the p value is statistical significance (<0.05) of gene expression between parenchymal and non-parenchymal fraction by two-way ANOVA. * indicate the p value is statistical significance (<0.05) between groups by post-hoc analysis following one-way ANOVA.

Sucnr1 mRNA expression is almost completely depleted in the hepatocyte enriched fraction in LiSucnr1KO mice compared to controls. There was also a trend for depletion of Sucnr1 in the non-parenchymal fraction in LiSucnr1KO mice compared to controls although levels were higher than in the hepatocyte fraction of LiSucnr1KO mice (Figure 16). We also noted that although Cre is supposed to express selectively in hepatocytes when driven by the albumin promoter, we were able to detect Cre expression in the non-parenchymal cell enriched fraction of the LiSucnr1KO mice compared to the control Sucnr1-floxed mice (Figure 16). This finding suggests that the Alb-Cre transgene may also express in non-parenchymal cells and may be capable of directing knockout of target genes in some non-parenchymal cells as well as hepatocytes. Thus, based on this result, we could not definitively conclude that the 92% reduction in liver Sucnr1 expression observed in bulk liver tissue (Figure 15) was exclusively due to reduction of Sucnr1 in hepatocytes versus non-parenchymal cells.

To further investigate this, we generated the hepatocyte-specific Sucnr1 knock-out (HepSucnr1KO) mice and their controls using either the Tbg-Cre AAV or GFP AAV as detailed in 2.1.1.3. The same set of experiments were then repeated using the HepSucnr1KO mice and Sucnr1-floxed mice as controls. As expected, using the Tbg-Cre AAV, there is minimal Cre expression in the non-parenchymal cell fractions of HepSucnr1KO mice (Figure 17). Sucnr1 expression is significantly higher in the hepatocyte enriched fraction than the non-parenchymal cell enriched fraction and

reduced exclusively in this fraction with hepatocyte specific Cre expression confirming that *Sucnr1* is predominantly expressed in the hepatic parenchymal cells, and not non-parenchymal cells.

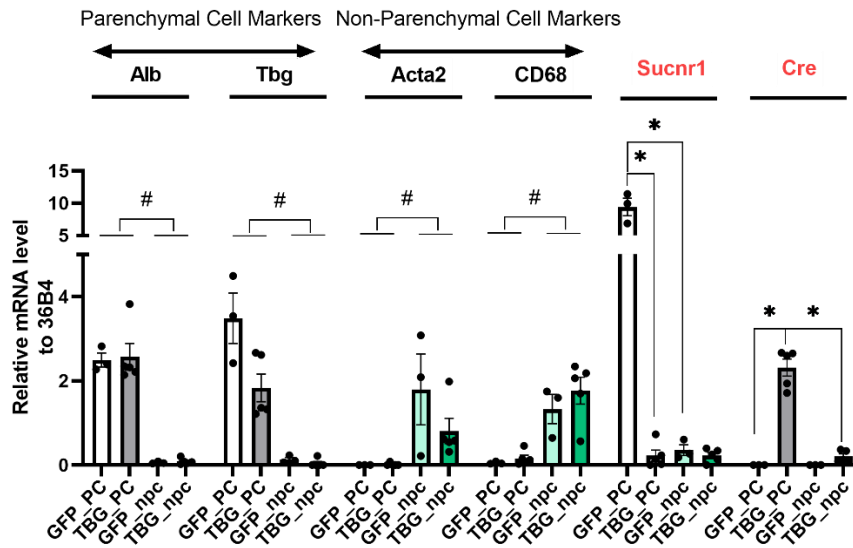


Figure 17: *Sucnr1* is predominantly expressed in the hepatocytes

The mRNA levels of genes were assessed in the liver parenchymal fraction (PC) versus non-parenchymal (NPC) fraction in ad-lib sacrificed GFP AAV versus TBG-Cre AAV injected *Sucnr1*-floxed males by qPCR. Animals were analyzed after 10 days post retro-orbital injection of AAVs. n= 4 in each group. * indicate the p value is statistical significance (<0.05) of gene expression between parenchymal and non-parenchymal fraction by two-way ANOVA. * indicate the p value is statistical significance (<0.05) between groups by post-hoc analysis following one-way ANOVA.

4.2.3 Acute exposure of the liver to succinate attenuates phosphorylation of some targets of hepatic glucagon signaling

As I have shown that *Sucnr1* is predominantly expressed in hepatocytes and might serve as a target of gut-derived succinate, I next pursued the potential for succinate to mediate acute signaling events in the liver. As a Gi-coupled cell-surface protein receptor, we hypothesized that *Sucnr1* would oppose Gs-signaling activated via the glucagon receptor and down-regulate adenylyl cyclase associated cAMP generation and associated signaling events. Glucagon receptor is the most abundantly expressed Gs-coupled receptor in the hepatocytes, and a well-established regulator of liver function in part through activation of PKA signaling [86]. In this regard, we assessed whether succinate could attenuate glucagon's ability to enhance PKA signaling in mice.

To approach this question, we used our *in vivo* portal perfusion model with multiple perfusion conditions: normal saline, glucagon alone, succinate alone, and glucagon plus succinate. Specifically, we used a perfusion rate of 15 ul/min which permits continuous perfusion into the portal vein without causing volume overload in the timeframe of this experiment [87]. As previous studies demonstrated that glucagon concentrations between 100 pM and 1 nM are sufficient to activate the glucagon receptor in hepatocytes [88], we chose to infuse glucagon to achieve a final portal concentration of either approximately 100 pM or 1 nM. Similarly, succinate concentrations above 200 uM are sufficient to fully activate the succinate receptor [89], thus, the final portal concentration of succinate used in this study was 200 uM. Considering that the portal

blood flow rate in mice is ~ 2 ml/min [32] and the portal infusion rate used in this study was 15 ul/min, infused glucagon solutions were prepared at either 13.33 or 133.3 mM while the infused succinate solution were prepared at 26.4 mM in normal saline.

As expected, glucagon perfusion for 20 minutes quickly activated hepatic PKA signaling as demonstrated by significant increases in phosphorylated PKA substrates (Figure 18A, B). Succinate perfusion alone for 20 minutes did not change the hepatic PKA signaling significantly, although succinate perfusion tended to decrease the phospho-PKA substrate levels at some selected molecular weights (~ 30KD and ~ 78 KD) (Figure 18A, B). In contrast, if mice were pretreated with succinate for 5 minutes and then perfused together with glucagon for another 5 minutes, immunoblots indicated that succinate was capable of reducing glucagon-mediated phosphorylation of PKA substrates (Figure 18C, D). This attenuation was more obvious at selected molecular weights, particularly at ~ 30 KD (Figure 18C, D). These observations were potentially consistent with our hypothesis that gut-derived succinate might be capable of antagonizing glucagon signaling through activation of *Sucnr1*. If so, this might have significant implications for the pathogenesis of metabolic diseases including diabetes where glucagon plays a prominent role [90].

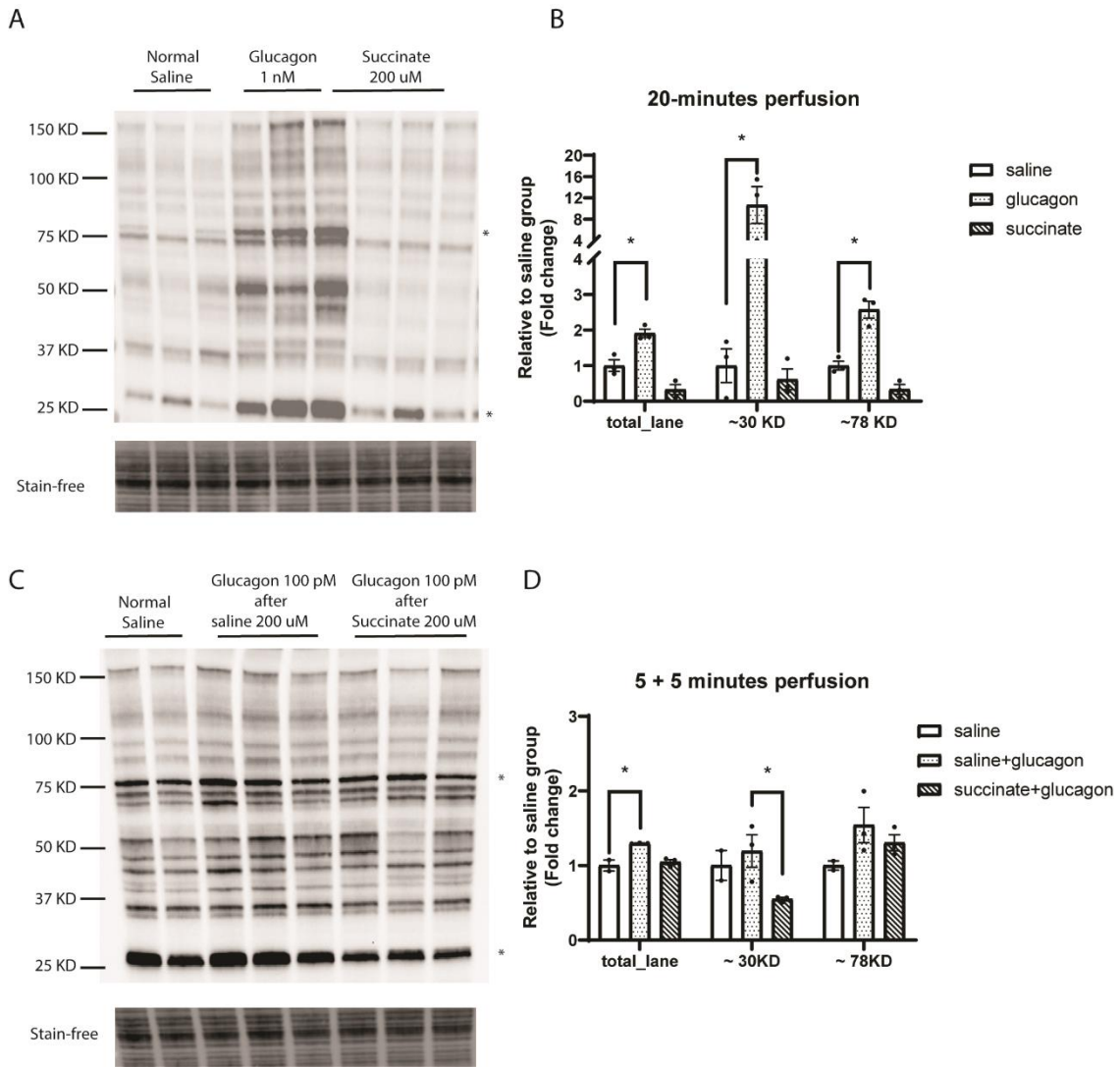


Figure 18: Succinate attenuates the phosphorylation of selected hepatic substrates that are phosphorylated following glucagon treatment.

Immuno-blot (A) and quantification (B) of phospho-PKA substrates levels in the liver tissues after 20 minutes portal perfusion of normal saline, glucagon (1 nM final concentration), and sodium succinate (200 uM final concentration) by Western Blot. Immuno-blot (C) and quantification (D) of phospho-PKA substrates levels in the liver tissues after portal perfusion with normal saline for 10 minutes, glucagon (100 pM final concentration) for 5 minutes after 5 minutes' perfusion with either saline or sodium succinate (200 uM final concentration). * indicate statistical significance ($p < 0.05$) of post hoc analysis after one-way ANOVA.

As succinate perfusion attenuated the phosphorylation of selected PKA substrates, we further explored the protein composition of these significantly altered bands (~ 30 KD, and ~ 78 KD) by proteomics. To enhance detection, we enriched for phosphorylated PKA substrates by immunoprecipitation. Briefly, 400 µg protein lysates from liver samples of mice described in Figure 18A were used. After enriching for phospho-PKA substrates by immunoprecipitation, protein lysates were loaded on SDS-PAGE gel for electrophoresis. After staining with colloidal blue, sections of the gel between 25 to 37 KD and 70 to 90 KD were excised under UV illumination. After recovering proteins from the gel, proteins were purified, digested with trypsin, and analyzed by LC/MS.

A total of 107 proteins were identified, with 68 proteins identified in the 25 to 37 KD band and 56 proteins identified within samples from the gel around 70 to 90 KD. By comparing the protein in saline versus glucagon treated samples, we identified only a single protein that was enriched in glucagon treated samples in either band - the Doublecortin like kinase 3 (DCLK3) (Figure 19A).

DCLK3 is a Serine/threonine-protein kinase that is preferentially expressed in neurons in the striatum and dentate gyrus. It is reported that the expression levels of DCLK3 is highly associated with the development of Huntington disease by regulating nucleosome/chromatin remodeling [91]. DCLK3 is known to be phosphorylated by PKA, but its function in the liver has not been studied. Identifying DCLK3's function in liver

and exploring the association of DCLK3 with glucagon and succinate signaling may be of interest in future studies.

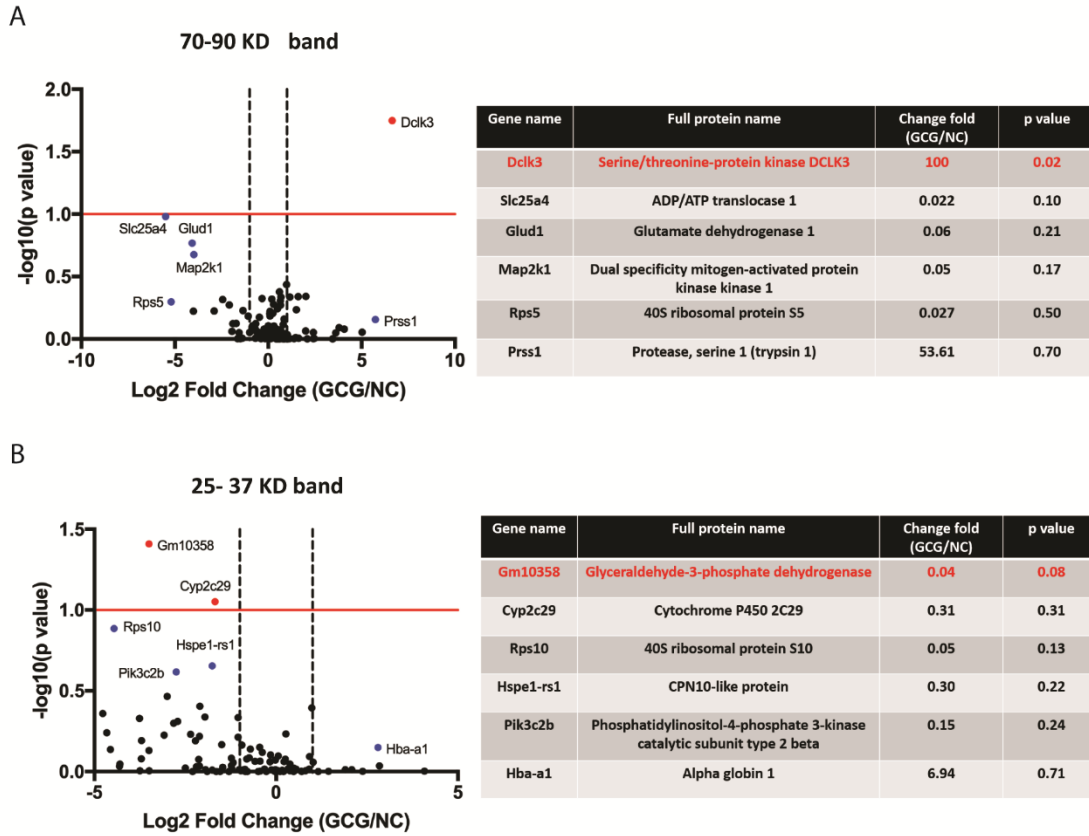


Figure 19: Protein discovery of phospho-PKA-substrates bands that responsive to acute portal succinate perfusion

Volcano plot and the top 6 differentially expressed PKA substrates associated proteins in the liver perfused with saline in contrast to glucagon for 20 minutes that are within 70 to 90 KD (A), and 25 to 37 KD (B).

4.2.4 Hepatic Sucnr1 knock-out has minimal effects on metabolic parameters

Increased circulating succinate has been observed in the setting of cardiometabolic disease [27, 28]. According to the EC50 and dose-effect curves of succinate for Sucnr1, the reported increases might be expected to double or triple the activity of Sucnr1 [50]. Thus, the succinate-Sucnr1 signaling has the potential to play a regulatory role in cardiometabolic disease. A recent study from Rossi and colleagues showed that activation Gi signaling in hepatocytes impairs glucose homeostasis and knocking down hepatic Gi signaling protected against diet-induced metabolic disease. Unfortunately, Rossi and colleagues did not clarify which specific Gi-coupled receptor(s) is/are mainly responsible for this regulatory effect. As we observed that the Gi-coupled Sucnr1 is expressed in hepatocytes and is the most highly expressed Gi-coupled GPCR in hepatocytes, we hypothesized that hepatic Sucnr1 might regulate liver metabolic function and glucose homeostasis.

Six-weeks-old LiSucnr1KO males and their littermate controls were challenged with chow versus high-fat/high-sucrose (HFHS, 45% Fat, 40% Sucrose) diet for 8 weeks. Eight weeks of HFHS diet induced significant obesity, adiposity, and glucose intolerance (Figure 20A - D). However, in contrast with our hypothesis that hepatic Sucnr1 might regulate glucose homeostasis or other metabolic parameters, liver-specific KO of Sucnr1 did not affect any of the measured physiological features including glucose tolerance (Figure 20A - D).

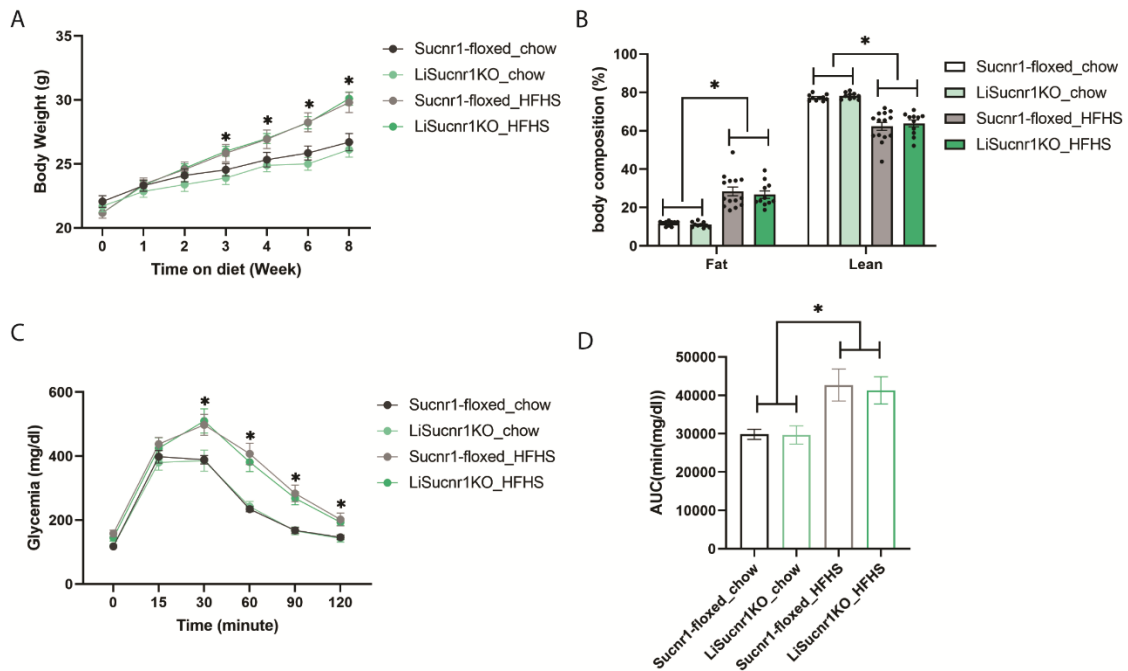


Figure 20: Hepatic *Sucnr1* knockout does not change metabolic phenotypes in high fat high sucrose induced metabolic disorder model

Body weight (A), body composition (B), glucose tolerance (C), and area under the curve (AUC) of the glucose tolerance test of *LiSucnr1KO* mice and their litter controls. n= 8-10 in each group. * indicates comparisons between diets reached statistical significance (<0.05) by two-way ANOVA.

Glucagon regulates not only glycemia, but also has marked effects on hepatic amino acid catabolism and its secretion is potently stimulated by dietary amino acids [92]. Therefore, we examined whether added amino acids in the form of a mixed meal which stimulates both glucagon and insulin secretion would elicit a glycemic phenotype in *LiSucnr1KO* mice. As was the case in the glucose tolerance test, the glycemic excursion increased in HFHS fed mice compared to chow controls. Chow-fed *LiSucnr1KO* mice had a 14% reduction in peak glycemia (15 min) compared to littermate controls, while the

HFHS-fed LiSucnr1KO mice tended to have 1.12-fold higher peak glycemia levels (Figure 21A). However, these effects are modest and there was no significant difference in area under the curve between LiSucnr1KO and littermate controls on either diet (Figure 21B). As glucagon signaling has profound effects on hepatic amino acid metabolism, we measured the ad libitum fed circulating amino acid levels in the LiSucnr1KO mice and their littermate controls. HFHS diet induced an increase in total circulating amino acid levels in the control Sucnr1-floxed animals, with significant increases specifically in circulating alanine and valine. In contrast, this induction was not apparent in the LiSucnr1KO mice (Figure 21C). These data may suggest that hepatic Sucnr1 plays a modest role facilitating the increase in some circulating amino acids that is observed with obesity that occurs with hypercaloric feeding. However, when we assessed the phospho-PKA substrate levels in these mice as a surrogate of hepatic glucagon signaling, we did not identify any significant changes in phosphorylated PKA substrate levels between LiSucnr1KO mice and controls (Figure 21D, 21E). This suggests that hepatic Sucnr1 does not have robust inhibitory effects on glucagon signaling. Moreover, we hypothesized that Sucnr1 would inhibit glucagon signaling. As glucagon drives catabolism of amino acids, we would have expected that loss of an opposing Sucnr1-mediated signal would have increased amino acid catabolism and reduced circulating amino acids. If anything, we observed the opposite (Figure 21C). Altogether, these data indicate that succinate, through hepatic Sucnr1, does not play a significant role in opposing hepatic glucagon signaling.

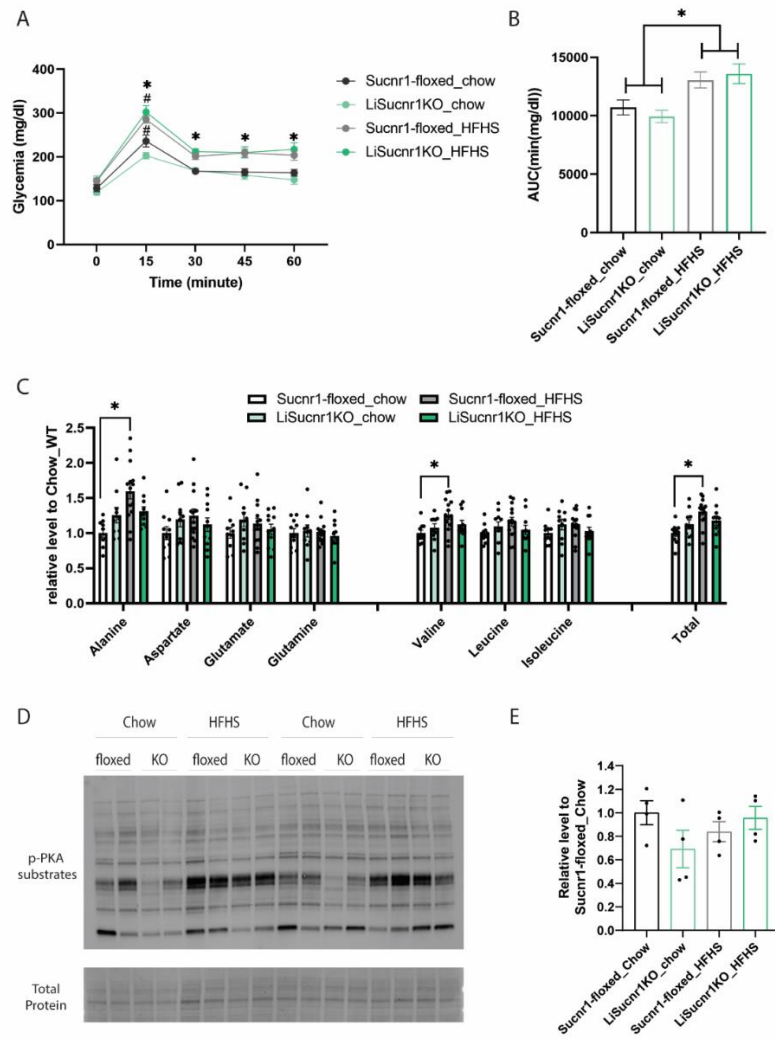


Figure 21: Liver Sucnr1 has modest regulatory effects of amino acid homeostasis

Mix-meal tolerance test (A), area under the curve of mix-meal tolerance test (B), circulating amino acid levels (C), and hepatic phosphor-PKA substrate levels (D, E) of LiSucnr1KO mice and their litter controls. n= 8-10 in each group. * indicates comparisons between diets reached statistically significance (<0.05) while # indicates comparisons between genotypes reached statistically significance (<0.05).

4.2.4 Explore hepatic Sucnr1's role on hepatic gene expression

Given the limited effect of Sucnr1 KO on measured metabolic parameters and additional observations inconsistent with our initial hypothesis that Sucnr1 might function to oppose Gcgr signaling, we next sought an unbiased approach to investigate potential functions of hepatic Sucnr. To do this we employed an unbiased approach assessing the impact of Sucnr1 on the hepatic transcriptome in liver tissue samples from LiSucnr1KO mice and their littermate controls by RNA-seq. In total, transcripts from 23,106 genes were identified in at least half of the samples. Among them, 510 genes were differentially expressed using liberal cutoff criteria without adjustment for multiple comparisons ($P < 0.05$, student's t-test) (Figure 22A, Appendix A). However, only 2 genes remained statistically significant after adjustment for a false discovery rate (FDR < 0.1 by Benjamini-Hochberg procedure) (Figure 22B). The largest change in mRNA levels was in the Sucnr1 transcript, which confirms successful knockout by the Cre-LoxP system (Figure 21B). The next most highly regulated gene is thiopurine methyltransferase (Tpmt) (1.87-fold increase in LiSucnr1KO compared to controls, $p = 0.0021$, FDR = 0.03), which is an enzyme of uncertain physiological function but potential clinical relevance, as it is required for catabolism of the immunosuppressive thiopurine class of drugs [93]. Variants in Tpmt that reduce enzyme activity and impair thiopurine catabolism pose significant risk of severe adverse drug reactions including myelosuppression, gastrointestinal intolerance, pancreatitis and hypersensitivity [94].

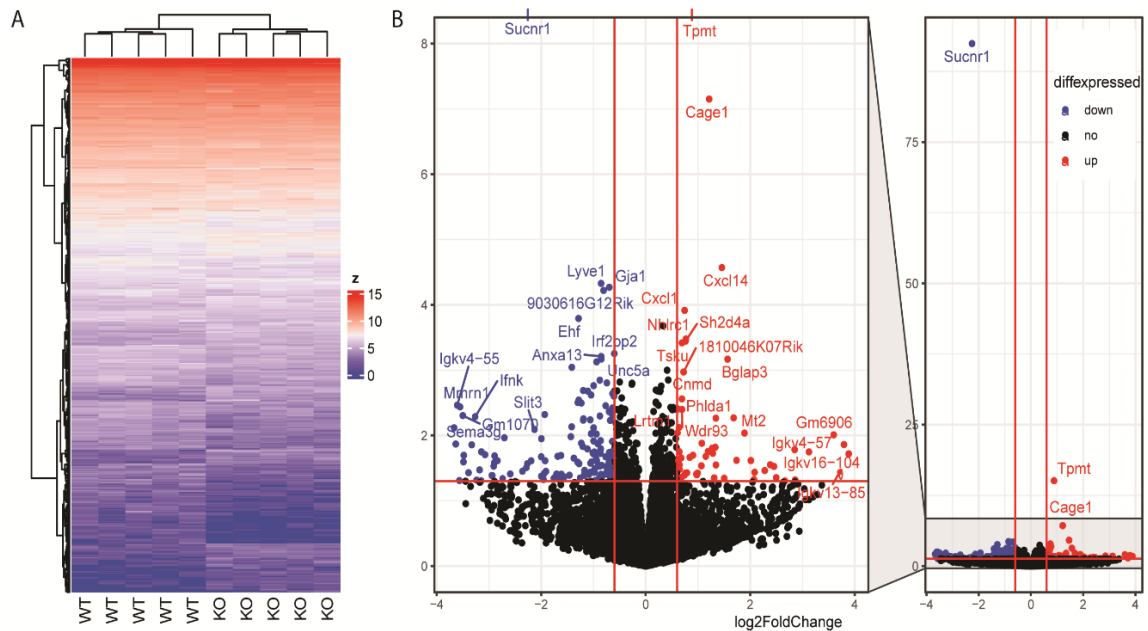


Figure 22: Liver *Sucnr1* knockout induce modest gene expression changes

Heat plot (A) and volcano plot (B) of the differentially expressed genes with a p value less than 0.05 by student's t test in the liver tissues of *Sucnr1*-floxed and Li*Sucnr1*KO mice by RNA-seq. For the heatmap, color refers to the frequency of the Euclidean distances between samples. The volcano plot is plotted using log₂FoldChange as the x-axis and -log₁₀(p value) as the y axis. n= 5 in each group.

By conducting pathway analysis using the enrichR package with the KEGG_2019_Mouse database [95], we observed that several gene sets associated with amino acid metabolism such as arginine biosynthesis (p = 0.000041, FDR = 0.005), alanine, aspartate and glutamate metabolism arginine (p = 0.00058, FDR = 0.037) and arginine and proline metabolism (p = 0.0018, FDR = 0.076) are the top up-regulated pathways in the Li*Sucnr1*KO compared to the *Sucnr1*-floxed littermate controls (Figure 22). Specifically, genes including Glutamate-pyruvate transaminase (GPT), Glutamate-pyruvate

transaminase 2 (GPT2), glutamate-ammonia ligase (Glul), Proline Dehydrogenase (Prodh), and Aldehyde Dehydrogenase 4 Family Member A1 (Aldh4a1) contributed significantly to enrichment for these pathways. These findings may correspond to the modest regulatory effects of hepatic *Sucnr1* on amino acid catabolism that we observed in the diet-induced metabolic disorders model detailed in 4.2.2. However, as indicated earlier, the trend induced by *Sucnr1* knockout conflicts with our original hypothesis that activation of *Sucnr1* might inhibit glucagon signaling in the liver.

Interestingly, *Gpt*, a previously established target of glucagon signaling in the liver, tends to increase in the absence of *Sucnr1* [96]. However, we saw no changes in other canonical transcriptional targets downstream of glucagon signaling.

Pathway analysis also suggests that hepatic *Sucnr1* may potentially participate in the regulation of carbohydrate homeostasis based on enrichment for genes involved in starch and sucrose metabolism ($p = 0.046$, FDR = 0.568) such as *Gck* and *Amy1* and decreased carbohydrate digestion & absorption ($p = 0.0039$, FDR = 0.134) including *G6pc* and *Sglt1* and *FoxO* and *Akt* signaling ($p = 0.0011$, FDR = 0.05) (Figure 23). Other differentially expressed gene sets included sets associated with liver infection including HPV infection ($p = 0.0011$, FDR = 0.055) and parasite infection ($p = 0.0053$, FDR = 0.153), and cancers including basal cell carcinoma ($p = 0.0043$, FDR = 0.133), hepatocellular carcinoma ($p = 0.0093$, FDR = 0.232), and ECM-receptor interaction ($p = 0.000035$, FDR = 0.004). This suggests that *Sucnr1* has the potential to participate in the regulatory effects

of liver immunity and inflammation. However, overall, there are limited differentially expressed genes between LiSucnr1KO and controls, suggesting hepatic Sucnr1 has only modest regulatory effects in the conditions that we studied these mice. Genes involved in the top 20 differentially expressed pathways are listed in Table 5 and Table 6.

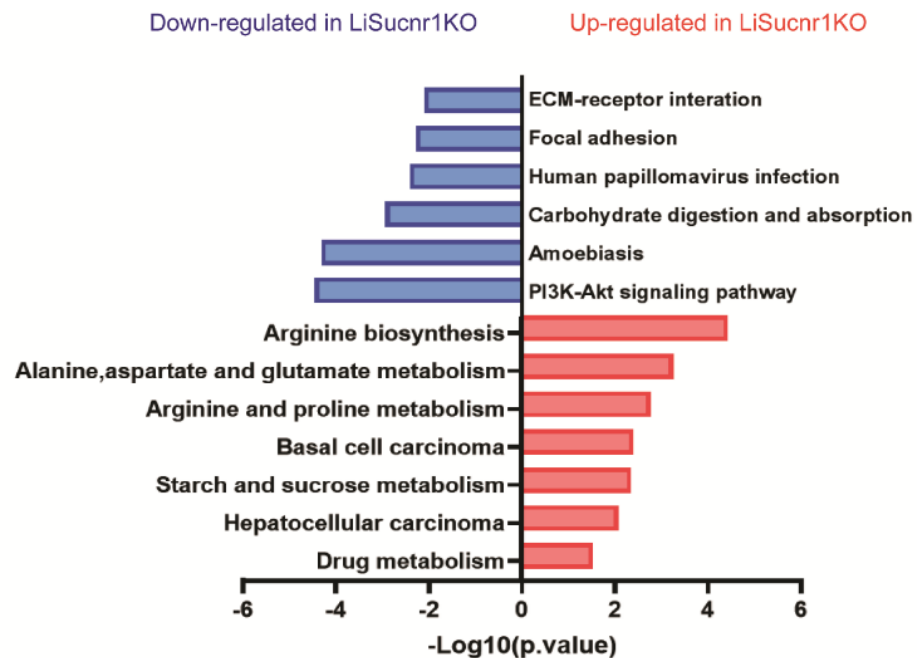


Figure 23: Differentially expressed pathways induced by liver Sucnr1 knockout

Pathway analysis (KEGG_2019_Mouse) has been conducted by EnrichR to illustrate the differentially expressed pathway in the liver tissues of Sucnr1-floxed and LiSucnr1KO mice. Red indicates the up-regulated pathways while blue indicates the down-regulated pathways in the LiSucnr1KO liver versus controls. n= 5 in each group.

Table 5: Top 20 up-regulated KEGG Pathways in LiSucnr1KO than controls

	Term	P.value	FDR	Genes
1	Arginine biosynthesis	3.97E-05	0.004964	ACY1; GPT2; GPT; GLUL
2	Alanine, aspartate and glutamate metabolism	0.000584	0.036503	ALDH4A1; GPT2; GPT; GLUL
3	Neomycin, kanamycin and gentamicin biosynthesis	0.051174	0.568093	GCK
4	Arginine and proline metabolism	0.001832	0.076343	GAMT; ALDH4A1; OAT; PRODH
5	Basal cell carcinoma	0.004266	0.133298	GADD45A; WNT9B; FZD8; GADD45G
6	Collecting duct acid secretion	0.032141	0.502197	SLC12A7; ATP6V0D2
7	Maturity onset diabetes of the young	0.032141	0.502197	GCK; FOXA2
8	Starch and sucrose metabolism	0.046426	0.568093	AMY1; GCK
9	Hepatocellular carcinoma	0.00928	0.232	GADD45A; DPF1; WNT9B; FZD8; GSTT1; GADD45G
10	Thyroid cancer	0.057004	0.568093	GADD45A; GADD45G
11	Drug metabolism	0.031769	0.502197	TPMT; FMO1; GSTT1; FMO4
12	Mineral absorption	0.077261	0.568093	MT2; MT1
13	Complement and coagulation cascades	0.064759	0.568093	CD59A; F11; CD46
14	Retinol metabolism	0.070117	0.568093	CYP2C68; CYP2A5; CYP2A4
15	Chemical carcinogenesis	0.075669	0.568093	CBR1; CYP2C68; GSTT1
16	Valine, leucine and isoleucine degradation	0.11614	0.685283	MCCC2; BCAT2
17	Breast cancer	0.068556	0.568093	GADD45A; WNT9B; FZD8; GADD45G
18	Endometrial cancer	0.123028	0.685283	GADD45A; GADD45G
19	Gastric cancer	0.072664	0.568093	GADD45A; WNT9B; FZD8; GADD45G
20	Cell cycle	0.138151	0.685283	GADD45A; E2F5; GADD45G

Table 6: Top 20 down-regulated KEGG Pathways in LiSucnr1KO than controls

	Term	P.value	FDR	Genes
1	ECM-receptor interaction	3.47E-05	0.00447	LAMA5; TNXB; LAMC3; LAMB2; COL6A2; TNC; SPP1; LAMC2
2	Focal adhesion	4.94E-05	0.00447	PDGFRB; LAMA5; TNXB; LAMC3; LAMB2; COL6A2; SPP1; TNC; PAK6; LAMC2; CRKL; IGF1R
3	Human papillomavirus infection	0.001146	0.05526	PTGER4; PDGFRB; LAMA5; TNXB; LAMC3; LAMB2; TNC; ISG15; LAMC2; LFNG; MFNG; COL6A2; SPP1; WNT4
4	Toxoplasmosis	0.001221	0.05526	GNAO1; LAMA5; LAMC3; IL10RB; LAMB2; TAB2; LAMC2
5	Carbohydrate digestion and absorption	0.003865	0.13992	G6PC; HKDC1; SLC5A1; TAS1R3
6	Amoebiasis	0.005283	0.15313	LAMA5; PLCB4; MUC2; LAMC3; LAMB2; LAMC2
7	Axon guidance	0.005922	0.15313	CAMK2D; ABLIM2; UNC5A; SEMA4D; SEMA3G; PAK6; SLIT3; WNT4
8	Glutamatergic synapse	0.007483	0.16015	GNAO1; PLCB4; HOMER3; CACNA1C; SHANK3; SHANK2
9	PI3K-Akt signaling pathway	0.007963	0.16015	PDGFRB; LAMA5; TNXB; G6PC; LAMC3; LAMB2; COL6A2; SPP1; TNC; LAMC2; PCK1; IGF1R
10	Wnt signaling pathway	0.010616	0.19215	SFRP1; CAMK2D; PLCB4; DAAM2; SFRP5; CTNNBIP1; WNT4
11	FoxO signaling pathway	0.014724	0.24228	G6PC; CCNG2; SETD7; HOMER3; PCK1; IGF1R
12	Long-term potentiation	0.018166	0.26181	CAMK2D; PLCB4; RPS6KA2; CACNA1C
13	Glucagon signaling pathway	0.018804	0.26181	CAMK2D; G6PC; PLCB4; SIK1; PCK1
14	Gastric acid secretion	0.025159	0.29973	CAMK2D; PLCB4; KCNJ16; KCNJ2

15	Renin secretion	0.027416	0.29973	PTGER4; PLCB4; CACNA1C; KCNJ2
16	Cholinergic synapse	0.027799	0.29973	GNAO1; CAMK2D; PLCB4; CACNA1C; KCNJ2
17	Hedgehog signaling pathway	0.028151	0.29973	EVC2; EVC; PTCH2
18	Pathways in cancer	0.031833	0.3201	PTGER4; PDGFRB; LAMA5; CAMK2D; GSTP2; LAMC3; LAMB2; PTCH2; LAMC2; CRKL; RUNX1; IGF1R; PLCB4; WNT4
19	Type II diabetes mellitus	0.035204	0.32072	HKDC1; PRKCD; CACNA1C
20	Neurotrophin signaling pathway	0.035807	0.32072	CAMK2D; IRAK2; RPS6KA2; PRKCD; CRKL

4.2.5 Exploration of *Sucnr1* function in human exome sequencing data

To gain further insight into potential functions of *Sucnr1*, we assessed recently released UK Biobank exome sequencing data for phenotypic associations with coding variants in *Sucnr1* [97]. Interestingly, according to this dataset, putative loss of function variants in *Sucnr1* associate with uncharacterized liver inflammation at sub-genome wide significance levels ($P = 0.000068$, $\text{Beta} = 0.29$, SKAT-O burden test) [97]. These variants did not associate with any other phenotype at comparable significance levels. These data suggest a role for hepatic *Sucnr1* specifically in liver inflammation.

4.3 Discussion

Recent studies suggest the succinate-Sucnr1 signaling axis regulates pleiotropic biological activities including urine filtration [51], immune responses [52, 53], and thermogenesis [54, 63]. Consistent with these functions, Sucnr1 is highly expressed in the kidney, immune cells, and adipose tissue [80]. In this study, we have investigated the expression of Sucnr1 in the liver by analyzing publicly available single-cell RNA-sequencing datasets and showed that Sucnr1 expression in hepatocytes is at least comparable to that in the liver non-parenchymal cells including hepatic stellate cells, Kupffer cells, and endothelial cells (Figure 13 and Figure 14). This finding directly contradicts prior literature that suggested that Sucnr1 was predominantly expressed in non-parenchymal cells with little to no expression in hepatocytes [12, 81]. The view that “Sucnr1 barely expresses in hepatocytes” is supported by studies conducted by Correa and colleagues and Liu and colleagues where they had not detected any mRNA and protein expression of Sucnr1 in cultured isolated primary hepatocytes [12, 81]. However, in their studies, RNA expression was measured in cultured primary cells. It was well-established that significant dedifferentiation occurs as soon as 6 hours after isolating and plating primary hepatocytes, associated with downregulation of many genes expressed that are expressed in fully differentiated hepatocytes [82]. This possibility is supported by studies where RNA-sequencing was conducted in freshly isolated primary hepatocytes, and compared with primary hepatocytes after culturing for 1 or 3 days [83]. This study

showed that the expression of *Sucnr1* decreased by 90% after 1 day in culture and was undetectable after 3 days in culture [83]. It should be noted that the expression of most GPCRs diminished in culture including the glucagon receptor [83]. These results inform upon the limitations of using cultured primary cells to make strong conclusions as to whether genes are expressed or not expressed in relevant cell types *in vivo*.

A recent study from Mills and colleagues compared *Sucnr1* expression in hepatocytes versus liver non-parenchymal cells by fluorescent in situ hybridization using frozen liver sections [79]. Unfortunately, the staining pattern of *Sucnr1* in this study was strongly non-specific, which limits the conclusions that can be drawn from their work.

In our study, we freshly isolate liver parenchymal versus non-parenchymal fractions in distinct genetic mouse models: *Sucnr1*-floxed, liver-specific (Alb-Cre) *Sucnr1* knock-out, and hepatocyte-specific (AAV-TBG-Cre) knock-out mice. The entire isolation process required no more than 1 hour and the isolated cells were immediately transferred to TRI reagent to minimize degradation of RNA. Our data show that *Sucnr1* expression is significantly higher in hepatocytes than in the liver non-parenchymal cells (Figure 17 and Figure 18). Considering the fact that hepatocyte accounts for ~70% to 80% of total cells in the liver, this finding suggests that succinate-*Sucnr1* signaling may participate in the regulation of hepatocyte function.

We initially hypothesized that *Sucnr1* would oppose *Gcgr* and participate in the regulation of glucose and amino acid homeostasis. However, our *in vivo* characterization

did not demonstrate robust effects of *Sucnr1* KO on relevant phenotypes. We observed modest effects on the regulation of the glycemic response to a mixed-meal tolerance test and a subtle trend for changes in circulating amino acid levels. However, the direction of change in the circulating amino acid levels in Li*Sucnr1*KO mice is inconsistent with our hypothesis that *Sucnr1* inhibits glucagon signaling. Overall, we conclude that *Sucnr1* does not play a major role in regulating metabolic parameters associated with glucagon signaling.

Therefore, we sought an unbiased method to begin to elucidate the function of *Sucnr1*. Via RNA-sequencing of liver samples from Li*Sucnr1*KO mice and controls, we demonstrated that hepatic *Sucnr1* knock-out induced modest changes in gene expression (Figure 21). To our surprise, the only significantly altered gene after Benjamini-Hochberg adjustment, other than *Sucnr1* itself, is thiopurine methyltransferase (*Tpmt*). *Tpmt* is highly expressed in endocrine tissues such as thyroid gland, and digestive tissues including liver and gastrointestinal tract [97]. *Tpmt* catalyzes the breakdown of 6-thioguanine and azathioprine, which are important therapies for certain types of cancers and immune diseases [98]. In this regard, measuring *Tpmt* activity is a common procedure in clinics for patients undergoing treatment with 6-thioguanine and azathioprine as variants in *Tpmt* which affect enzyme activity impact dosing regimens [99]. However, the normal physiological function of *Tpmt* is uncertain.

Interestingly, in a GWAS study conducted in cattle, genetic variants in *Tpmt* associated with parasite burden of a liver fluke [100]. Consistent with the possibility that *Sucnr1* mediated regulation of *Tpmt* may be important in the response to parasites, succinate is one of the common products of protist parasites including amoebae, helminth, diplomonads, trichomonads, and trypanosomatids [101]. Moreover, gene sets associated with parasitic infections including amoebiasis and toxoplasmosis emerged as significant in our gene set enrichment analysis. Additionally, recent exome sequencing data from the UK Biobank suggests that loss of function variants in *Sucnr1* in humans associates with liver inflammation. One other piece of data pointing to a relationship between *Sucnr1* and parasitic infections is that *Sucnr1* is also highly expressed in intestinal tuft cells which is an intestinal cell type that plays a major role in responding to bacterial and parasitic infections [102].

Thus, exploring whether hepatic succinate-*Sucnr1* signaling participates in the regulation of liver parasitic infections and whether this regulation is mediated via *Tpmt* are promising directions for future research. Whether or not gut-derived circulating succinate might also play a role in this biology also remains to be evaluated.

4.4 Conclusion

In the liver *Sucnr1* is predominantly expressed in hepatocytes and much less so in liver non-parenchymal cells. Given the intestinal contribution to circulating succinate and the elevated levels in portal compared to peripheral circulation, hepatic *Sucnr1* is well-positioned to respond to this potential gut-derived signal. Our initial studies suggest potential roles for hepatic *Sucnr1* in amino acid metabolism and liver inflammation. However, additional studies will be required to fully evaluate hepatic *Sucnr1* function.

5. Investigation into the use of the gut-derived TCA cycle intermediates as biomarkers of intestinal metabolism in metabolic disease

5.1 Introduction

Metformin is a first-line anti-diabetic drug that is widely prescribed worldwide. In addition to its benefits for treating diabetes, metformin may also have benefit for treating obesity [103], non-alcohol fatty liver disease [104], Alzheimer's disease [105], and even some cancers [106, 107]. The beneficial effects of metformin for diabetes are often attributed to its effects on reducing hepatic glucose production [108]. However, despite intensive investigation for decades, the major target organs and the underlying mechanism mediating its beneficial effects remain controversial [109].

The most common side effect of metformin is gastrointestinal symptoms including vomiting, bloating, and diarrhea [110]. Studies have shown that metformin is concentrated in intestinal tissue and its concentration there is 100- to 300-fold higher than that in serum [111, 112]. Interestingly, metformin's preference for the gut is independent of the route of delivery, as study shows that intravenous injected metformin also accumulates in the intestine tissue [113]. Moreover, studies suggest that restricting metformin absorption in the gut blunts its effects on lowering glucose production [114], while intravenous injection of metformin fails to increase glucose production [115]. The liver also concentrates metformin but to a lesser degree than intestinal tissue [113]. The

role of intestinal tissue versus liver in metformin action remains uncertain. Additionally, the biological effects of metformin on intestinal function have received far less attention than its effects in liver.

Our work showed that intestinal tissue is a major contributor to circulating TCA cycle intermediates (Section 3). Additionally, studies from our lab and others have shown that fructose is extensively metabolized in the small intestine [57, 116], and that carbon in fructose is readily incorporated into gut-derived TCA cycle intermediates ([57] and Figure 3). We hypothesized that intestinal fructose metabolism and TCA cycle intermediate production could be used to probe intestinal metabolism *in vivo*. Moreover, we hypothesized that this approach could be used to investigate the ability of metformin to regulate multiple aspects of intestinal metabolism. Successful completion of this study might not only advance our insights into metformin's effects on intestinal metabolism, but could also provide a promising strategy to evaluate intestinal metabolism using non-invasive techniques in a range of applications.

5.2 Results

5.2.1 Establish a short-term metformin intervention animal model

In human type-2 diabetes patients, a short-term (7 days) of metformin treatment significantly improves glucose tolerance without altering body weight [117]. To better

understand the effects of metformin in adverse metabolic conditions, 18-week-old wildtype C57BL/6J mice were preconditioned with 1 week of high-fat/high-sucrose diet (45% Fat, 40% Sucrose). After that, animals were oral gavaged daily with either metformin or water for two weeks (Figure 24). We used a dose of 250 mg metformin / kg body weight which is a dose comparable to the dose used in human patients and sufficient to improve glucose tolerance and increase intestinal production of the peptide hormone GDF15 independently of changes in body weight in a prior publication [118].

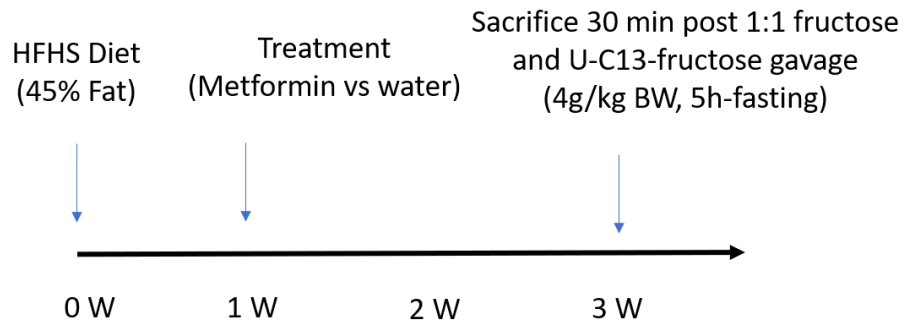


Figure 24: Timeline of the metformin study

5.2.2 Short-term metformin treatment improves glucose tolerance

After 2 weeks of treatment, the body weight of mice in the metformin group (33.5 ± 2.7 g, Figure 25A) was similar to that of the control group (34.2 ± 2.1 g, Figure 25A). Similarly, the fasting glycemia levels remained comparable between the water group and metformin group (Figure 25B). Although no differences in body weight or fasting

glycemia were observed, 2 weeks of metformin treatment significantly improved glucose intolerance (Figure 25C, 25D). These results indicate that short-term metformin administration is sufficient to enhance systemic glucose homeostasis independently of changes in body weight.

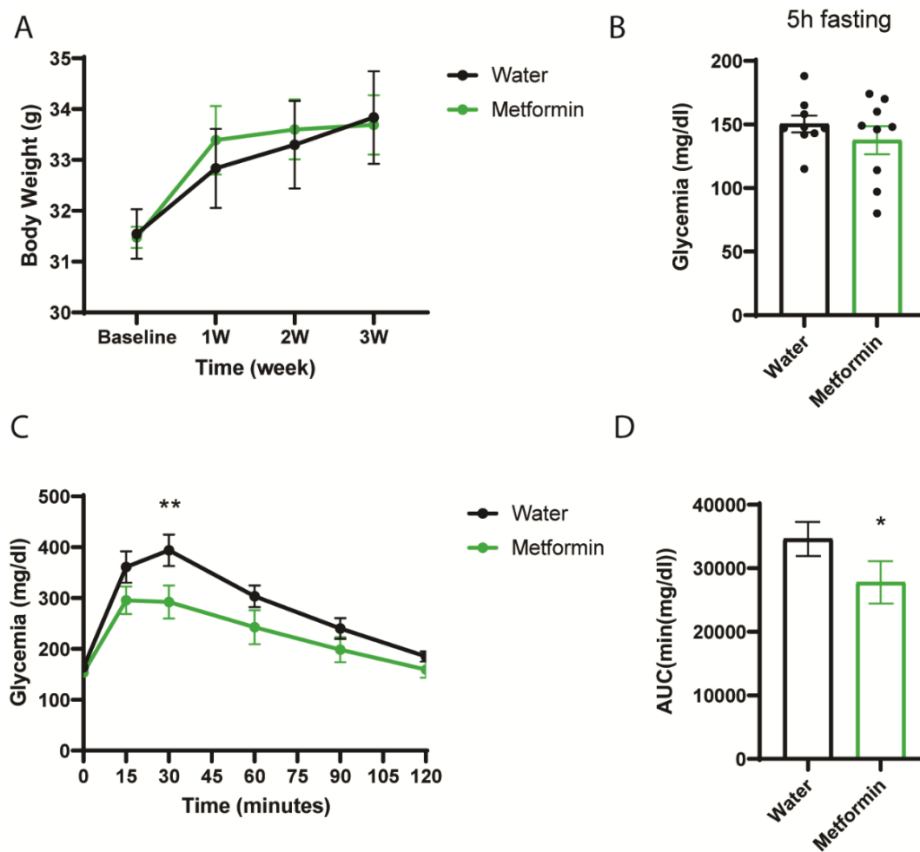


Figure 25: Short-term of metformin treatment improves glucose tolerance

Body weight (A), fasting glycemia (B), glucose tolerance test (C) and area under the curve of glucose tolerance test (D) of wildtype C57BL/6J mice that were treated with either water or metformin for 2 weeks. n=9 in each group. p<0.05; ** p<0.01. Data were analyzed by student's t test between water and metformin group.

5.2.3 Short-term metformin treatment decreased fructose metabolism in the intestine tissue

After 2 weeks of metformin versus control treatment, animals from all groups were sacrificed 30 minutes after oral-gavage with 1:1 unlabeled fructose and universal carbon-13 labeled fructose (U-C13-fructose) at a dose of 4g/kg. GC/MS was conducted to assess fructose metabolism in the intestine tissue, portal blood, and liver tissues. A graphical abstract of intestinal fructose metabolism is depicted in Figure 26.

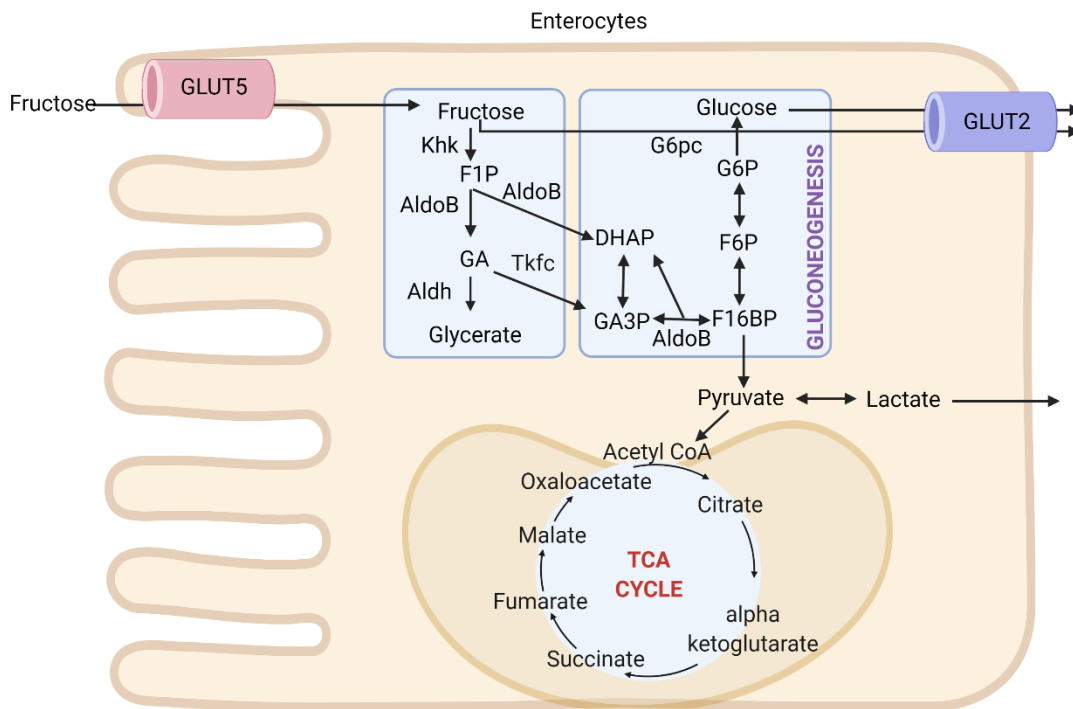


Figure 26: Intestinal fructose metabolism

The levels of both M+0 and M+6 isotopes of fructose-1-phosphate (F1P), were significantly decreased in the intestinal tissue of mice in the metformin group compared to control (Figure 27A). Metformin also significantly decreased the enrichment of three-carbon metabolites, glyceraldehyde 3-phosphate (GA3P) and glycerate (Figure 27B and C). These data suggest that fructose catabolism to three-carbon metabolites is significantly decreased by metformin treatment in the intestine tissue.

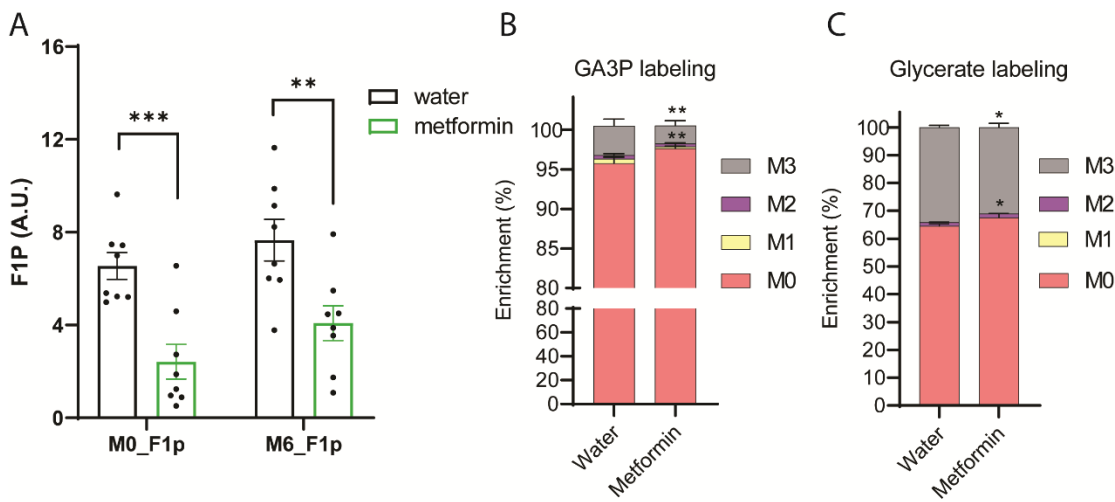


Figure 27: Metformin decrease fructose metabolism in the intestine tissue

Total ion counts of F1P (A), enrichment of GA3P (B) and Glycerate (C) in the intestinal tissue were measured by GC/MS using M6-F6P as internal standards. n=8 in each group. Two samples were excluded from GC/MS analysis due to poor sample quality. p<0.05; ** p<0.01; *** p<0.001. Data were analyzed by student's t test.

5.2.4 Metformin treatment decreases the flux from pyruvate into TCA cycle of PDH in the intestine tissue

We next investigated the role of metformin on intestinal metabolism by assessing the flux of labeled fructose-derived metabolites into the TCA cycle. Metformin treatment reduced enrichment of labeled carbon in pyruvate and the TCA cycle intermediates (Figure 28 A - D). The degree of reduced labeling was more pronounced in the TCA cycle intermediates than in pyruvate (Figure 28 A - D). These results suggest the possibility that metformin reduced flux through pyruvate dehydrogenase (PDH). In support of this hypothesis, the protein levels of pyruvate dehydrogenase E1 component subunit alpha (PDHA), the enzyme responsible for pyruvate decarboxylation into acetyl-CoA, were reduced by metformin treatment (Figure 28 E, F). Phosphorylation of PDHA Ser293 inhibits the activity of pyruvate dehydrogenase complex. We observed an increase in the ratio of phosphorylated PDHA Ser293 to PDHA in the metformin group as the reduction in total PDHA was larger than the reduction in phosphorylated PDH. Altogether, these results suggest that 2 weeks of metformin treatment may inhibit intestinal pyruvate dehydrogenase activity and decrease flux of substrate into the TCA cycle.

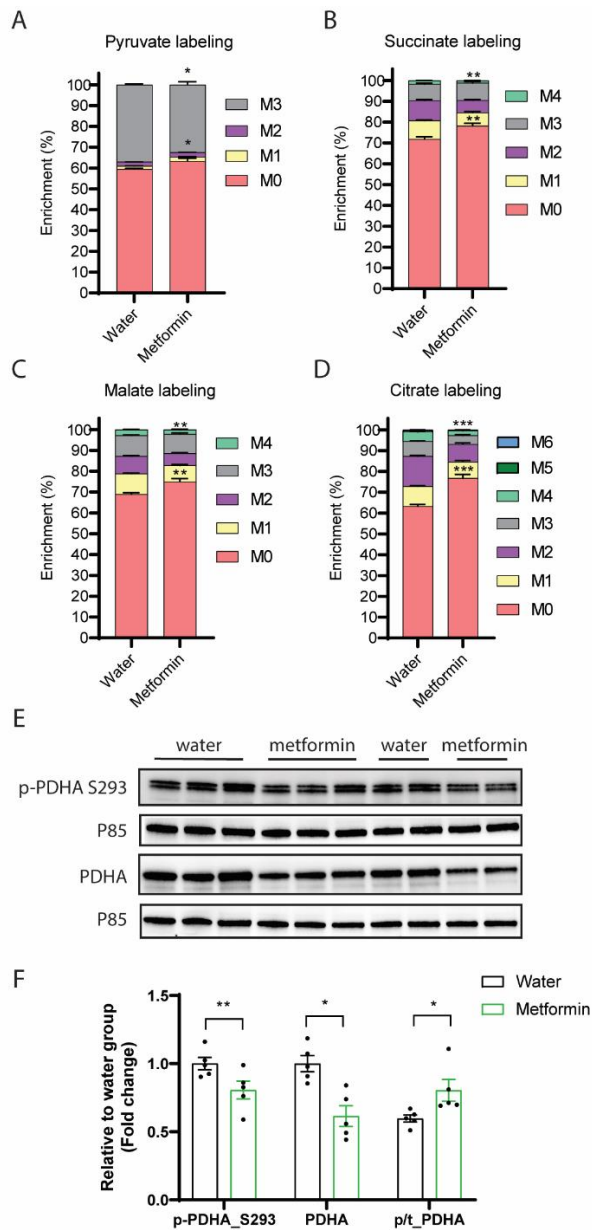


Figure 28: Metformin decreased the flux of labeled substrate into the TCA cycle in association with reduced pyruvate dehydrogenase

The enrichment of pyruvate (A), Succinate (B), Malate (C), and Citrate (D) in the intestine tissue. The blot (E) and quantification (F) of phospho-PDHA S293 and total PDHA by Western Blot. n=9 in metabolomics study and n=5 in the Western Blot. p<0.05; ** p<0.01; *** p<0.001. Data were analyzed by student's t test.

5.2.5 Metformin altered citrate concentrations in the intestine tissue and portal plasma

One interesting finding from our quantification of intestinal TCA cycle intermediate levels is that metformin significantly decreased citrate levels (Figure 29A). Agreeing with this finding, citrate levels were also remarkably blunted in the portal plasma (Figure 29B). In contrast to the decrease of citrate levels, malate levels were upregulated in the portal plasma (Figure 29B). These opposite trends suggest possible impairment in flux from malate to citrate in the TCA cycle. It is known that high levels of metformin can inhibit complex I activity, which is coupled to malate dehydrogenase [119]. It is possible that in the intestine where metformin is highly concentrated, an inhibited complex I activity results in reduced conversion of malate to citrate, reflected in the increased malate levels and decreased citrate levels in portal plasma.

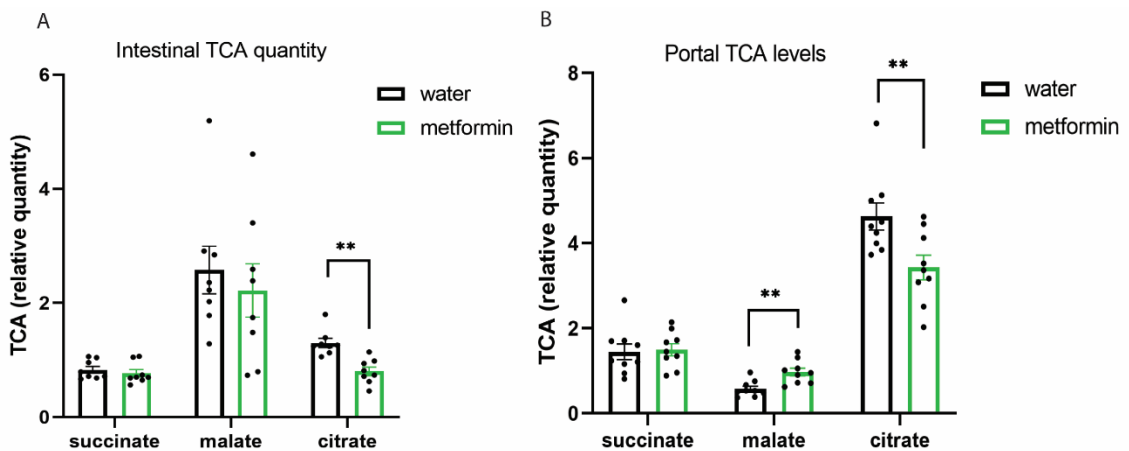


Figure 29: Metformin decreased citrate levels in the intestine tissue and portal plasma

Intestinal (A) and portal (B) TCA cycle intermediates levels after 30 minutes post fructose gavage. n=9 in each group. ** p<0.01. Data were analyzed by student's t test.

5.2.6 Decreased intestinal fructose metabolism induced by metformin is associated with increased AMPK signaling

We next investigated molecular mechanisms that might contribute to metformin's apparent effects to reduce fructose metabolism. Fructose metabolism starts by the production of F1P catalyzed by ketohexokinase (Khk), after which F1P is cleaved to form dihydroxyacetone phosphate (DHAP) and glyceraldehyde 3-phosphate (GA3P) by Aldolase B (AldoB) [67]. Carbohydrate-responsive element-binding protein (ChREBP), a transcriptional factor that is extensively induced by fructose exposure, is suggested to promote the expression of Khk and AldoB transcriptionally [120]. We measured the mRNA levels of the fructose sensing transcription factor ChREBP and fructolytic enzymes Khk and AldoB in the intestinal tissue. The mRNA levels of ChREBP, Khk and AldoB all remained comparable between the water and metformin group (Figure 30A), suggesting that the effects of short-term metformin treatment on fructose metabolism is unlikely to be mediated through transcriptional regulation of fructolytic enzymes. Additionally, the protein levels of both Khk and AldoB remained comparable between the water and metformin groups (Figure 30B), suggesting the effects of short-term metformin on fructose metabolism are not regulated by translation of key fructolytic enzymes.

AMPK, a well-known cellular energy sensor that monitors cellular energy charge (reflected in the AMP to ATP ratio), is robustly activated by metformin treatment [121]. We therefore investigated whether AMPK activity may regulate fructose metabolism.

Previous studies showed that the phosphorylation of Thr172 correlates with AMPK activity [122]. As the measurement of AMP, ADP, and ATP in the intestinal tissue remains a technical challenge for our group, we assessed the ratio of phospho-AMPK Thr172 levels to total AMPK-alpha levels as a surrogate of AMPK activity (Figure 30 C, D). Consistent with the hypothesis, increased AMPK phosphorylation was detected in the intestinal tissue in the metformin group. This could potentially arise from increased AMP/ATP ratio in the intestine tissue although this has not been measured directly. As discussed above, metformin treatment decreased the labeling of TCA cycle intermediates from isotope precursors as an indicator of reduced TCA cycle flux (Figure 28). Because TCA cycle flux accounts for most ATP production, the decreased TCA cycle flux in the intestine tissue of metformin treated animals may potentially impair ATP generation, leading to an increase in AMP/ATP ratio and activation of AMPK signaling in the intestine tissue. In addition, a large amount of ATP is consumed via fructose phosphorylation by KHK following an oral fructose load, providing another mechanism for lowering ATP and impairing fructose metabolism [123, 124].

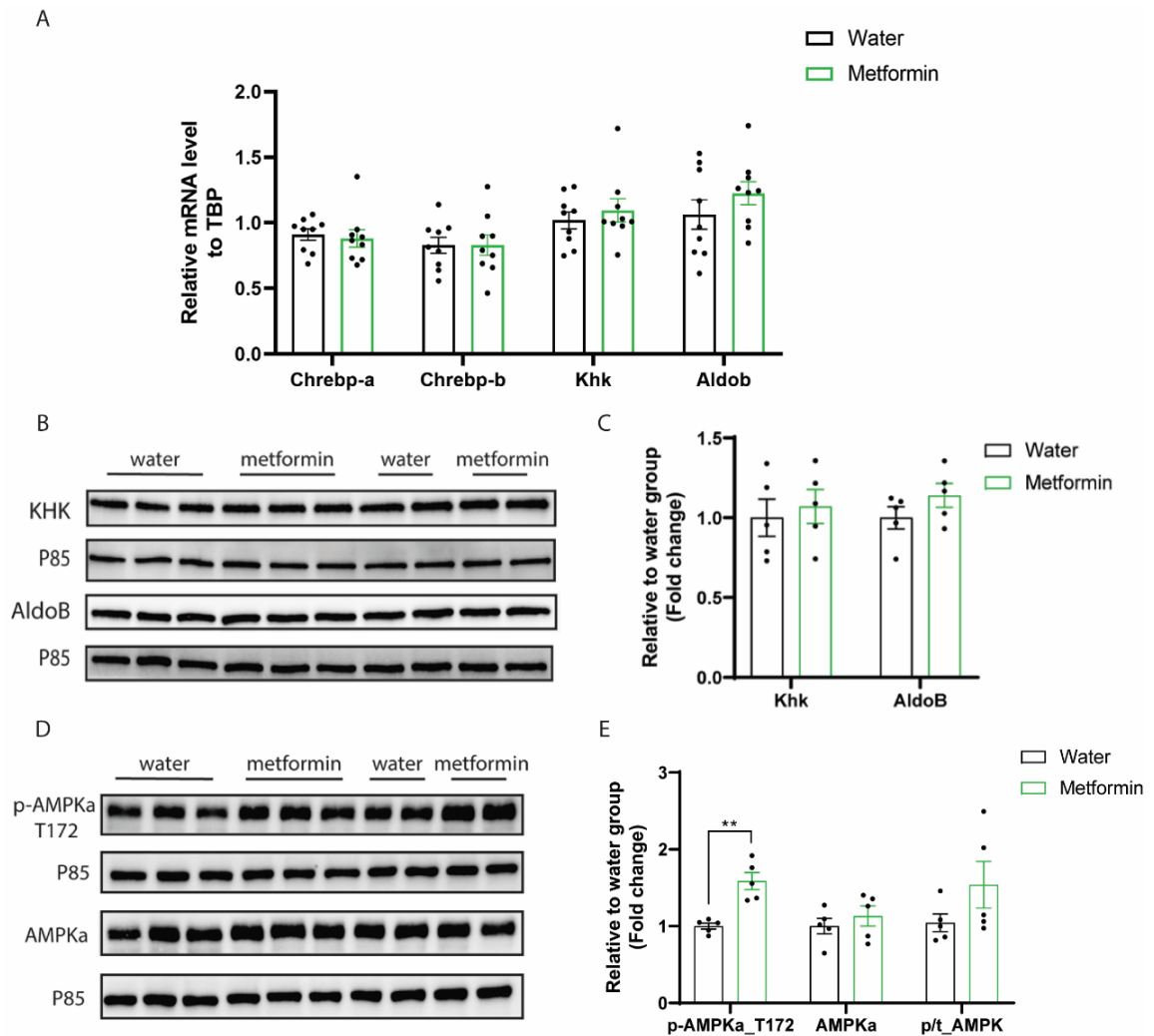


Figure 30: The effects of decreased intestinal fructose metabolism induced by metformin associates with increased activity of AMPK signaling

A. mRNA levels of fructose sensing transcriptional factor and fructolytic enzymes in intestine tissue were assessed by qPCR. The blot (B) and quantification (C) of Khk and AldoB by Western Blot. n=9 in qPCR; n=5 in Western Blot experiment. p<0.05; ** p<0.01; *** p<0.001. Data were analyzed by student's t test.

5.2.7 Short-term metformin treatment inhibits intestinal glucose production

It is well-established that metformin inhibits endogenous glucose production and it is commonly assumed that this occurs via reduction in hepatic glucose production [125]. However, we and others have provided evidence that the intestine is also a major site of glucose production [116, 126]. No studies have investigated whether metformin could impact intestinal glucose production. In this study, we did not identify any differences in systemic (tail vein) glycemia between metformin treated mice and controls (Figure 31 A). However, both the M+0 and M+3 isotope of portal glucose were significantly decreased in the metformin group when compared to control (Figure 31 B). Similarly, levels of the M+0, M+3, and M+6 isotopes of glucose were significantly lower in the intestine tissue of metformin treated mice (Figure 31 C). These data suggest that short-term metformin treatment is sufficient to decrease net intestinal glucose production, although this decrease may not be sufficient to reduce systemic glycemia. Intestinal expression of key gluconeogenic genes, G6pc and PCK1, was significantly reduced by short-term metformin treatment (Figure 31 D). Altogether, these data strongly suggest that 2 weeks of metformin treatment is sufficient to inhibit intestinal glucose production, and this may be mediated in part through negative regulation of intestinal gluconeogenic enzyme expression.

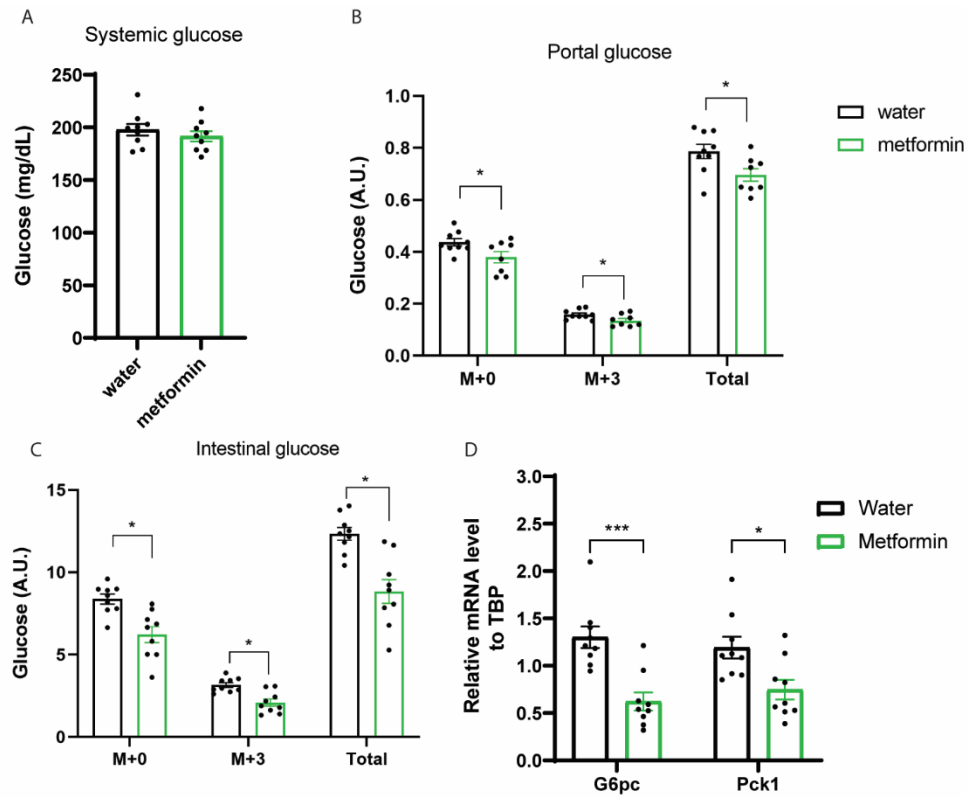


Figure 31: Metformin decrease intestinal glucose production

Systemic (A) and portal (B) glucose levels after fructose gavage. Systemic glucose levels were measured with the tail blood samples using the glucose oxidation kit. Portal glucose levels were measured with the portal blood samples using GC/MS. mRNA levels of gluconeogenic genes were measured by qPCR. n=9 in each group. p<0.05; ** p<0.01; *** p<0.001. Data were analyzed by student's t test.

5.2.8 Short-term metformin treatment decreases the delivery of fructose and fructose-derived metabolites to the liver

Recent studies suggest that the intestine shields the liver from exposure to fructose [57], and only hepatic fructose metabolism accounts for the fructose-induced diseases [127]. As we have shown above that metformin decrease fructose metabolism and flux into the TCA cycle in the intestine tissue, we next explored the potential effects of metformin on fructose delivery to the liver tissue. In this regard, we assessed the levels of fructose and fructose-derived metabolites in the portal blood. Metformin treatment decreased portal fructose levels by ~40% (Figure 32 A). Metformin treatment also reduced the enrichment of isotope-labeled TCA cycle intermediates in the portal circulation (Figure 32 B, C, D). These results indicate that metformin impairs the delivery of fructose and fructose-derived metabolites to the liver via the portal vein. Consistent with this, the levels of both the M+0 and M+6 isotopomer of F1P decreased in the liver tissues of metformin treated mice (Figure 32 E). The levels of hepatic GA3P decreased similarly with metformin treatment (Figure 32 F).

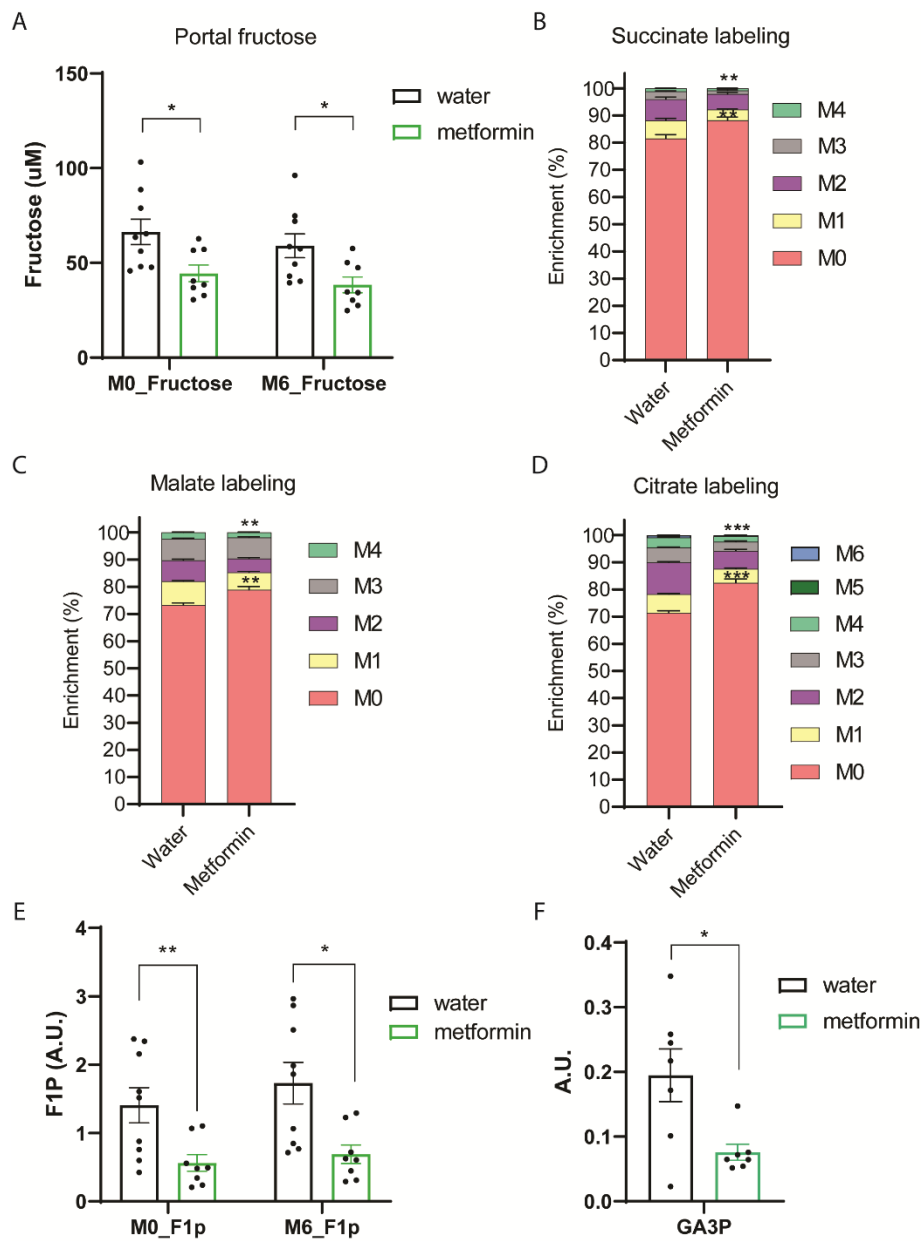


Figure 32: Metformin decrease fructose delivery to the liver

A. Portal fructose levels were measured by GC/MS using M2-fructose as internal standard. The enrichment of succinate (B), malate (C), and citrate (D) were measured by GC/MS using norvaline as internal standard. The F1P levels (E), and GA3P levels (F) were measured by GC/MS using M6-F6P as internal standard. $p < 0.05$; ** $p < 0.01$; *** $p < 0.001$. Data were analyzed by student's t test.

5.3 Discussion

Despite the fact that metformin is widely prescribed and investigated for years, the major effect tissue(s) accounting for metformin's role in lowering glucose production and its underlying mechanism remain uncertain. Overall, the view that metformin's effects and mechanism depend on concentration is accepted in the field [128]. In humans, metformin is typically used at a dose of 1.5 – 2.5 g daily which results in an effective plasma concentration in the ~5 to 10 μM range [129]. In mice, to achieve a ~5 μM plasma concentration requires a dose of ~ 250 mg/kg orally [130]. In contrast to the low circulating concentrations, metformin concentrates in specific tissues, including the intestine and liver tissues which reached ~ 5 mM, and ~ 100 μM respectively [113, 131]. Accordingly, studies suggest that metformin's effects appear to be dose-dependent. Specifically, a relatively low dose of metformin (50 to 80 μM) is sufficient to activate AMPK activity and reduce glucose production by the LBK-AMPK pathway [132]. Additionally, a recent study suggests that therapeutic concentration of metformin (5 to 30 μM) could activate lysosomal AMPK by binding to PEN2-ATP6AP1 to inhibit vATPase without altering AMP and ATP levels [133]. On the other hand, metformin is also reported to activate AMPK signaling via inhibiting Complex I of the mitochondrial electron transport chain at higher concentrations (~ 150 μM) [119]. Thus, the concentration of metformin in target tissue may determine metformin's effects and mechanism of action.

As discussed above, metformin concentrates to high levels in intestinal tissue [111, 112]. Additionally, studies reveal that intravenous administration of metformin or reducing intestinal metformin absorption impairs metformin's effects on lowering glucose production [114, 115]. Despite these data indicating that the intestine may be relevant for metformin action, few studies have investigated the role of metformin on intestinal functions and its association with systemic glucose homeostasis.

In this study, we hypothesized that we could use intestinal fructose metabolism and TCA cycle intermediate production after an isotope-labeled oral fructose bolus to probe intestinal metabolism after short-term metformin treatment. Indeed, we demonstrated that metformin decreased intestinal fructose metabolism, incorporation of fructose-derived substrate into the TCA cycle, reduced intestinal glucose production, and reduced the delivery of fructose to the liver. These data indicate that our fructose gavage methodology is able to produce a range of valuable metabolic measurements that inform upon intestinal metabolism in vivo. Thinking translationally, this approach may be useful in large-scale studies of human intestinal metabolism. In this regard, this approach has the potential to open a new era for investigating intestinal metabolic function.

With the prevalence high fructose corn syrup in the typical Western diet, fructose and fructose related disease has attracted increasing attention. Studies conducted in both human and rodents support the hypothesis that increased fructose consumption contributes to metabolic disorders including obesity, insulin resistance, and NAFLD [134-

136]. Intestinal tissue is a major site of fructose metabolism and shields the liver from fructose induced metabolic disease [57], as hepatic fructose metabolism appears to be essential for the development of fructose related pathologies like increased *de novo* lipogenesis and insulin resistance [137]. One prior study suggested that fructose-induced metabolic disease may be attenuated by metformin treatment in mice although this was attributed to an effect of metformin to alter the microbiome and protect against deterioration of gut barrier function [138]. Nevertheless, our results are consistent with protective effects of metformin against fructose-induced metabolic disease as we demonstrated that metformin decreased fructose delivery to the liver , as indicated by decreases in portal fructose and hepatic fructose-derived metabolites in metformin-treated animals. (Figure 31). In this regard, metformin may serve as a promising strategy to protect against fructose-induced metabolic disease.

In addition to decreasing fructose delivery to the liver, we also demonstrated that metformin decreased intestinal fructose metabolism using isotope-tracing metabolomics. Specifically, intestinal F1P levels were nearly halved in metformin-treated animals when compared to controls (Figure 28). Additionally, significantly lower enrichment of isotope labeling was detected in three-carbon fructose metabolites, pyruvate, and TCA cycle metabolites (Figure 28, 29). It is interesting that metformin treatment not only decreased intestinal fructose metabolism, but also reduced the amount of fructose delivered to the liver. The decrease in both of these processes

suggests the possibility that metformin treatment reduced intestinal fructose absorption. Future studies should focus on whether and how metformin alters intestinal epithelial absorptive function and substrate transport.

Mechanistically, despite the remarkable inhibition of fructose metabolism induced by metformin treatment, the mRNA and protein levels of fructolytic enzymes remained unchanged, suggesting that metformin has no effect on expression of fructose metabolism-related enzymes at either the transcriptional or translational level. On the other hand, increased phosphorylation of AMPK at Thr172 was detected in the intestinal tissue in the metformin-treated group, suggesting increased AMP/ATP ratio (Figure 29). The flux of substrate into the TCA cycle was reduced in metformin treated mice. That might be consistent with reduced TCA cycle flux and reduced ATP production. However, this has not yet been directly measured. Additionally, decreased expression level of pyruvate dehydrogenase protein and increased phosphorylation of PDHA1 at Ser 293, a surrogate for decreased PDH activity, were observed in the intestine tissue of metformin-treated mice (Figure 28). This result may be somewhat consistent with previous findings which indicated that metformin acutely inhibits pyruvate dehydrogenase flux in the kidney [139]. However, in this case the inhibition was attributed to metformin mediated changes in kidney redox state. In contrast, two weeks of metformin treatment failed to alter the expression level and activity of pyruvate dehydrogenase in muscles [140]. As metformin trends to concentrate in the intestine, liver, and kidney tissues [141], it is

possible that the regulatory effects of metformin on pyruvate dehydrogenase are dose- and tissue-dependent. Future studies could further validate metformin's effects on the activation of AMPK activity and the inhibition of PDH activity, while also further exploring underlying regulatory mechanisms.

5.4 Conclusion

Using a fructose gavage approach, we have shown that metformin decreased fructose metabolism, TCA cycle flux, and glucose production in the intestine. Measurement of circulating TCA cycle metabolites following oral administration of labeled substrates like fructose has the potential to serve as a quick and effective method for assessing intestinal metabolism in a range of physiological and pathophysiological conditions, including in human subjects.

6. Conclusions and future directions

In this body of work, we explored a potential mechanism for how the TCA cycle intermediate succinate connects intestinal metabolism to the regulation of liver function. Specifically, we first proposed that gut is the major source of circulating succinate by showing a marked portal-to-tail gradient in plasma succinate. Using conventional versus germ-free mice, we further demonstrated that gut microbiota is not a major contributor to circulating succinate. Moreover, by comparing the capacity of intestinal succinate absorption to endogenous succinate production, we demonstrated that endogenous intestinal succinate production far exceeds external succinate absorption in normal physiological conditions. Altogether, we showed that the intestine tissue is a major contributor to circulating succinate.

Elevated circulating succinate levels are a biomarker of cardiometabolic disease [27]. In this regard, exploring regulatory factors of intestinal succinate production and its association with the development of cardiometabolic disease will be an important next step. Whether the increase in circulating succinate associates with changes in intestinal succinate production and/or altered mitochondrial function requires further investigation.

The large amounts of intestine-derived succinate are first delivered to the liver tissue where succinate receptor *Sucnr1* is expressed at high levels. Thus, we proposed that liver may be a major target of the gut-derived succinate. By analyzing publicly

accessible single-cell RNA sequencing datasets, we observed that *Sucnr1* is expressed in both hepatocyte and liver non-parenchymal cells. By conducting parenchymal and non-parenchymal cell enrichment after *in situ* liver digestion with the hepatocyte specific *Sucnr1* knockout mice and their controls, we show for the first time that *Sucnr1* is predominantly expressed in the hepatocytes, and to a much lesser degree in non-parenchymal cells. This novel finding contrasts with previously published data which may have arrived at erroneous conclusions due to the culture conditions used in those studies. Our work in this area will provide a solid foundation for future studies to investigate the role of succinate signaling in the liver.

The RNA-sequencing data from our initial study suggests potential roles of hepatic *Sucnr1* in amino acid metabolism and liver inflammation. However, additional studies will be required to fully evaluate the potential functions of hepatic *Sucnr1* in this context. Since succinate is a major end-product secreted by many parasites and our RNA-sequencing data suggests a connection between hepatic *Sucnr1* and some parasitic infections, it is possible that the succinate-*Sucnr1* signaling axis is predominately involved in an adaptive response to parasitic infections of the liver. Again, this will require further investigation.

Taking advantage of our finding that intestinal tissue is a major contributor to portal TCA cycle intermediates, we proposed to use the isotope tracing of fructose-derived TCA cycle intermediates to probe intestinal metabolism in the setting of

metformin treatment. Using this approach, we are the first to show that metformin decreased intestinal fructose metabolism, TCA cycle flux, and glucose production, which supports our hypothesis that this approach has the potential to serve as a robust approach to assess intestinal metabolic function *in vivo*.

The mechanism by which metformin mediates its beneficial effects remains highly controversial. AMPK responds to changes in energy cellular status such as glucose deprivation to maintain energy homeostasis by inhibiting anabolic processes while promoting catabolic processes. Our results are consistent with a potential role for AMPK to mediate some of metformin's effects as we observed increased phosphorylation of AMPK Thr172. We have not yet measured the levels of AMP and ATP and are currently validating assays to make such measurements. Similarly, we observed increased PDHA1 phosphorylation at Ser293 as a surrogate of inhibited PDH activity. The measurement of AMP to ATP ratio and PDH activity could potentially validate our interpretation.

Altogether, this study provides a foundation for future studies to explore the role of intestine in regulating circulating succinate, hepatic *Sucnr1* signaling, and a promising new approach using TCA cycle metabolites produced by the intestine to probe intestinal metabolism *in vivo*.

Appendix A

Table 7: Top 50 differentially expressed genes between the LiSucnr1KO liver versus controls using the p values smaller than 0.05 as criteria

SYMBOL	baseMean	log2FoldChange	lfcSE	stat	pvalue
Sucnr1	586.2669	-2.25499	0.110156	-20.4708	3.92E-93
Tpmt	1738.371	0.882724	0.109602	8.053906	8.02E-16
Cage1	34.82912	1.214441	0.225336	5.38946	7.07E-08
Cxcl14	127.227	1.457099	0.347099	4.197933	2.69E-05
Lyve1	169.9793	-0.85426	0.209876	-4.07032	4.69E-05
Gja1	106.0263	-0.69607	0.172365	-4.03833	5.38E-05
9030616G12Rik	347.2285	-0.80659	0.201037	-4.01214	6.02E-05
Cxcl1	168.6995	0.744347	0.193703	3.842721	0.000122
Ehf	25.65114	-1.28581	0.340856	-3.7723	0.000162
Prodh	4927.777	0.333608	0.090001	3.706726	0.00021
Nhlrc1	51.82678	0.768897	0.214305	3.587864	0.000333
Sh2d4a	166.1305	0.760238	0.213129	3.567037	0.000361
Tsku	1811.932	0.693179	0.195161	3.551834	0.000383
Irf2bp2	2674.982	-0.60136	0.174207	-3.452	0.000556
Anxa13	37.50029	-0.85268	0.24903	-3.42399	0.000617
Unc5a	46.39115	-0.85138	0.250515	-3.39851	0.000678
Bglap3	13.33287	1.566732	0.461144	3.397488	0.00068
Parp8	28.18613	-0.94069	0.279003	-3.37161	0.000747
Gm7599	28.66531	-1.41464	0.426289	-3.31849	0.000905
Rnf43	975.7324	0.409028	0.12434	3.289594	0.001003
1810046K07Rik	55.13835	0.724305	0.221352	3.272184	0.001067
Tgfbr3l	154.8847	0.430817	0.134987	3.191544	0.001415
Galnt15	73.75503	-0.87902	0.275578	-3.18972	0.001424
Atp11a	874.5822	-0.49826	0.157154	-3.17053	0.001522
Syt7	62.22553	-0.7441	0.235325	-3.16203	0.001567
Aadac	12123.5	-0.26161	0.082831	-3.15842	0.001586
Zfp385a	900.6044	-0.26529	0.084297	-3.14706	0.001649
Gnao1	19.24987	-0.99705	0.31824	-3.13301	0.00173
Slc23a1	2242.538	0.296778	0.094829	3.129622	0.00175
F11	3523.375	0.196018	0.063482	3.087756	0.002017
Gm9353	13.55885	-1.19521	0.387724	-3.08263	0.002052
Cstf3	436.1032	0.281045	0.091236	3.080413	0.002067
Acy1	884.4822	0.216271	0.070218	3.080006	0.00207
Cbfa2t3	137.7062	-0.54898	0.178299	-3.07902	0.002077
Hic1	128.258	-0.59951	0.194892	-3.07609	0.002097
Elf5	17.58257	-1.10733	0.360118	-3.07491	0.002106
Mtif3	522.3777	0.272899	0.088848	3.071521	0.00213

Pck1	61174.97	-0.63566	0.20834	-3.05106	0.00228
Muc2	5.58644	-2.06964	0.680713	-3.04039	0.002363
Prdm16	17.06662	-1.04541	0.344393	-3.03551	0.002401
Lratd1	57.89258	-0.60683	0.20079	-3.02222	0.002509
Gbp6	81.77772	-0.45996	0.153083	-3.00465	0.002659
Cnmd	94.07574	0.692153	0.23121	2.993613	0.002757
Cttnbp2	12.15017	-1.2819	0.429977	-2.98131	0.00287
Inf2	2410.928	0.195395	0.066027	2.95932	0.003083
Tubb4a	10.62963	-1.29941	0.439772	-2.95474	0.003129
Igkv4-55	3.677063	-3.60691	1.232929	-2.92548	0.003439
Sult1d1	2184.944	0.243182	0.083145	2.924814	0.003447

References

1. Lund P. Sir Hans Krebs (1900-1981). *Clinical science* (London, England : 1979). 1982;63(3):225-30. Epub 1982/09/01. doi: 10.1042/cs0630225. PubMed PMID: 7047048.
2. Fernie AR, Carrari F, Sweetlove LJ. Respiratory metabolism: glycolysis, the TCA cycle and mitochondrial electron transport. *Current opinion in plant biology*. 2004;7(3):254-61. Epub 2004/05/12. doi: 10.1016/j.pbi.2004.03.007. PubMed PMID: 15134745.
3. van der Blik AM, Sedensky MM, Morgan PG. Cell Biology of the Mitochondrion. *Genetics*. 2017;207(3):843-71. Epub 2017/11/04. doi: 10.1534/genetics.117.300262. PubMed PMID: 29097398; PubMed Central PMCID: PMC5676242.
4. Yu S, Meng S, Xiang M, Ma H. Phosphoenolpyruvate carboxykinase in cell metabolism: Roles and mechanisms beyond gluconeogenesis. *Molecular metabolism*. 2021;53:101257. Epub 2021/05/22. doi: 10.1016/j.molmet.2021.101257. PubMed PMID: 34020084; PubMed Central PMCID: PMC8190478.
5. Stern JR, Ochoa S. Enzymatic synthesis of citric acid by condensation of acetate and oxalacetate. *The Journal of biological chemistry*. 1949;179(1):491. Epub 1949/05/01. PubMed PMID: 18119265.
6. Monné M, Voza A, Lasorsa FM, Porcelli V, Palmieri F. Mitochondrial Carriers for Aspartate, Glutamate and Other Amino Acids: A Review. *Int J Mol Sci*. 2019;20(18). Epub 2019/09/13. doi: 10.3390/ijms20184456. PubMed PMID: 31510000; PubMed Central PMCID: PMC6769469.
7. Wang J, Liu Y, Lian K, Shentu X, Fang J, Shao J, et al. BCAA Catabolic Defect Alters Glucose Metabolism in Lean Mice. *Frontiers in physiology*. 2019;10:1140. Epub 2019/09/26. doi: 10.3389/fphys.2019.01140. PubMed PMID: 31551816; PubMed Central PMCID: PMC6738029.
8. Salminen A, Jouhten P, Sarajärvi T, Haapasalo A, Hiltunen M. Hypoxia and GABA shunt activation in the pathogenesis of Alzheimer's disease. *Neurochemistry international*. 2016;92:13-24. Epub 2015/12/01. doi: 10.1016/j.neuint.2015.11.005. PubMed PMID: 26617286.

9. Chouchani ET, Pell VR, Gaude E, Aksentijević D, Sundier SY, Robb EL, et al. Ischaemic accumulation of succinate controls reperfusion injury through mitochondrial ROS. *Nature*. 2014;515(7527):431-5. Epub 2014/11/11. doi: 10.1038/nature13909. PubMed PMID: 25383517; PubMed Central PMCID: PMC4255242.
10. Tannahill GM, Curtis AM, Adamik J, Palsson-McDermott EM, McGettrick AF, Goel G, et al. Succinate is an inflammatory signal that induces IL-1 β through HIF-1 α . *Nature*. 2013;496(7444):238-42. Epub 2013/03/29. doi: 10.1038/nature11986. PubMed PMID: 23535595; PubMed Central PMCID: PMC4031686.
11. Zhang J, Wang YT, Miller JH, Day MM, Munger JC, Brookes PS. Accumulation of Succinate in Cardiac Ischemia Primarily Occurs via Canonical Krebs Cycle Activity. *Cell reports*. 2018;23(9):2617-28. Epub 2018/05/31. doi: 10.1016/j.celrep.2018.04.104. PubMed PMID: 29847793; PubMed Central PMCID: PMC6002783.
12. Correa PR, Kruglov EA, Thompson M, Leite MF, Dranoff JA, Nathanson MH. Succinate is a paracrine signal for liver damage. *Journal of hepatology*. 2007;47(2):262-9. Epub 2007/04/25. doi: 10.1016/j.jhep.2007.03.016. PubMed PMID: 17451837; PubMed Central PMCID: PMC1986575.
13. Kamarauskaite J, Baniene R, Trumbeckas D, Strazdauskas A, Trumbeckaite S. Increased Succinate Accumulation Induces ROS Generation in In Vivo Ischemia/Reperfusion-Affected Rat Kidney Mitochondria. *BioMed research international*. 2020;2020:8855585. Epub 2020/10/27. doi: 10.1155/2020/8855585. PubMed PMID: 33102598; PubMed Central PMCID: PMC7578729.
14. Yang M, Pollard PJ. Succinate: a new epigenetic hacker. *Cancer cell*. 2013;23(6):709-11. Epub 2013/06/15. doi: 10.1016/j.ccr.2013.05.015. PubMed PMID: 23763995.
15. Fernández-Veledo S, Ceperuelo-Mallafre V, Vendrell J. Rethinking succinate: an unexpected hormone-like metabolite in energy homeostasis. *Trends in endocrinology and metabolism: TEM*. 2021;32(9):680-92. Epub 2021/07/25. doi: 10.1016/j.tem.2021.06.003. PubMed PMID: 34301438.
16. Krzak G, Willis CM, Smith JA, Pluchino S, Peruzzotti-Jametti L. Succinate Receptor 1: An Emerging Regulator of Myeloid Cell Function in Inflammation. *Trends in immunology*. 2021;42(1):45-58. Epub 2020/12/07. doi: 10.1016/j.it.2020.11.004. PubMed PMID: 33279412.

17. Bailis W, Shyer JA, Zhao J, Canaveras JCG, Al Khazal FJ, Qu R, et al. Distinct modes of mitochondrial metabolism uncouple T cell differentiation and function. *Nature*. 2019;571(7765):403-7. Epub 2019/06/21. doi: 10.1038/s41586-019-1311-3. PubMed PMID: 31217581; PubMed Central PMCID: PMC6939459.
18. Caielli S, Veiga DT, Balasubramanian P, Athale S, Domic B, Murat E, et al. A CD4(+) T cell population expanded in lupus blood provides B cell help through interleukin-10 and succinate. *Nature medicine*. 2019;25(1):75-81. Epub 2018/11/28. doi: 10.1038/s41591-018-0254-9. PubMed PMID: 30478422; PubMed Central PMCID: PMC6325012.
19. Liu Y, Xu R, Gu H, Zhang E, Qu J, Cao W, et al. Metabolic reprogramming in macrophage responses. *Biomarker research*. 2021;9(1):1. Epub 2021/01/08. doi: 10.1186/s40364-020-00251-y. PubMed PMID: 33407885; PubMed Central PMCID: PMC67786975.
20. Trauelsen M, Hiron TK, Lin D, Petersen JE, Breton B, Husted AS, et al. Extracellular succinate hyperpolarizes M2 macrophages through SUCNR1/GPR91-mediated Gq signaling. *Cell reports*. 2021;35(11):109246. Epub 2021/06/17. doi: 10.1016/j.celrep.2021.109246. PubMed PMID: 34133934.
21. Connors J, Dawe N, Van Limbergen J. The Role of Succinate in the Regulation of Intestinal Inflammation. *Nutrients*. 2018;11(1). Epub 2018/12/26. doi: 10.3390/nu11010025. PubMed PMID: 30583500; PubMed Central PMCID: PMC6356305.
22. Littlewood-Evans A, Sarret S, Apfel V, Loesle P, Dawson J, Zhang J, et al. GPR91 senses extracellular succinate released from inflammatory macrophages and exacerbates rheumatoid arthritis. *The Journal of experimental medicine*. 2016;213(9):1655-62. Epub 2016/08/03. doi: 10.1084/jem.20160061. PubMed PMID: 27481132; PubMed Central PMCID: PMC4995082.
23. Harber KJ, de Goede KE, Verberk SGS, Meinster E, de Vries HE, van Weeghel M, et al. Succinate Is an Inflammation-Induced Immunoregulatory Metabolite in Macrophages. *Metabolites*. 2020;10(9). Epub 2020/09/19. doi: 10.3390/metabo10090372. PubMed PMID: 32942769; PubMed Central PMCID: PMC7569821.
24. McCreath KJ, Espada S, Gálvez BG, Benito M, de Molina A, Sepúlveda P, et al. Targeted disruption of the SUCNR1 metabolic receptor leads to dichotomous effects on

obesity. *Diabetes*. 2015;64(4):1154-67. Epub 2014/10/30. doi: 10.2337/db14-0346. PubMed PMID: 25352636.

25. Wang T, Xu YQ, Yuan YX, Xu PW, Zhang C, Li F, et al. Succinate induces skeletal muscle fiber remodeling via SUCNR1 signaling. *EMBO reports*. 2021;22(6):e53027. Epub 2021/06/08. doi: 10.15252/embr.202153027. PubMed PMID: 34097347; PubMed Central PMCID: PMC8183402.

26. Xu G, Yuan Y, Luo P, Yang J, Zhou J, Zhu C, et al. Acute Succinate Administration Increases Oxidative Phosphorylation and Skeletal Muscle Explosive Strength via SUCNR1. *Frontiers in veterinary science*. 2021;8:808863. Epub 2022/02/01. doi: 10.3389/fvets.2021.808863. PubMed PMID: 35097053; PubMed Central PMCID: PMC8795363.

27. Serena C, Ceperuelo-Mallafre V, Keiran N, Queipo-Ortuno MI, Bernal R, Gomez-Huelgas R, et al. Elevated circulating levels of succinate in human obesity are linked to specific gut microbiota. *The ISME journal*. 2018;12(7):1642-57. Epub 2018/02/13. doi: 10.1038/s41396-018-0068-2. PubMed PMID: 29434314; PubMed Central PMCID: PMC6018807.

28. Sadagopan N, Li W, Roberds SL, Major T, Preston GM, Yu Y, et al. Circulating succinate is elevated in rodent models of hypertension and metabolic disease. *American journal of hypertension*. 2007;20(11):1209-15. Epub 2007/10/24. doi: 10.1016/j.amjhyper.2007.05.010. PubMed PMID: 17954369.

29. Staňková P, Kučera O, Peterová E, Elkalaf M, Rychtrmoc D, Melek J, et al. Western Diet Decreases the Liver Mitochondrial Oxidative Flux of Succinate: Insight from a Murine NAFLD Model. *Int J Mol Sci*. 2021;22(13). Epub 2021/07/03. doi: 10.3390/ijms22136908. PubMed PMID: 34199098; PubMed Central PMCID: PMC8268937.

30. Osuna-Prieto FJ, Martinez-Tellez B, Ortiz-Alvarez L, Di X, Jurado-Fasoli L, Xu H, et al. Elevated plasma succinate levels are linked to higher cardiovascular disease risk factors in young adults. *Cardiovascular diabetology*. 2021;20(1):151. Epub 2021/07/29. doi: 10.1186/s12933-021-01333-3. PubMed PMID: 34315463; PubMed Central PMCID: PMC8314524.

31. Ceperuelo-Mallafre V, Llauradó G, Keiran N, Benaiges E, Astiarraga B, Martínez L, et al. Preoperative Circulating Succinate Levels as a Biomarker for Diabetes Remission

- After Bariatric Surgery. *Diabetes care*. 2019;42(10):1956-65. Epub 2019/08/04. doi: 10.2337/dc19-0114. PubMed PMID: 31375523.
32. Xie C, Wei W, Zhang T, Dirsch O, Dahmen U. Monitoring of systemic and hepatic hemodynamic parameters in mice. *Journal of visualized experiments : JoVE*. 2014;(92):e51955. Epub 2014/10/29. doi: 10.3791/51955. PubMed PMID: 25350047; PubMed Central PMCID: PMC4692415.
33. Chen M, Wang J, Lu J, Bond MC, Ren XR, Lyerly HK, et al. The anti-helminthic niclosamide inhibits Wnt/Frizzled1 signaling. *Biochemistry*. 2009;48(43):10267-74. Epub 2009/09/24. doi: 10.1021/bi9009677. PubMed PMID: 19772353; PubMed Central PMCID: PMC2801776.
34. Sato T, Vries RG, Snippert HJ, van de Wetering M, Barker N, Stange DE, et al. Single Lgr5 stem cells build crypt-villus structures in vitro without a mesenchymal niche. *Nature*. 2009;459(7244):262-5. Epub 2009/03/31. doi: 10.1038/nature07935. PubMed PMID: 19329995.
35. Bu P, Chen KY, Xiang K, Johnson C, Crown SB, Rakhilin N, et al. Aldolase B-Mediated Fructose Metabolism Drives Metabolic Reprogramming of Colon Cancer Liver Metastasis. *Cell metabolism*. 2018;27(6):1249-62.e4. Epub 2018/05/01. doi: 10.1016/j.cmet.2018.04.003. PubMed PMID: 29706565; PubMed Central PMCID: PMC5990465.
36. He W, Wang Y, Xie EJ, Barry MA, Zhang GF. Metabolic perturbations mediated by propionyl-CoA accumulation in organs of mouse model of propionic acidemia. *Molecular genetics and metabolism*. 2021;134(3):257-66. Epub 2021/10/13. doi: 10.1016/j.ymgme.2021.09.009. PubMed PMID: 34635437.
37. Fernandez CA, Des Rosiers C, Previs SF, David F, Brunengraber H. Correction of ¹³C mass isotopomer distributions for natural stable isotope abundance. *Journal of mass spectrometry : JMS*. 1996;31(3):255-62. Epub 1996/03/01. doi: 10.1002/(sici)1096-9888(199603)31:3<255::Aid-jms290>3.0.Co;2-3. PubMed PMID: 8799277.
38. Zhang GF, Jensen MV, Gray SM, El K, Wang Y, Lu D, et al. Reductive TCA cycle metabolism fuels glutamine- and glucose-stimulated insulin secretion. *Cell metabolism*. 2020. Epub 2020/12/16. doi: 10.1016/j.cmet.2020.11.020. PubMed PMID: 33321098.
39. de Sena Brandine G, Smith AD. Falco: high-speed FastQC emulation for quality control of sequencing data. *F1000Research*. 2019;8:1874. Epub 2019/11/07. doi:

10.12688/f1000research.21142.2. PubMed PMID: 33552473; PubMed Central PMCID: PMCPMC7845152.

40. Dobin A, Davis CA, Schlesinger F, Drenkow J, Zaleski C, Jha S, et al. STAR: ultrafast universal RNA-seq aligner. *Bioinformatics (Oxford, England)*. 2013;29(1):15-21. Epub 2012/10/30. doi: 10.1093/bioinformatics/bts635. PubMed PMID: 23104886; PubMed Central PMCID: PMCPMC3530905.

41. Liao Y, Smyth GK, Shi W. The Subread aligner: fast, accurate and scalable read mapping by seed-and-vote. *Nucleic acids research*. 2013;41(10):e108. Epub 2013/04/06. doi: 10.1093/nar/gkt214. PubMed PMID: 23558742; PubMed Central PMCID: PMCPMC3664803.

42. Robinson MD, McCarthy DJ, Smyth GK. edgeR: a Bioconductor package for differential expression analysis of digital gene expression data. *Bioinformatics (Oxford, England)*. 2010;26(1):139-40. Epub 2009/11/17. doi: 10.1093/bioinformatics/btp616. PubMed PMID: 19910308; PubMed Central PMCID: PMCPMC2796818.

43. Chen EY, Tan CM, Kou Y, Duan Q, Wang Z, Meirelles GV, et al. Enrichr: interactive and collaborative HTML5 gene list enrichment analysis tool. *BMC bioinformatics*. 2013;14:128. Epub 2013/04/17. doi: 10.1186/1471-2105-14-128. PubMed PMID: 23586463; PubMed Central PMCID: PMCPMC3637064.

44. Xiong X, Kuang H, Ansari S, Liu T, Gong J, Wang S, et al. Landscape of Intercellular Crosstalk in Healthy and NASH Liver Revealed by Single-Cell Secretome Gene Analysis. *Mol Cell*. 2019;75(3):644-60.e5. Epub 2019/08/10. doi: 10.1016/j.molcel.2019.07.028. PubMed PMID: 31398325; PubMed Central PMCID: PMCPMC7262680.

45. Halpern KB, Shenhav R, Matcovitch-Natan O, Toth B, Lemze D, Golan M, et al. Single-cell spatial reconstruction reveals global division of labour in the mammalian liver. *Nature*. 2017;542(7641):352-6. Epub 2017/02/07. doi: 10.1038/nature21065. PubMed PMID: 28166538; PubMed Central PMCID: PMCPMC5321580.

46. Patro R, Duggal G, Love MI, Irizarry RA, Kingsford C. Salmon provides fast and bias-aware quantification of transcript expression. *Nature methods*. 2017;14(4):417-9. Epub 2017/03/07. doi: 10.1038/nmeth.4197. PubMed PMID: 28263959; PubMed Central PMCID: PMCPMC5600148.

47. Zhou H, Wang F, Tao P. t-Distributed Stochastic Neighbor Embedding Method with the Least Information Loss for Macromolecular Simulations. *Journal of chemical theory and computation*. 2018;14(11):5499-510. Epub 2018/09/27. doi: 10.1021/acs.jctc.8b00652. PubMed PMID: 30252473; PubMed Central PMCID: PMC6679899.
48. Zhu D, Rostami MR, Zuo WL, Leopold PL, Crystal RG. Single-Cell Transcriptome Analysis of Mouse Liver Cell-Specific Tropism and Transcriptional Dysregulation Following Intravenous Administration of AAVrh.10 Vectors. *Human gene therapy*. 2020;31(9-10):590-604. Epub 2020/03/08. doi: 10.1089/hum.2019.366. PubMed PMID: 32143547; PubMed Central PMCID: PMC67232697.
49. Owen OE, Kalhan SC, Hanson RW. The key role of anaplerosis and cataplerosis for citric acid cycle function. *The Journal of biological chemistry*. 2002;277(34):30409-12. Epub 2002/06/28. doi: 10.1074/jbc.R200006200. PubMed PMID: 12087111.
50. He W, Miao FJ, Lin DC, Schwandner RT, Wang Z, Gao J, et al. Citric acid cycle intermediates as ligands for orphan G-protein-coupled receptors. *Nature*. 2004;429(6988):188-93. Epub 2004/05/14. doi: 10.1038/nature02488. PubMed PMID: 15141213.
51. Toma I, Kang JJ, Sipos A, Vargas S, Bansal E, Hanner F, et al. Succinate receptor GPR91 provides a direct link between high glucose levels and renin release in murine and rabbit kidney. *The Journal of clinical investigation*. 2008;118(7):2526-34. Epub 2008/06/07. doi: 10.1172/jci33293. PubMed PMID: 18535668; PubMed Central PMCID: PMC2413183.
52. Lampropoulou V, Sergushichev A, Bambouskova M, Nair S, Vincent EE, Loginicheva E, et al. Itaconate Links Inhibition of Succinate Dehydrogenase with Macrophage Metabolic Remodeling and Regulation of Inflammation. *Cell metabolism*. 2016;24(1):158-66. Epub 2016/07/05. doi: 10.1016/j.cmet.2016.06.004. PubMed PMID: 27374498; PubMed Central PMCID: PMC5108454.
53. Rubic T, Lametschwandtner G, Jost S, Hinteregger S, Kund J, Carballido-Perrig N, et al. Triggering the succinate receptor GPR91 on dendritic cells enhances immunity. *Nature immunology*. 2008;9(11):1261-9. Epub 2008/09/30. doi: 10.1038/ni.1657. PubMed PMID: 18820681.
54. Mills EL, Pierce KA, Jedrychowski MP, Garrity R, Winther S, Vidoni S, et al. Accumulation of succinate controls activation of adipose tissue thermogenesis. *Nature*.

2018;560(7716):102-6. Epub 2018/07/20. doi: 10.1038/s41586-018-0353-2. PubMed PMID: 30022159; PubMed Central PMCID: PMCPMC7045287.

55. Cho EH. Succinate as a Regulator of Hepatic Stellate Cells in Liver Fibrosis. *Front Endocrinol (Lausanne)*. 2018;9:455. Epub 2018/09/07. doi: 10.3389/fendo.2018.00455. PubMed PMID: 30186230; PubMed Central PMCID: PMCPMC6110815.

56. De Vadder F, Kovatcheva-Datchary P, Zitoun C, Duchamp A, Backhed F, Mithieux G. Microbiota-Produced Succinate Improves Glucose Homeostasis via Intestinal Gluconeogenesis. *Cell metabolism*. 2016;24(1):151-7. Epub 2016/07/15. doi: 10.1016/j.cmet.2016.06.013. PubMed PMID: 27411015.

57. Jang C, Hui S, Lu W, Cowan AJ, Morscher RJ, Lee G, et al. The Small Intestine Converts Dietary Fructose into Glucose and Organic Acids. *Cell metabolism*. 2018;27(2):351-61.e3. Epub 2018/02/08. doi: 10.1016/j.cmet.2017.12.016. PubMed PMID: 29414685; PubMed Central PMCID: PMCPMC6032988.

58. Zhao S, Jang C, Liu J, Uehara K, Gilbert M, Izzo L, et al. Dietary fructose feeds hepatic lipogenesis via microbiota-derived acetate. *Nature*. 2020;579(7800):586-91. Epub 2020/03/28. doi: 10.1038/s41586-020-2101-7. PubMed PMID: 32214246; PubMed Central PMCID: PMCPMC7416516.

59. Macfarlane S, Macfarlane GT. Composition and metabolic activities of bacterial biofilms colonizing food residues in the human gut. *Applied and environmental microbiology*. 2006;72(9):6204-11. Epub 2006/09/08. doi: 10.1128/aem.00754-06. PubMed PMID: 16957247; PubMed Central PMCID: PMCPMC1563644.

60. Mills E, O'Neill LA. Succinate: a metabolic signal in inflammation. *Trends in cell biology*. 2014;24(5):313-20. Epub 2013/12/24. doi: 10.1016/j.tcb.2013.11.008. PubMed PMID: 24361092.

61. Ahn S, Jung J, Jang IA, Madsen EL, Park W. Role of Glyoxylate Shunt in Oxidative Stress Response. *The Journal of biological chemistry*. 2016;291(22):11928-38. Epub 2016/04/03. doi: 10.1074/jbc.M115.708149. PubMed PMID: 27036942; PubMed Central PMCID: PMCPMC4882458.

62. Woting A, Blaut M. Small Intestinal Permeability and Gut-Transit Time Determined with Low and High Molecular Weight Fluorescein Isothiocyanate-Dextran in C3H Mice. *Nutrients*. 2018;10(6). Epub 2018/05/31. doi: 10.3390/nu10060685. PubMed PMID: 29843428; PubMed Central PMCID: PMCPMC6024777.

63. Liu X, Chen Y, Zhao L, Tian Q, deAvila JM, Zhu MJ, et al. Dietary succinate supplementation to maternal mice improves fetal brown adipose tissue development and thermogenesis of female offspring. *The Journal of nutritional biochemistry*. 2021;108908. Epub 2021/11/22. doi: 10.1016/j.jnutbio.2021.108908. PubMed PMID: 34801687.
64. Nadjombati MS, McGinty JW, Lyons-Cohen MR, Jaffe JB, DiPeso L, Schneider C, et al. Detection of Succinate by Intestinal Tuft Cells Triggers a Type 2 Innate Immune Circuit. *Immunity*. 2018;49(1):33-41.e7. Epub 2018/07/19. doi: 10.1016/j.immuni.2018.06.016. PubMed PMID: 30021144; PubMed Central PMCID: PMC6084797.
65. Nilsson R. Validity of natural isotope abundance correction for metabolic flux analysis. *Mathematical biosciences*. 2020;330:108481. Epub 2020/10/03. doi: 10.1016/j.mbs.2020.108481. PubMed PMID: 33007317.
66. Borowy CS, Ashurst JV. *Physiology, Zero and First Order Kinetics*. StatPearls. Treasure Island (FL): StatPearls Publishing Copyright © 2021, StatPearls Publishing LLC.; 2021.
67. Hannou SA, Haslam DE, McKeown NM, Herman MA. Fructose metabolism and metabolic disease. *The Journal of clinical investigation*. 2018;128(2):545-55. Epub 2018/02/02. doi: 10.1172/jci96702. PubMed PMID: 29388924; PubMed Central PMCID: PMC5785258.
68. Herman MA, Birnbaum MJ. Molecular aspects of fructose metabolism and metabolic disease. *Cell metabolism*. 2021. Epub 2021/10/08. doi: 10.1016/j.cmet.2021.09.010. PubMed PMID: 34619074.
69. Tretter L, Patocs A, Chinopoulos C. Succinate, an intermediate in metabolism, signal transduction, ROS, hypoxia, and tumorigenesis. *Biochimica et biophysica acta*. 2016;1857(8):1086-101. Epub 2016/03/15. doi: 10.1016/j.bbabbio.2016.03.012. PubMed PMID: 26971832.
70. Jang C, Hui S, Zeng X, Cowan AJ, Wang L, Chen L, et al. Metabolite Exchange between Mammalian Organs Quantified in Pigs. *Cell metabolism*. 2019;30(3):594-606.e3. Epub 2019/07/02. doi: 10.1016/j.cmet.2019.06.002. PubMed PMID: 31257152; PubMed Central PMCID: PMC6726553.

71. Kishida K, Pearce SC, Yu S, Gao N, Ferraris RP. Nutrient sensing by absorptive and secretory progenies of small intestinal stem cells. *American journal of physiology Gastrointestinal and liver physiology*. 2017;312(6):G592-g605. Epub 2017/03/25. doi: 10.1152/ajpgi.00416.2016. PubMed PMID: 28336548; PubMed Central PMCID: PMC5495913.
72. Al-Jawadi A, Patel CR, Shiarella RJ, Romelus E, Auvinen M, Guardia J, et al. Cell-Type-Specific, Ketohexokinase-Dependent Induction by Fructose of Lipogenic Gene Expression in Mouse Small Intestine. *The Journal of nutrition*. 2020;150(7):1722-30. Epub 2020/05/10. doi: 10.1093/jn/nxaa113. PubMed PMID: 32386219; PubMed Central PMCID: PMC7330472.
73. Wijermars LG, Schaapherder AF, Kostidis S, Wüst RC, Lindeman JH. Succinate Accumulation and Ischemia-Reperfusion Injury: Of Mice but Not Men, a Study in Renal Ischemia-Reperfusion. *American journal of transplantation : official journal of the American Society of Transplantation and the American Society of Transplant Surgeons*. 2016;16(9):2741-6. Epub 2016/03/22. doi: 10.1111/ajt.13793. PubMed PMID: 26999803.
74. Chan TS, Cassim S, Raymond VA, Gottschalk S, Merlen G, Zwingmann C, et al. Upregulation of Krebs cycle and anaerobic glycolysis activity early after onset of liver ischemia. *PloS one*. 2018;13(6):e0199177. Epub 2018/06/15. doi: 10.1371/journal.pone.0199177. PubMed PMID: 29902244; PubMed Central PMCID: PMC6002017
- de Montréal is a philanthropic chair administered by Université de Montréal that was initially founded through a joint initiative of the Canadian Liver Foundation and Novartis to help promote research in the field of liver disease. There are no patents, products in development or marketed products to declare. This does not alter our adherence to PLOS ONE policies on sharing data and materials.
75. Reddy A, Bozi LHM, Yaghi OK, Mills EL, Xiao H, Nicholson HE, et al. pH-Gated Succinate Secretion Regulates Muscle Remodeling in Response to Exercise. *Cell*. 2020;183(1):62-75.e17. Epub 2020/09/19. doi: 10.1016/j.cell.2020.08.039. PubMed PMID: 32946811; PubMed Central PMCID: PMC7778787.
76. Tang WH, Kitai T, Hazen SL. Gut Microbiota in Cardiovascular Health and Disease. *Circulation research*. 2017;120(7):1183-96. Epub 2017/04/01. doi: 10.1161/circresaha.117.309715. PubMed PMID: 28360349; PubMed Central PMCID: PMC5390330.
77. Turnbaugh PJ, Hamady M, Yatsunenko T, Cantarel BL, Duncan A, Ley RE, et al. A core gut microbiome in obese and lean twins. *Nature*. 2009;457(7228):480-4. Epub

2008/12/02. doi: 10.1038/nature07540. PubMed PMID: 19043404; PubMed Central PMCID: PMCPMC2677729.

78. Rajas F, Bruni N, Montano S, Zitoun C, Mithieux G. The glucose-6 phosphatase gene is expressed in human and rat small intestine: regulation of expression in fasted and diabetic rats. *Gastroenterology*. 1999;117(1):132-9. Epub 1999/06/26. doi: 10.1016/s0016-5085(99)70559-7. PubMed PMID: 10381919.

79. Mills EL, Harmon C, Jedrychowski MP, Xiao H, Garrity R, Tran NV, et al. UCP1 governs liver extracellular succinate and inflammatory pathogenesis. *Nature metabolism*. 2021;3(5):604-17. Epub 2021/05/19. doi: 10.1038/s42255-021-00389-5. PubMed PMID: 34002097; PubMed Central PMCID: PMCPMC8207988.

80. Regard JB, Sato IT, Coughlin SR. Anatomical profiling of G protein-coupled receptor expression. *Cell*. 2008;135(3):561-71. Epub 2008/11/06. doi: 10.1016/j.cell.2008.08.040. PubMed PMID: 18984166; PubMed Central PMCID: PMCPMC2590943.

81. Liu XJ, Xie L, Du K, Liu C, Zhang NP, Gu CJ, et al. Succinate-GPR-91 receptor signalling is responsible for nonalcoholic steatohepatitis-associated fibrosis: Effects of DHA supplementation. *Liver international : official journal of the International Association for the Study of the Liver*. 2020;40(4):830-43. Epub 2020/01/07. doi: 10.1111/liv.14370. PubMed PMID: 31903720.

82. Olsavsky Goyak KM, Laurenzana EM, Omiecinski CJ. Hepatocyte differentiation. *Methods in molecular biology (Clifton, NJ)*. 2010;640:115-38. Epub 2010/07/21. doi: 10.1007/978-1-60761-688-7_6. PubMed PMID: 20645049; PubMed Central PMCID: PMCPMC6690360.

83. Sun P, Zhang G, Su X, Jin C, Yu B, Yu X, et al. Maintenance of Primary Hepatocyte Functions In Vitro by Inhibiting Mechanical Tension-Induced YAP Activation. *Cell reports*. 2019;29(10):3212-22.e4. Epub 2019/12/05. doi: 10.1016/j.celrep.2019.10.128. PubMed PMID: 31801084.

84. Barrett T, Wilhite SE, Ledoux P, Evangelista C, Kim IF, Tomashevsky M, et al. NCBI GEO: archive for functional genomics data sets--update. *Nucleic acids research*. 2013;41(Database issue):D991-5. Epub 2012/11/30. doi: 10.1093/nar/gks1193. PubMed PMID: 23193258; PubMed Central PMCID: PMCPMC3531084.

85. Aizarani N, Saviano A, Sagar, Maily L, Durand S, Herman JS, et al. A human liver cell atlas reveals heterogeneity and epithelial progenitors. *Nature*. 2019;572(7768):199-204. Epub 2019/07/12. doi: 10.1038/s41586-019-1373-2. PubMed PMID: 31292543; PubMed Central PMCID: PMC6687507.
86. Jiang G, Zhang BB. Glucagon and regulation of glucose metabolism. *American journal of physiology Endocrinology and metabolism*. 2003;284(4):E671-8. Epub 2003/03/11. doi: 10.1152/ajpendo.00492.2002. PubMed PMID: 12626323.
87. Diehl KH, Hull R, Morton D, Pfister R, Rabemampianina Y, Smith D, et al. A good practice guide to the administration of substances and removal of blood, including routes and volumes. *Journal of applied toxicology : JAT*. 2001;21(1):15-23. Epub 2001/02/17. doi: 10.1002/jat.727. PubMed PMID: 11180276.
88. Zou H, Liu Q, Meng L, Zhou J, Da C, Wu X, et al. Chemical genetic-based phenotypic screen reveals novel regulators of gluconeogenesis in human primary hepatocytes. *NPJ genomic medicine*. 2018;3:20. Epub 2018/08/23. doi: 10.1038/s41525-018-0062-7. PubMed PMID: 30131871; PubMed Central PMCID: PMC6093908 & Co. provided support in the form of salaries for authors and funding for research materials, but did not have any additional role in the study design, data collection and analysis, decision to publish, or preparation of the manuscript.
89. Hu J, Li T, Du S, Chen Y, Wang S, Xiong F, et al. The MAPK signaling pathway mediates the GPR91-dependent release of VEGF from RGC-5 cells. *International journal of molecular medicine*. 2015;36(1):130-8. Epub 2015/05/06. doi: 10.3892/ijmm.2015.2195. PubMed PMID: 25936351; PubMed Central PMCID: PMC64494573.
90. Janah L, Kjeldsen S, Galsgaard KD, Winther-Sorensen M, Stojanovska E, Pedersen J, et al. Glucagon Receptor Signaling and Glucagon Resistance. *Int J Mol Sci*. 2019;20(13). Epub 2019/07/10. doi: 10.3390/ijms20133314. PubMed PMID: 31284506; PubMed Central PMCID: PMC6651628.
91. Galvan L, Francelle L, Gaillard MC, de Longprez L, Carrillo-de Sauvage MA, Liot G, et al. The striatal kinase DCLK3 produces neuroprotection against mutant huntingtin. *Brain : a journal of neurology*. 2018;141(5):1434-54. Epub 2018/03/14. doi: 10.1093/brain/awy057. PubMed PMID: 29534157; PubMed Central PMCID: PMC65917821.
92. Winther-Sørensen M, Galsgaard KD, Santos A, Trammell SAJ, Sulek K, Kuhre RE, et al. Glucagon acutely regulates hepatic amino acid catabolism and the effect may

be disturbed by steatosis. *Molecular metabolism*. 2020;42:101080. Epub 2020/09/17. doi: 10.1016/j.molmet.2020.101080. PubMed PMID: 32937194; PubMed Central PMCID: PMC7560169.

93. Zaza G, Cheok M, Krynetskaia N, Thorn C, Stocco G, Hebert JM, et al. Thiopurine pathway. *Pharmacogenetics and genomics*. 2010;20(9):573-4. Epub 2009/12/03. doi: 10.1097/FPC.0b013e328334338f. PubMed PMID: 19952870; PubMed Central PMCID: PMC3098750.

94. Asadov C, Aliyeva G, Mustafayeva K. Thiopurine S-Methyltransferase as a Pharmacogenetic Biomarker: Significance of Testing and Review of Major Methods. *Cardiovascular & hematological agents in medicinal chemistry*. 2017;15(1):23-30. Epub 2017/05/30. doi: 10.2174/1871525715666170529091921. PubMed PMID: 28552060; PubMed Central PMCID: PMC5740490.

95. Kuleshov MV, Jones MR, Rouillard AD, Fernandez NF, Duan Q, Wang Z, et al. Enrichr: a comprehensive gene set enrichment analysis web server 2016 update. *Nucleic acids research*. 2016;44(W1):W90-7. Epub 2016/05/05. doi: 10.1093/nar/gkw377. PubMed PMID: 27141961; PubMed Central PMCID: PMC4987924.

96. Bozadjieva Kramer N, Lubaczeuski C, Blandino-Rosano M, Barker G, Gittes GK, Caicedo A, et al. Glucagon Resistance and Decreased Susceptibility to Diabetes in a Model of Chronic Hyperglucagonemia. *Diabetes*. 2021;70(2):477-91. Epub 2020/11/27. doi: 10.2337/db20-0440. PubMed PMID: 33239450; PubMed Central PMCID: PMC7881862.

97. Watters JW, Zhang W, Meucci MA, Hou W, Ma MK, McLeod HL. Analysis of variation in mouse TPMT genotype, expression and activity. *Pharmacogenetics*. 2004;14(4):247-54. Epub 2004/04/15. doi: 10.1097/00008571-200404000-00004. PubMed PMID: 15083069.

98. Marinaki AM, Arenas-Hernandez M. Reducing risk in thiopurine therapy. *Xenobiotica; the fate of foreign compounds in biological systems*. 2020;50(1):101-9. Epub 2019/11/05. doi: 10.1080/00498254.2019.1688424. PubMed PMID: 31682552.

99. Lee MN, Woo HI, Lee YM, Kang B, Kim JW, Choe YH, et al. Successful azathioprine treatment with metabolite monitoring in a pediatric inflammatory bowel disease patient homozygous for TPMT*3C. *Yonsei medical journal*. 2013;54(6):1545-9. Epub 2013/10/22. doi: 10.3349/ymj.2013.54.6.1545. PubMed PMID: 24142665; PubMed Central PMCID: PMC3809851.

100. Gibson J, Russ TC, Clarke TK, Howard DM, Hillary RF, Evans KL, et al. A meta-analysis of genome-wide association studies of epigenetic age acceleration. *PLoS genetics*. 2019;15(11):e1008104. Epub 2019/11/19. doi: 10.1371/journal.pgen.1008104. PubMed PMID: 31738745; PubMed Central PMCID: PMC6886870.
101. Bringaud F, Ebikeme C, Boshart M. Acetate and succinate production in amoebae, helminths, diplomonads, trichomonads and trypanosomatids: common and diverse metabolic strategies used by parasitic lower eukaryotes. *Parasitology*. 2010;137(9):1315-31. Epub 2009/12/24. doi: 10.1017/s0031182009991843. PubMed PMID: 20028611.
102. Lei W, Ren W, Ohmoto M, Urban JF, Jr., Matsumoto I, Margolskee RF, et al. Activation of intestinal tuft cell-expressed *Sucnr1* triggers type 2 immunity in the mouse small intestine. *Proceedings of the National Academy of Sciences of the United States of America*. 2018;115(21):5552-7. Epub 2018/05/08. doi: 10.1073/pnas.1720758115. PubMed PMID: 29735652; PubMed Central PMCID: PMC6003470.
103. Yerevanian A, Soukas AA. Metformin: Mechanisms in Human Obesity and Weight Loss. *Current obesity reports*. 2019;8(2):156-64. Epub 2019/03/16. doi: 10.1007/s13679-019-00335-3. PubMed PMID: 30874963; PubMed Central PMCID: PMC6520185.
104. Lin HZ, Yang SQ, Chuckaree C, Kuhajda F, Ronnet G, Diehl AM. Metformin reverses fatty liver disease in obese, leptin-deficient mice. *Nature medicine*. 2000;6(9):998-1003. Epub 2000/09/06. doi: 10.1038/79697. PubMed PMID: 10973319.
105. Farr SA, Roesler E, Niehoff ML, Roby DA, McKee A, Morley JE. Metformin Improves Learning and Memory in the SAMP8 Mouse Model of Alzheimer's Disease. *Journal of Alzheimer's disease : JAD*. 2019;68(4):1699-710. Epub 2019/04/09. doi: 10.3233/jad-181240. PubMed PMID: 30958364.
106. Cerezo M, Tichet M, Abbe P, Ohanna M, Lehraiki A, Rouaud F, et al. Metformin blocks melanoma invasion and metastasis development in AMPK/p53-dependent manner. *Molecular cancer therapeutics*. 2013;12(8):1605-15. Epub 2013/06/07. doi: 10.1158/1535-7163.Mct-12-1226-t. PubMed PMID: 23741061.
107. Linnard-Palmer L. The use of simulation for pediatric oncology nursing safety principles: ensuring competent practice through the use of a mnemonic, chemotherapy

road maps and case-based learning. *Journal of pediatric nursing*. 2012;27(3):283-6. Epub 2012/03/07. doi: 10.1016/j.pedn.2012.02.001. PubMed PMID: 22391150.

108. Johnson AB, Webster JM, Sum CF, Heseltine L, Argyraki M, Cooper BG, et al. The impact of metformin therapy on hepatic glucose production and skeletal muscle glycogen synthase activity in overweight type II diabetic patients. *Metabolism: clinical and experimental*. 1993;42(9):1217-22. Epub 1993/09/01. doi: 10.1016/0026-0495(93)90284-u. PubMed PMID: 8412779.

109. Tulipano G. Integrated or Independent Actions of Metformin in Target Tissues Underlying Its Current Use and New Possible Applications in the Endocrine and Metabolic Disorder Area. *Int J Mol Sci*. 2021;22(23). Epub 2021/12/11. doi: 10.3390/ijms222313068. PubMed PMID: 34884872; PubMed Central PMCID: PMC8658259.

110. Garber AJ, Duncan TG, Goodman AM, Mills DJ, Rohlf JL. Efficacy of metformin in type II diabetes: results of a double-blind, placebo-controlled, dose-response trial. *The American journal of medicine*. 1997;103(6):491-7. Epub 1998/01/16. doi: 10.1016/s0002-9343(97)00254-4. PubMed PMID: 9428832.

111. Tanja JJ, Langlass TM. Metformin: a biguanide. *The Diabetes educator*. 1995;21(6):509-10, 13-4. Epub 1995/11/01. PubMed PMID: 8549253.

112. Zhang Q, Hu N. Effects of Metformin on the Gut Microbiota in Obesity and Type 2 Diabetes Mellitus. *Diabetes, metabolic syndrome and obesity : targets and therapy*. 2020;13:5003-14. Epub 2020/12/29. doi: 10.2147/dmso.S286430. PubMed PMID: 33364804; PubMed Central PMCID: PMC8658259.

113. Wilcock C, Bailey CJ. Accumulation of metformin by tissues of the normal and diabetic mouse. *Xenobiotica; the fate of foreign compounds in biological systems*. 1994;24(1):49-57. Epub 1994/01/01. doi: 10.3109/00498259409043220. PubMed PMID: 8165821.

114. Buse JB, DeFronzo RA, Rosenstock J, Kim T, Burns C, Skare S, et al. The Primary Glucose-Lowering Effect of Metformin Resides in the Gut, Not the Circulation: Results From Short-term Pharmacokinetic and 12-Week Dose-Ranging Studies. *Diabetes care*. 2016;39(2):198-205. Epub 2015/08/20. doi: 10.2337/dc15-0488. PubMed PMID: 26285584.

115. Sum CF, Webster JM, Johnson AB, Catalano C, Cooper BG, Taylor R. The effect of intravenous metformin on glucose metabolism during hyperglycaemia in type 2

diabetes. *Diabetic medicine : a journal of the British Diabetic Association*. 1992;9(1):61-5. Epub 1992/01/01. doi: 10.1111/j.1464-5491.1992.tb01716.x. PubMed PMID: 1551312.

116. Kim M, Astapova II, Flier SN, Hannou SA, Doridot L, Sargsyan A, et al. Intestinal, but not hepatic, ChREBP is required for fructose tolerance. *JCI insight*. 2017;2(24). Epub 2017/12/22. doi: 10.1172/jci.insight.96703. PubMed PMID: 29263303; PubMed Central PMCID: PMC5752301.

117. Eriksson A, Attvall S, Bonnier M, Eriksson JW, Rosander B, Karlsson FA. Short-term effects of metformin in type 2 diabetes. *Diabetes, obesity & metabolism*. 2007;9(4):483-9. Epub 2007/06/26. doi: 10.1111/j.1463-1326.2006.00624.x. PubMed PMID: 17587390.

118. Coll AP, Chen M, Taskar P, Rimmington D, Patel S, Tadross JA, et al. GDF15 mediates the effects of metformin on body weight and energy balance. *Nature*. 2020;578(7795):444-8. Epub 2019/12/26. doi: 10.1038/s41586-019-1911-y. PubMed PMID: 31875646; PubMed Central PMCID: PMC7234839.

119. Owen MR, Doran E, Halestrap AP. Evidence that metformin exerts its anti-diabetic effects through inhibition of complex 1 of the mitochondrial respiratory chain. *The Biochemical journal*. 2000;348 Pt 3(Pt 3):607-14. Epub 2000/06/07. PubMed PMID: 10839993; PubMed Central PMCID: PMC1221104.

120. Kim MS, Krawczyk SA, Doridot L, Fowler AJ, Wang JX, Trauger SA, et al. ChREBP regulates fructose-induced glucose production independently of insulin signaling. *The Journal of clinical investigation*. 2016;126(11):4372-86. Epub 2016/11/02. doi: 10.1172/jci81993. PubMed PMID: 27669460; PubMed Central PMCID: PMC5096918.

121. Zhou G, Myers R, Li Y, Chen Y, Shen X, Fenyk-Melody J, et al. Role of AMP-activated protein kinase in mechanism of metformin action. *The Journal of clinical investigation*. 2001;108(8):1167-74. Epub 2001/10/17. doi: 10.1172/jci13505. PubMed PMID: 11602624; PubMed Central PMCID: PMC209533.

122. Zang M, Zuccollo A, Hou X, Nagata D, Walsh K, Herscovitz H, et al. AMP-activated protein kinase is required for the lipid-lowering effect of metformin in insulin-resistant human HepG2 cells. *The Journal of biological chemistry*. 2004;279(46):47898-905. Epub 2004/09/17. doi: 10.1074/jbc.M408149200. PubMed PMID: 15371448.

123. Kinote A, Faria JA, Roman EA, Solon C, Razolli DS, Ignacio-Souza LM, et al. Fructose-induced hypothalamic AMPK activation stimulates hepatic PEPCK and gluconeogenesis due to increased corticosterone levels. *Endocrinology*. 2012;153(8):3633-45. Epub 2012/05/16. doi: 10.1210/en.2012-1341. PubMed PMID: 22585831.
124. Kogut MD, Roe TF, Ng W, Nonnel GN. Fructose-induced hyperuricemia: observations in normal children and in patients with hereditary fructose intolerance and galactosemia. *Pediatric research*. 1975;9(10):774-8. Epub 1975/10/01. doi: 10.1203/00006450-197510000-00005. PubMed PMID: 1187240.
125. Rena G, Hardie DG, Pearson ER. The mechanisms of action of metformin. *Diabetologia*. 2017;60(9):1577-85. Epub 2017/08/05. doi: 10.1007/s00125-017-4342-z. PubMed PMID: 28776086; PubMed Central PMCID: PMC552828.
126. De Vadder F, Kovatcheva-Datchary P, Zitoun C, Duchampt A, Bäckhed F, Mithieux G. Microbiota-Produced Succinate Improves Glucose Homeostasis via Intestinal Gluconeogenesis. *Cell metabolism*. 2016;24(1):151-7. Epub 2016/07/15. doi: 10.1016/j.cmet.2016.06.013. PubMed PMID: 27411015.
127. Jang C, Wada S, Yang S, Gosis B, Zeng X, Zhang Z, et al. The small intestine shields the liver from fructose-induced steatosis. *Nature metabolism*. 2020;2(7):586-93. Epub 2020/07/23. doi: 10.1038/s42255-020-0222-9. PubMed PMID: 32694791; PubMed Central PMCID: PMC8020332.
128. He L, Wondisford FE. Metformin action: concentrations matter. *Cell metabolism*. 2015;21(2):159-62. Epub 2015/02/05. doi: 10.1016/j.cmet.2015.01.003. PubMed PMID: 25651170.
129. Graham GG, Punt J, Arora M, Day RO, Doogue MP, Duong JK, et al. Clinical pharmacokinetics of metformin. *Clinical pharmacokinetics*. 2011;50(2):81-98. Epub 2011/01/19. doi: 10.2165/11534750-000000000-00000. PubMed PMID: 21241070.
130. Chandel NS, Avizonis D, Reczek CR, Weinberg SE, Menz S, Neuhaus R, et al. Are Metformin Doses Used in Murine Cancer Models Clinically Relevant? *Cell metabolism*. 2016;23(4):569-70. Epub 2016/04/15. doi: 10.1016/j.cmet.2016.03.010. PubMed PMID: 27076070.
131. Bailey CJ, Wilcock C, Scarpello JH. Metformin and the intestine. *Diabetologia*. 2008;51(8):1552-3. Epub 2008/06/06. doi: 10.1007/s00125-008-1053-5. PubMed PMID: 18528677.

132. Cao J, Meng S, Chang E, Beckwith-Fickas K, Xiong L, Cole RN, et al. Low concentrations of metformin suppress glucose production in hepatocytes through AMP-activated protein kinase (AMPK). *The Journal of biological chemistry*. 2014;289(30):20435-46. Epub 2014/06/15. doi: 10.1074/jbc.M114.567271. PubMed PMID: 24928508; PubMed Central PMCID: PMC4110255.
133. Ma T, Tian X, Zhang B, Li M, Wang Y, Yang C, et al. Low-dose metformin targets the lysosomal AMPK pathway through PEN2. *Nature*. 2022. Epub 2022/02/25. doi: 10.1038/s41586-022-04431-8. PubMed PMID: 35197629.
134. Khan TA, Sievenpiper JL. Controversies about sugars: results from systematic reviews and meta-analyses on obesity, cardiometabolic disease and diabetes. *European journal of nutrition*. 2016;55(Suppl 2):25-43. Epub 2016/12/03. doi: 10.1007/s00394-016-1345-3. PubMed PMID: 27900447; PubMed Central PMCID: PMC4517419.
135. Ma J, McKeown NM, Hwang SJ, Hoffmann U, Jacques PF, Fox CS. Sugar-Sweetened Beverage Consumption Is Associated With Change of Visceral Adipose Tissue Over 6 Years of Follow-Up. *Circulation*. 2016;133(4):370-7. Epub 2016/01/13. doi: 10.1161/circulationaha.115.018704. PubMed PMID: 26755505; PubMed Central PMCID: PMC4729662.
136. Toop CR, Gentili S. Fructose Beverage Consumption Induces a Metabolic Syndrome Phenotype in the Rat: A Systematic Review and Meta-Analysis. *Nutrients*. 2016;8(9). Epub 2016/09/23. doi: 10.3390/nu8090577. PubMed PMID: 27657120; PubMed Central PMCID: PMC5037561.
137. Andres-Hernando A, Orlicky DJ, Kuwabara M, Ishimoto T, Nakagawa T, Johnson RJ, et al. Deletion of Fructokinase in the Liver or in the Intestine Reveals Differential Effects on Sugar-Induced Metabolic Dysfunction. *Cell metabolism*. 2020;32(1):117-27.e3. Epub 2020/06/06. doi: 10.1016/j.cmet.2020.05.012. PubMed PMID: 32502381; PubMed Central PMCID: PMC7347444.
138. Spruss A, Kanuri G, Stahl C, Bischoff SC, Bergheim I. Metformin protects against the development of fructose-induced steatosis in mice: role of the intestinal barrier function. *Laboratory investigation; a journal of technical methods and pathology*. 2012;92(7):1020-32. Epub 2012/04/25. doi: 10.1038/labinvest.2012.75. PubMed PMID: 22525431.

139. Qi H, Nielsen PM, Schroeder M, Bertelsen LB, Palm F, Laustsen C. Acute renal metabolic effect of metformin assessed with hyperpolarised MRI in rats. *Diabetologia*. 2018;61(2):445-54. Epub 2017/09/25. doi: 10.1007/s00125-017-4445-6. PubMed PMID: 28936623.
140. Kristensen JM, Larsen S, Helge JW, Dela F, Wojtaszewski JF. Two weeks of metformin treatment enhances mitochondrial respiration in skeletal muscle of AMPK kinase dead but not wild type mice. *PloS one*. 2013;8(1):e53533. Epub 2013/01/24. doi: 10.1371/journal.pone.0053533. PubMed PMID: 23341947; PubMed Central PMCID: PMC3544921.
141. Pan Q, Lu X, Zhao C, Liao S, Chen X, Guo F, et al. Metformin: the updated protective property in kidney disease. *Aging*. 2020;12(9):8742-59. Epub 2020/05/05. doi: 10.18632/aging.103095. PubMed PMID: 32364526; PubMed Central PMCID: PMC7244070.

Biography

Wenxin Tong

Education

Duke University, Durham, NC – Ph.D. in Pharmacology, 2022

Shanghai Jiao Tong University, Shanghai, China – M.S. in Internal Medicine, 2017

Wuhan University, Wuhan, China– Bachelor of Medicine (M.D. equivalent), 2014

Publication

- **Wenxin Tong**, Sarah A. Hannou, Guofang Zhang, You Wang, Inna Astapova, Ashot Sargsyan, Mark A. Herman. The intestine tissue is a major contributor of circulating succinate. (submitted for publication).
- Ludivine Doridot, Sarah A Hannou, Sarah A Krawczyk, **Wenxin Tong**, Mi-Sung Kim, Inna Astapova, Mark A Herman. A Systems Approach Dissociates Fructose-Induced Liver Triglyceride from Hypertriglyceridemia and Hyperinsulinemia in Male Mice. *Nutrients*. 2021 Oct 18;13(10):3642
- Ashot Sargsyan, Ludivine Doridot, Sarah A Hannou, **Wenxin Tong**, Phillip J White, Paul A Grimsrud, Inna Astapova, Linus Tsai, Mark A Herman. HGFAC is a ChREBP Regulated Hepatokine that Enhances Glucose and Lipid Homeostasis. (In revision, *JCI insight*)
- **Wenxin Tong**, Liping Ju, Weihong Sun, Jingyan Tian. Liraglutide ameliorate non-alcohol fatty liver disease by enhancing mitochondrial architecture and promoting autophagy through SIRT1/SIRT3-FOXO3a pathway. *Hepatology Research*. 2016 46:933-943.
- Liping Ju, **Wenxin Tong (co-first author)**, Miaoyan Qiu, Weili Shen, Jingyan Tian. Endurance exercise ameliorates low birthweight developed catch-up growth related metabolic dysfunctions in a mouse model. *Endocrine Journal*. 2016 63(3): 275-2852016 46:933-943.
- Liping Ju, **Wenxin Tong (co-first author)**, Weihong Sun, Jingyan Tian. Antioxidant MMCC ameliorates catch-up growth related metabolic dysfunction. *Oncotarget*. 2017;8(59):99931-9.
- Hailuan Zeng, Renchao Tong, **Wenxin Tong**, Qiaoling Yang, Aizhen Xiong, Jingyan Tian. Metabolic Biomarkers for Prognostic Prediction of Pre-diabetes: results from a longitudinal cohort study. *Scientific reports*. 2017;7(1):6575.
- Miaoyan Qiu, Xiaomin Song, Liping Ju, **Wenxin Tong**, Jingyan Tian. Effects of prediabetes alone or plus hypertension on subsequent occurrence of cardiovascular disease and diabetes: a longitudinal study. *Hypertension*. 2015; 65: 525-530.

- Xiaomin Song, Miaoyan Qiu, **Wenxin Tong**, Sheng Zheng, Yan Jin, Yixin Wu, Weiqing Wang, Jingyan Tian. Gender-related affecting factors of prediabetes on its ten-year outcome. *BMJ Open Diabetes Research & Care*. 2016 May 10;4(1): e000169
- Yuyao Zhang, Chao Li, Gaofeng Yao, Linjuan Du, Xiaojun Zheng, Jiajun Sun, **Wenxin Tong**, Xiaobei Chen, Shengzhong Duan. Deletion of Macrophage Mineralocorticoid Receptor Protects Hepatic Steatosis and Insulin Resistance Through ER α /HGF/Met Pathway. *Diabetes*. 2017;66(6):1535-47
- Hong Zhang, Miaoyan Qiu, Yanyun Li, **Wenxin Tong**, Zhiling Che, Jingyan Tian. Risk factors of type 2 diabetes mellitus with major vascular complications. *Journal of internal medicine and Practice*. 2014, 30 (7): 548-552.
- Hao Shen, **Wenxin Tong**, Ling Zhang, Jianguo Wang, Kun Ding. Systematic evaluation and Meta-analysis of traditional Chinese herbs and western medicine therapy for prostatitis. *Occupation and Health*. 2012, 28(21): 2628-2631
- Cheng Gong, Quanyan Liu, **Wenxin Tong**, Zhisu Liu. The efficiency and Safety of laparoscopic surgery for colorectal carcinoma : a systematic review. *Chinese J Surgery*. 2011, 49(4): 346-450.

Honors and Awards

- *Duke Scholar in Nutrition and Metabolism, Duke Scholars in Molecular Medicine, Duke University, 2021*
- *Chancellor's Scholarship, Duke University, 2017*
- *Excellent Graduates of Shanghai Jiao Tong University, Shanghai Jiao Tong University, 2017*
- *China National Scholarship, Ministry of Education of China, 2016*
- *Excellent Graduates of Wuhan University, Wuhan University, 2014*
- *Excellent Student leader of Wuhan University, Wuhan University, 2014*
- *China National Scholarship, Ministry of Education China, 2011*